

中图分类号: TP391
密 级: 公开

单位代号: 10280
学 号: 19860119

上海大学



博士学位论文

SHANGHAI UNIVERSITY
DOCTOR'S DISSERTATION

题 目	Digitized-Counterdiabatic Quantum Computing
-----	--

作 者 _____ Narendra Narayana Hegade
学科专业 _____ 理论物理
导 师 _____ Prof. Dr. Enrique Solano
完成日期 _____ 二〇二三年一月

姓名: Narendra Narayana Hegade

学号: 19860119

论文题目: Digitized-Counterdiabatic Quantum Computing

上海大学

本论文经答辩委员会全体委员审查,确认符合上海大学博士学位论文质量要求。

答辩委员会签名: 工作单位 职称

主任: *Kihwan Kim* Tsinghua University Professor

委员: *王立刚* Zhejiang University Professor

张永平 Shanghai University Professor

Ram IIIT Hyderabad, India Professor

陈志 Shanghai University Professor

导师: 

答辩日期: 2023-06-26

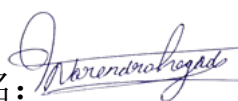
姓 名: Narendra Narayana Hegade

学号: 19860119

论文题目: Digitized-Counterdiabatic Quantum Computing

原创性声明

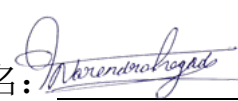
本人声明: 所呈交的论文是本人在导师指导下进行的研究工作。除了文中特别加以标注和致谢的地方外, 论文中不包含其他人已发表或撰写过的研究成果。参与同一工作的其他同志对本研究所做的任何贡献均已在论文中作了明确的说明并表示了谢意。

签 名:  日期: 2023-06-26

本论文使用授权说明

本人完全了解上海大学有关保留、使用学位论文的规定, 即: 学校有权保留论文及送交论文复印件, 允许论文被查阅和借阅; 学校可以公布论文的全部或部分内容。

(保密的论文在解密后应遵守此规定)

签 名:  导师签名:  日期: 2023-06-26

上海大学理学博士学位论文

Digitized-Counterdiabatic Quantum Computing

姓 名： Narendra Narayana Hegade

导 师： Prof. Dr. Enrique Solano

学科专业： 理论物理

上海大学理学院

2023 年 01 月

A Dissertation Submitted to Shanghai University for the Degree of
Doctor of Philosophy
in Science

Digitized-Counterdiabatic Quantum Computing

Candidate: Narendra Narayana Hegade

Supervisor: Prof. Dr. Enrique Solano

Major: Theoretical Physics

College of Sciences, Shanghai University

January, 2023

摘要

量子计算是一种利用量子力学系统特性进行计算的新方法，绝热量子计算 (AQC) 就是其中一种通用的模型，它能通过把问题的解译码到哈密顿量的基态从而解决任何计算问题。然而，当前量子硬件不可避免的退相干误差对缓慢的绝热演化造成了限制。因此，人们必须依赖于有限时间的反向透热补偿演化，但这会导致本征态之间的激发，从而导致算法的成功率降低。AQC 的另一个主要挑战是需要构建一个可以实现任意非随机相互作用的通用相干绝热量子计算机。受启发于所有的这些挑战，本论文提出“数字化反向透热补偿量子计算”(DCQC) 作为一种新范例，通过反向透热补偿的方法来提高量子计算结果，从而在量子门模型的量子计算机上实现绝热算法的新方法。该方法不仅可以通过抑制反向透热的激发来加速绝热过程，而且提供了可以实现任意相互作用的灵活性，从而适用于有噪声的中型量子计算机。

除此之外，我们的研究表明当应用于解决组合优化问题时 DCQC 方法就像一个非随机催化剂，与使用随机哈密顿量的传统量子退火方法相比，它提供了基态成功率的多项式增强。另外，我们还讨论了 DCQC 的扩展方法，即经典—量子混合算法用于构建一个高效的模拟算法，该算法通过提供更好的近似率和更快地收敛到浅层量子线路的全局解决方案，从而实现更好的性能。此外，DCQC 方法还可用于解决基于当前超导量子比特和囚禁离子系统的噪声量子计算机的更多有趣且重要的计算问题，如组合优化问题、多体基态的备置、质因数分解、投资组合优化等。我们推测，在具有数百万量子比特计算能力的容错量子计算机构建之前，DCQC 方法可能会是量子计算届的领先候选方法。

关键词： 绝热量子计算；量子绝热捷径技术；反向透热补偿；量子算法；量子模拟。

ABSTRACT

Quantum computing is a novel approach to do computation by exploiting the properties of quantum mechanical systems. Adiabatic quantum computing (AQC) is one such universal model of quantum computation, capable of solving any computational problem by encoding the solution in the ground state of a Hamiltonian. However, the inevitable decoherence errors of the current quantum hardware pose a restriction on the slow adiabatic evolution. Consequently, one has to rely on finite time non-adiabatic evolution, which results in excitations between eigenstates, reducing the algorithm's success probability. Another major challenge of AQC is building a universal coherent adiabatic quantum computer that can realize arbitrary non-stoquastic interactions. Inspired by all these challenges, this thesis proposes "Digitized-counterdiabatic quantum computing" (DCQC) as a new paradigm to implement adiabatic quantum algorithms enhanced by counterdiabatic protocols on a gate model quantum computer. This novel approach not only speeds up the adiabatic process by suppressing the non-adiabatic excitations but also provides the flexibility to realize any arbitrary interactions making it suitable for noisy intermediate-scale quantum computers.

Furthermore, we show that the DCQC approach, when applied to combinatorial optimization problems, acts like a non-stoquastic catalyst and provides a polynomial enhancement in the ground state success probability compared to the traditional quantum annealing with stoquastic Hamiltonian. Also, we discuss the extension of the DCQC protocol for hybrid classical-quantum algorithms for constructing an efficient ansatz that performs better by giving a better approximation ratio and faster convergence to a global solution with shallow-depth quantum circuits. In addition, using the DCQC approach, we solve many interesting and important computational problems like combinatorial optimization problems, many-body ground state preparation, prime factorization, portfolio optimization, and many more on current noisy quantum computers based on superconducting qubits and trapped-ion systems. We presume that the DCQC paradigm might serve as a leading candidate in the quantum computing community before a fault-tolerant quantum computer with millions of qubits is built.

Keywords: Adiabatic quantum computing; Shortcuts to adiabaticity; Counterdiabatic protocol; Quantum algorithms; Quantum simulation.

目 录

第一章	Introduction	1
1.1	The potential of quantum computing	1
1.2	Noisy intermediate-scale quantum computers	2
1.3	Quantum simulation	3
1.4	Motivation	4
1.5	Outline of the thesis	4
第二章	Adiabatic Quantum Computation and Counterdiabatic Protocols	8
2.1	Adiabatic quantum computation	8
2.1.1	Proof of adiabatic theorem	9
2.2	Digitized-adiabatic evolution	11
2.3	Shortcuts to adiabaticity	12
2.3.1	Transitionless quantum driving	12
2.3.2	Approximate CD-driving from the variational method	12
2.4	Conclusion	13
第三章	Shortcuts to Adiabaticity in Digitized-Adiabatic Quantum Computing	15
3.1	Introduction	15
3.2	Single spin system	17
3.3	Local counterdiabatic driving	20
3.3.1	Local CD from Berry's algorithm	21
3.3.2	Local CD from variational approach	23
3.4	Approximate counterdiabatic protocol	25
3.5	Preparation of topological order	29
3.6	Ground state of hydrogen molecule (H_2)	32
3.7	Method of digitization	34
3.8	Approximate CD term using variational method	36
3.9	Error Analysis	37
3.9.1	Gate error	38
3.9.2	Measurement error mitigation	39
3.10	Conclusion	40

第四章	Digitized-Counterdiabatic Quantum Optimization	41
4.1	Introduction	41
4.2	Counterdiabatic driving as a non-stoquastic catalyst	43
4.3	Digitized counterdiabatic driving	45
4.4	Experimental implementation	49
4.5	Discussion and conclusion	50
第五章	Digitized-Counterdiabatic Quantum Approximate Optimization Algorithm ...	54
5.1	Introduction	54
5.2	Digitized-counterdiabatic quantum approximate optimization algorithm	56
5.3	Ising spin models	60
5.4	Classical optimization problems	61
5.5	P -spin Model	64
5.6	Discussion and conclusion	66
第六章	Digitized-Counterdiabatic Quantum Factorization	67
6.1	Introduction	67
6.2	Approach 1: Direct optimization	68
6.3	Approach 2: Binary multiplication table	70
6.4	Experimental analysis	74
6.5	Conclusions	75
第七章	Portfolio Optimization with Digitized-Counterdiabatic Quantum Algorithms .	78
7.1	Introduction	78
7.2	Markowitz portfolio optimization	80
7.3	Digitized-counterdiabatic quantum computing	82
7.4	Digitized-counterdiabatic quantum approximate optimization algorithm	88
7.5	Conclusion	91
第八章	Conclusions	93
插图索引		96
表格索引		103
附录 A	Additional Calculation and results for Digitized-Counterdiabatic Quantum Factorization.	104
A.1	Calculation of local CD term	104
A.1.1	Example-1: quantum factorization of 217 using the direct optimization method	106

A.1.2 Example-2: quantum factorization of $35 = 7 \times 5$	106
A.1.3 Example-3: quantum factorization of 2479 using the binary multiplication table	107
参考文献	109
作者在攻读博士学位期间发表的论文与研究成果	124
作者在攻读博士学位期间所作的项目	126
致 谢	127

第一章 Introduction

1.1 The potential of quantum computing

The concept of quantum computation was developed in the early 1980s as a new means to perform computational tasks by exploiting quantum mechanical properties [1, 2]. As Richard Feynman proposed, an obvious application of quantum computers is for simulating complex quantum many-body systems [3]. However, the proposal of Shor's and Grover's algorithm [4] sparked massive interest in developing quantum algorithms for various applications, including quantum simulation, combinatorial optimization, quantum chemistry, machine learning, and many more.

Classical computers process information using strings of bits. In contrast, quantum computers use qubits, two-level quantum systems with special properties like superposition and entanglement. However, these qubits need to be isolated from the environmental noise to maintain the quantum mechanical properties. At the same time, it requires controlling the qubits by applying external interactions for performing different operations and measurements to get the output. So for building large-scale quantum computers, it is essential to correct the errors caused by any external means by using error correction techniques. And quantum error correction (QEC) is a field of research that addresses this problem in detail. However, the experimental advancement toward building a universal fault-tolerant quantum computer with a low error rate and long coherence time would take decades. The QEC requires building a scalable quantum computer with an error below a certain threshold. However, increasing the number of qubits while maintaining the error threshold required for QEC is a challenging problem. These difficulties motivated us to explore the potential of current noisy quantum computers. Recently there has been a huge interest in using noisy intermediate-scale quantum (NISQ) computers for solving certain computational problems which are challenging to solve on classical computers. And many hardware players like Google, IBM, IonQ, etc., aim to build a quantum computer with a few hundred to thousand qubits in the near future. These near-term quantum computers will have a limited number of noisy qubits, with limited coherence time, imperfect gate operations, and suffer from other sources of environmental errors. Achieving a quantum advantage from these devices requires creative ideas in developing hardware-aware quantum algorithms and efficient encoding of the problems.

1.2 Noisy intermediate-scale quantum computers

Despite all the limitations, NISQ computers are expected to perform quantum computations that are beyond the reach of classical computers. The potential applications of NISQ computers are vast. They could be used to solve problems in physics and chemistry that are intractable with existing classical simulation techniques. They could also be used to develop new drugs and materials and solve important industrial optimization problems. The development of NISQ computers is an active area of research, and there are already a number of prototypes in existence. Commercial NISQ computers are already available, and one can access them via the cloud.

Many of the NISQ algorithms rely on a hybrid classical-quantum setup, where computationally expensive tasks are performed on quantum computers while classical computers are used for relatively easy tasks. This hybrid setup is ideal for NISQ devices because of the limitations on the circuit depth. Generally, these hybrid algorithms are also known as variational quantum algorithms (VQA). There are mainly four components in VQA. i) Objective function: For a given computation problem, one could define an objective function, and minimizing or maximizing this function will give the optimal solution to the problem of interest. ii) Parametrized quantum circuit: Preparing a quantum state by applying parameterized unitary operations is essential to VQA. The states prepared by this variational circuit is also called ansatz state. iii) Measurement: In order to obtain information on the prepared state, one has to make a measurement of some observable, for example, measuring the expectation value of a Hamiltonian, which can be done efficiently on a quantum computer. iv) Classical optimization: Updating the variational parameters of the quantum circuit with the aim of minimizing an objective function is done on a classical computer.

The future of NISQ computation is very exciting. With continued research and development, NISQ computers will become more powerful and more widely available. They will open up new possibilities for scientific discovery and enable us to solve problems that are currently beyond our reach. However, achieving a quantum advantage from these devices is still an open problem and an active area of research. One of the main motivations of this thesis is to develop NISQ algorithms to achieve a quantum advantage using near-term quantum computers.

1.3 Quantum simulation

A numerical simulation of physical systems can help us better understand natural phenomena. The numerical solution of many physical systems of interest in fields such as quantum many-body systems in condensed matter physics, quantum chemistry, high energy physics, etc., is thought to be very difficult with a classical computer. Analytical methods are very difficult to solve the dynamics of physical systems described by mathematical models. Numerical simulation plays a key role in studying the dynamics of these systems. However, one of the major problems we often face in numerical computations is the enormous amount of memory and computing time necessary to solve them. We face this problem even at a very small system size for quantum systems. The main reason for this is the exponential growth of Hilbert space as quantum systems grow in size. To overcome this problem, in 1982, Richard Feynman proposed the idea of simulating the dynamics of a quantum system on a quantum simulator [3]

Quantum simulation is a method of using one quantum system to study the behavior of another quantum system. Here the former is an easily controllable and manipulable system, while the latter corresponds to some complex many-body quantum system [5–8]. By simulating the behavior of a quantum system on a quantum computer, one can gain a better understanding of how the system works and what its potential applications might be. One of the most promising applications of quantum simulation is in the area of quantum chemistry. By simulating the behavior of molecules on a quantum computer, researchers can gain a better understanding of the chemical properties of those molecules. This could lead to the development of new, more efficient methods for synthesizing and manufacturing chemicals. In addition to quantum chemistry, quantum simulation can also be used to study other condensed matter systems, such as high-temperature superconductors, fractional quantum Hall effect, and many more. By understanding how these systems work, researchers can develop new materials and devices with improved performance.

The potential applications of quantum simulation are nearly limitless, and the field is currently one of the most active areas of research in quantum computing. In the future, quantum simulation is likely to play a major role in many areas of science and engineering, from materials science to drug design. There are mainly three types of quantum simulation techniques, i) Digital quantum simulation ii) Analog quantum simulation, and iii) Hybrid digital-analog quantum simulation. Digital quantum simulators are the most versatile type of quantum simulator, as they can be used to simulate any type of quantum system by a sequence of quantum logic gates. Analog quantum simulators are limited to simulating

specific types of quantum systems, but they can achieve very high levels of fidelity. Hybrid quantum simulators are a combination of digital and analog quantum simulators, and they offer the best of both worlds in terms of versatility and fidelity. In this thesis, we exploit digital and digital-analog techniques to develop our algorithms.

1.4 Motivation

The concept of CD driving originated from shortcuts to adiabaticity was there for a long time. However, its applications were limited due to experimental constraints and the difficulty in extending this idea to many-body systems. The recent advancement in constructing the CD term using the variational approach opened up the possibility of efficiently obtaining the approximate CD term for many-body systems without requiring the knowledge of the instantaneous eigenstates. We found this feature to be particularly useful for adiabatic quantum computing. However, for many interesting quantum optimization problems, the obtained CD terms are non-stoquastic, making it challenging to realize such Hamiltonians on existing quantum annealers. Also, for obtaining a higher success probability in many-body systems, it is essential to consider higher-order multi-qubit CD terms; this is a challenging task for analog quantum computers and quantum annealers (which requires reducing the problem to QUBO form). Along with that, the lack of flexibility in realizing arbitrary interactions is one of the main drawbacks of analog quantum computers and quantum annealers. To overcome all these problems, we come up with DCQC protocols, which provide the flexibility to introduce arbitrary multi-qubit and non-stoquastic interactions. The model is also consistent with error correction, and error mitigation techniques are being developed for noisy quantum devices. Furthermore, DCQC serves as an alternative approach suitable for implementation on NISQ computers.

1.5 Outline of the thesis

The subject of this thesis is a combination of adiabatic quantum algorithms, shortcuts to adiabaticity by counterdiabatic driving, and its implementation by discretizing the continuous adiabatic evolution on gate-based quantum computers. In the following chapters, we discuss these three concepts in detail. Each of them carries its own advantages and challenges. Their combination helps to take advantage of each paradigm and also helps to overcome some of the challenges.

In **Chapter 2** (二), we introduce the concept of adiabatic quantum computation and

shortcuts to adiabaticity by counterdiabatic driving techniques. We start with the proof of the adiabatic theorem and discuss how the slow adiabatic process can be sped up using counterdiabatic driving techniques. By considering Berry's proposal on transitionless quantum driving, we provide an expression for the exact CD term and discuss its challenges and limitations for many-body quantum systems. We consider approximate CD protocols inspired by variational principles to circumvent the problems of exact CD terms. And finally, we discuss the advantage of implementing the adiabatic algorithms on a gate-model quantum computer using the Hamiltonian simulation techniques.

In **Chapter 3** (三), we address the application of shortcuts to adiabaticity (STA) by the counter-diabatic driving (CD) technique to enhance the digital adiabatic quantum computing paradigm in terms of fidelity and simulation time. We consider the exact CD driving protocol to study a few qubit systems and the approximate CD protocol based on a variational method to study many-body systems. We show the applicability of this technique in the preparation of bell state, N-qubit GHZ state, and topological orders with a shallow quantum circuit with very high fidelity. Also, we discuss the application of the digital-analog approach by using hardware native gates to implement the time evolution unitaries to reduce the circuit depth and gate counts further. In this regard, we consider a transmon-based quantum processor with fixed-frequency superconducting qubits to implement the digitized-counterdiabatic algorithms to find the ground state of the hydrogen (H_2) molecule. And we show that using native parameterized Cross-Resonance (CR) gates are advantageous over standard quantum logic gates.

One of the key applications of quantum computers is to solve combinatorial optimization problems, which are of huge interest to both science and industry. Adiabatic algorithms for quantum optimization are an important method for solving such problems. However, in AQC, one generally considers a stoquastic Hamiltonian, and quantum Monte Carlo algorithms can efficiently tackle such problems without facing the sign problem. In order to prevent classical simulability and achieve quantum speed-up, in **Chapter 4** (四), we propose a novel method called digitized-counterdiabatic quantum optimization (DCQO) for solving combinatorial optimization problems on current gate-based quantum computers. To illustrate the advantage of this method, we consider the problem of finding the ground state of a general Ising spin-glass Hamiltonian with all-to-all interactions. By introducing the simplest 2-local non-stoquastic counterdiabatic terms, we show a polynomial enhancement over the traditional AQC with stoquastic Hamiltonians.

A more suitable alternative method for NISQ devices is hybrid classical-quantum

algorithms that combine quantum computers and classical computers. The three main components of this algorithm are the parameterized quantum circuits, also known as ansatz, an objective function corresponding to the problem of interest, and a classical optimization part. Since the algorithm involves variational minimization of some cost function by iteratively updating the circuit parameters, these are also known as variational quantum algorithms (VQA). An essential part of VQA is finding a suitable ansatz to find the solution. In literature, there are many types of ansatz proposed for different tasks. We can categorize these ansatzes into two types, Hardware efficient ansatz, and problem-inspired ansatz. The Hardware efficient ansatz is experimentally more feasible since they consider the hardware constraints like connectivity and available gate set while constructing the ansatz. However, finding the optimal parameters with this ansatz is challenging because of the vanishing gradients in the optimization landscape. The problem-inspired ansatz might be more suitable to overcome this difficulty. However, the circuit depth of these ansatzes is relatively larger. Also, depending on the problem, it might require a complicated form of the circuits with multi-qubit and non-local interactions. One such variational quantum algorithm based on problem Inspired ansatz is the quantum approximate optimization algorithm (QAOA). Here the ansatz is a digitized version of the adiabatic evolution with a parameterized scheduling function. In order to improve the performance of this ansatz, in **Chapter 5** (五), we propose a CD-inspired method to construct the ansatz, where we introduce the counterdiabatic terms with extra parameters for each layer. This optimized method, known as digitized-counterdiabatic QAOA, can quickly find the solution with a few layers. Also, in some cases, both the circuit depth and the number of variational parameters can be reduced by a large factor using DC-QAOA.

In cryptography, many of the secure public-key encryption protocols are based on the fact that finding the prime factors of a very large number is a difficult task for classical computers. Shor's factoring algorithm can solve this problem in polynomial time on a quantum computer. However, the implementation of Shor's algorithm on a NISQ device is a difficult task. And so far, the largest number factored using this method on a quantum computer does not go beyond two digits. An alternative method is to use the adiabatic algorithm for factorization, where the problem of finding the prime factors is mapped to an optimization problem. An advantage of this method is that the number of qubits required for the computation scales linearly with the number of bits required to represent the integer N . However, the time complexity of this method is still unknown. And it's highly believed that adiabatic factorization with stoquastic Hamiltonian might not give significant speed-up

compared to classical algorithms. In **Chapter 6** (六), we introduce a method to speed up adiabatic factorization using counter-diabatic driving techniques, which can factor numbers much larger than those feasible using Shor's algorithm with the same number of qubits, which makes it more suitable for NISQ devices.

In **Chapter 7** (七), we discuss the application of digitized-counterdiabatic protocols to solve a discrete mean-variance portfolio optimization problem, showing its usefulness in a key finance application. This problem deals with optimizing the weights of the assets in a portfolio to give out returns based on the requirements of the asset manager, as is the case of maximum return and minimum risk. We select a large number of data instances and solve the problem using the digitized-counterdiabatic protocols. We obtain the approximate CD terms by considering variational minimization techniques that significantly enhance the success probability for most of the selected instances. We also show that the inclusion of these CD terms in hybrid classical-quantum algorithms like QAOA, namely DC-QAOA, improves success probabilities with a reduced number of iterations.

Finally, **Chapter 8** (八) gives a conclusion and future aspects of this thesis, while the appendix section contains detailed calculations from each chapter.

第二章 Adiabatic Quantum Computation and Counterdiabatic Protocols

2.1 Adiabatic quantum computation

In 1988, Appoloni et al. proposed the idea of encoding the solution of a computational problem in the ground state of a quantum Hamiltonian in the context of solving classical combinatorial optimization problems [9]. This idea was recognized as quantum annealing [10] as analogous to classical simulated annealing, where the simulated quantum fluctuation and tunneling were exploited to find the optimal solution to an optimization problem. Later this idea led to the development of a novel method of quantum computing called adiabatic quantum computation (AQC) by Farhi et al. in 2001 [11]. The key idea behind adiabatic quantum computation is to use the adiabatic theorem to keep the system in its ground state throughout the computation. The adiabatic theorem states that if a system is initially in its ground state and the Hamiltonian of the system is slowly varied, then the system will remain in its ground state. The Hamiltonian describing the adiabatic evolution is given by

$$H(\lambda(t)) = (1 - \lambda(t))H_i + \lambda(t)H_f, \quad (2.1)$$

where $\lambda(t)$ is a scheduling function. And, H_i corresponds to the initial Hamiltonian, whose ground state can be easily prepared. H_f corresponds to the final Hamiltonian, which encodes the solution to some computational problem.

Adiabatic quantum computation is also relatively insensitive to noise. This is because the system is always in its ground state during the computation, which is the state of lowest energy. This means that any errors that occur will not cause the system to become excited and will not lead to incorrect results. Adiabatic quantum computation is fault-tolerant against a restricted class of errors. This means that if an error does occur, it will not propagate and cause the entire computation to be incorrect. This is in contrast to the circuit model, where an error in one qubit can lead to errors in all of the qubits that are connected to it. The main disadvantage of adiabatic quantum computation is that it is relatively slow. This is because the time required for the computation is proportional to the inverse of the energy gap between the ground state and the first excited state of the final Hamiltonian. This can be a problem when trying to solve large problems, as the energy gap can become very small. There are a number of ways to speed up adiabatic quantum computation. One way is to use a

quantum annealer. A quantum annealer is a quantum computer that is specifically designed for adiabatic quantum computation. It uses a special type of quantum algorithm, called annealing, which can be used to solve certain types of optimization problems. Another way to speed up adiabatic quantum computation is to use a shortcut to adiabaticity. A shortcut to adiabaticity is a method of creating a Hamiltonian that has the same ground state as the desired final Hamiltonian but can be prepared much faster.

2.1.1 Proof of adiabatic theorem

The idea behind AQC comes from the adiabatic theorem. There are various approaches to proving this theorem. Here, we consider one such approach inspired by [12]. We start with a time-dependent Schrodinger equation given by

$$i \frac{\partial}{\partial t} |\psi(t)\rangle = H(t) |\psi(t)\rangle. \quad (2.2)$$

Here, we set $\hbar = 1$, and $|\psi(0)\rangle$ is the initial ground state corresponding to the Hamiltonian $H(0)$. The instantaneous eigenstates and the eigenvalues of the Hamiltonian $H(t)$ are defined as

$$H(t) |n(t)\rangle = E_n(t) |n(t)\rangle. \quad (2.3)$$

This forms a complete orthonormal set satisfying the condition $\langle n(t)|n(t)|n(t)|n(t)\rangle = 1$. In order to solve the Schrodinger equation, we expand $|\psi(t)\rangle$ as a linear combination of eigenstates $|n(t)\rangle$

$$|\psi(t)\rangle = \sum_n c_n(t) e^{i\theta_n(t)} |n(t)\rangle, \quad (2.4)$$

where $\theta_n(t)$ is a phase factor because of the time dependence of the eigenvalue E_n given by

$$\theta_n(t) = -i \int_0^t E_n(t') dt'. \quad (2.5)$$

By substituting Eq. (2.4) in the Schrodinger equation, we get

$$i \sum_n \left[\dot{c}_n |n(t)\rangle + c_n |\dot{n}(t)\rangle + i c_n |n(t)\rangle \dot{\theta}_n \right] e^{i\theta_n} = \sum_n c_n (H |n(t)\rangle) e^{i\theta_n}. \quad (2.6)$$

By substituting Eq. (2.3) and Eq. (2.5) gives

$$i \sum_n [\dot{c}_n |n(t)\rangle + c_n |\dot{n}(t)\rangle - i c_n E_n |n(t)\rangle] e^{i\theta_n} = \sum_n c_n E_n |n(t)\rangle e^{i\theta_n}. \quad (2.7)$$

After the cancellation, the equation simplifies to

$$\sum_n \dot{c}_n |n(t)\rangle e^{i\theta_n} = - \sum_n c_n |\dot{n}(t)\rangle e^{i\theta_n}. \quad (2.8)$$

Multiplying both sides by $\langle m|$, we get

$$\sum_n \dot{c}_n \langle m|n\rangle e^{i\theta_n} = - \sum_n c_n \langle m|\dot{n}\rangle e^{i\theta_n}, \quad (2.9)$$

and the orthonormality condition leads to

$$\dot{c}_m(t) = - \sum_n c_n \langle m|\dot{n}\rangle e^{i(\theta_n - \theta_m)}. \quad (2.10)$$

Now, we take the time derivative of Eq. (2.3) and multiply by $\langle m|$,

$$\langle m| \dot{H}|n\rangle + \langle m| H|\dot{n}\rangle = \dot{E}_n \delta_{mn} + E_n \langle m|\dot{n}\rangle. \quad (2.11)$$

Here, H is Hermitian, so we have $\langle m| H |\dot{n}\rangle = \langle m| H^\dagger |\dot{n}\rangle = E_n \langle m|\dot{n}\rangle$. For $n \neq m$ we get

$$\langle m| \dot{H}|n\rangle = (E_n - E_m) \langle m|\dot{n}\rangle. \quad (2.12)$$

Substituting Eq. (2.12) in Eq. (2.10) gives

$$\dot{c}_m(t) = -c_m \langle m|\dot{m}\rangle - \sum_{n \neq m} c_n \frac{\langle m| \dot{H}|n\rangle}{(E_n - E_m)} e^{-i \int_0^t (E_n^{t'} - E_m^{t'}) dt'}. \quad (2.13)$$

For slow evolution, we can drop the second term because \dot{H} is negligible, and we get

$$\dot{c}_m(t) = -c_m \langle m|\dot{m}\rangle. \quad (2.14)$$

The solution to this differential equation is given by

$$c_m(t) = c_m(0) e^{i\gamma_m(t)}, \quad (2.15)$$

where

$$\gamma_m(t) \equiv i \int_0^t \langle m(t')|\dot{m}(t')\rangle dt'. \quad (2.16)$$

For a system starting in the n th eigenstate, Eq. 2.4 reduces to

$$|\psi_n(t)\rangle = e^{i\theta_n(t)} e^{i\gamma_n(t)} |n(t)\rangle, \quad (2.17)$$

which implies that the system will remain in the n th eigenstate for all time t with only a change in phase.

2.2 Digitized-adiabatic evolution

There are various techniques to approximate the time evolution of a Hamiltonian to implement on a quantum computer. This section discusses how continuous adiabatic evolution can be implemented on a gate model quantum computer. Also, the digital implementation of the adiabatic evolution can help to overcome some of the experimental difficulties faced by current analog quantum computers and quantum annealers.

For the Hamiltonian corresponds to the adiabatic evolution given in Eq. (2.1), the time evolved state is given by

$$|\psi(T)\rangle = U(0, T) |\psi(0)\rangle, \text{ with } U(0, T) = \mathcal{T} e^{-i \int_0^T H(\lambda) dt}, \quad (2.18)$$

where \mathcal{T} is the time ordering operator. Here, the Hamiltonian can be decomposed into sum of local terms, *i.e.*, $H(\lambda) = \sum_j c_j(t) H_j$. We discretize the total time T into many small intervals of size δt . Using the first-order Trotter-Suzuki formula, we obtained the approximate time evolution operator given by

$$U_{\text{dig}}(0, T) = \prod_{k=1}^M \prod_j \exp \{-i\delta t c_j(k\delta t) H_j\}, \quad (2.19)$$

where M is the number of trotter steps. For this first-order approximation, the trotter error is of the order $\mathcal{O}(\delta t^2)$. There are many ways to approximate the time evolution operator by a product of unitaries, with different trade-offs between the number of operations and the accuracy of the approximation. The most general approach is to use the Baker-Campbell-Hausdorff formula to expand $U(0, T)$ as a product of unitary operators, which is then truncated at a suitable order.

2.3 Shortcuts to adiabaticity

2.3.1 Transitionless quantum driving

For an arbitrary time-dependent Hamiltonian $H_0(t)$ with instantaneous eigenstates $|n(t)\rangle$ and eigen energies $E_n(t)$ satisfy the equation,

$$H_0(t)|n(t)\rangle = E_n(t)|n(t)\rangle. \quad (2.20)$$

In general, the time-varying Hamiltonian introduces a transition between quantum states. However, for a slow evolution, the transition amplitude will be minimal. By considering the adiabatic approximation, the state driven by H_0 is given by

$$|\psi_n(t)\rangle = \exp \left\{ -\frac{i}{\hbar} \int_0^t d\tau E_n(\tau) - \int_0^t d\tau \langle n(\tau) | \partial_\tau n(\tau) \rangle \right\} |n(t)\rangle. \quad (2.21)$$

Now we look for a Hamiltonian $H(t)$ for which $|\psi_n(t)\rangle$ is the exact evolving state, which satisfies the Schrödinger equation

$$i\hbar \partial_t |\psi_n(t)\rangle = H(t) |\psi_n(t)\rangle.$$

In order to construct the Hamiltonian $H(t)$, we consider the time evolution operator

$$U(t) = \sum_n \exp \left\{ -\frac{i}{\hbar} \int_0^t d\tau E_n(\tau) - \int_0^t d\tau \langle n(\tau) | \partial_\tau n(\tau) \rangle \right\} |n(t)\rangle \langle n(0)|, \quad (2.22)$$

which is the solution of $i\hbar \partial_t U(t) = H(t)U(t)$. After simplification, we obtain

$$H(t) = \sum_n |n\rangle E_n \langle n| + i\hbar \sum_n (\langle \partial_t n | \langle n | - \langle n | \partial_t n \rangle | n \rangle \langle n |) \equiv H_0(t) + H_{CD}(t), \quad (2.23)$$

where the CD term H_{CD} can be written in an alternative form as

$$H_{CD}(t) = i\hbar \sum_{m \neq n} \sum \frac{|m\rangle \langle m | \partial_t H_0 | n \rangle \langle n |}{E_n - E_m}. \quad (2.24)$$

2.3.2 Approximate CD-driving from the variational method

When complex many-body systems are considered, the calculation of the exact CD term becomes difficult. Also, the form of the CD term can be severely complicated with different non-local and many-body interaction terms. Besides, it becomes rather difficult to implement systems with such interactions on current quantum computers. Because of the difficulty in calculating the exact CD term for many-body systems, it is essential to

look for an approximate solution. A recently proposed method by Sels and Polkovnikov [13], based on the variational approach, provides an alternative to calculate the approximate CD Hamiltonian with only local terms. For a given time-dependent Hamiltonian $H_0(\lambda(t))$, which is a function of some control parameter λ , we consider approximate gauge potential A_λ^* , which satisfies the equation

$$[i\partial_\lambda H_0 - [A_\lambda^*, H_0], H_0] = 0. \quad (2.25)$$

For the optimal solution, we have to minimize the operator distance between the exact gauge potential A_λ and the approximate gauge potential A_λ^* , which is equivalent to minimizing the action

$$S_\lambda(A_\lambda^*) = \text{Tr} [G_\lambda^2(A_\lambda^*)], \quad (2.26)$$

where the Hilbert-Schmidt norm G_λ is given by

$$G_\lambda(A_\lambda^*) = \partial_\lambda H_0 + i[A_\lambda^*, H_0]. \quad (2.27)$$

The nature of the CD term from variational calculation depends on the choice of appropriate adiabatic gauge potential A_λ^* . A recently proposed method gives a more general way to choose the gauge potential by using the nested commutator (NC) as in [14],

$$A_\lambda^{(l)} = i \sum_{k=1}^l \alpha_k(t) \underbrace{[H, [H, \dots, [H, \dots [H, \partial_\lambda H]]]]}_{2k-1}, \quad (2.28)$$

where l determines the order of the expansion, when $l \rightarrow \infty$, we will get the exact gauge potential. Depending on the required accuracy, we can keep the number of variational coefficients small.

2.4 Conclusion

In this chapter, we introduced three main concepts i) Adiabatic quantum computing, ii) Shortcuts to adiabaticity by counterdiabatic driving, and iii) digitized-adiabatic evolution on a gate-based quantum computer; these are the essential component of this thesis. The AQC provides an alternative way to do quantum computation by exploiting the adiabatic theorem. However, its application on current quantum computers is hindered because of its slow evolution. The counterdiabatic protocols provide a way to speed up adiabatic evolution. However, calculating and implementing the exact CD term for a many-body

system is challenging. The recently proposed approximate counterdiabatic protocols provide a way to overcome these challenges. And finally, the gate-model approach provides the required flexibility and controllability to implement adiabatic algorithms using quantum logic gates. In the next chapter, we discuss about combining these three concepts to develop a novel paradigm called digitized-counterdiabatic quantum computing and show its vast applications in NISQ devices for solving useful scientific and industrially relevant computational problems.

第三章 Shortcuts to Adiabaticity in Digitized-Adiabatic Quantum Computing

Shortcuts to adiabaticity are well-known methods for controlling the quantum dynamics beyond the adiabatic criteria, where counter-diabatic (CD) driving provides a promising means to speed up quantum many-body systems. In this chapter, we show the applicability of CD driving to enhance the digitized adiabatic quantum computing paradigm in terms of fidelity and total simulation time. We study the state evolution of an Ising spin chain using the digitized version of the standard CD driving and its variants derived from the variational approach. We apply this technique in the preparation of Bell and Greenberger-Horne-Zeilinger states with high fidelity using a very shallow quantum circuit. We implement this proposal in the IBM quantum computer, proving its usefulness for the speed up of adiabatic quantum computing in noisy intermediate-scale quantum devices.

3.1 Introduction

Quantum computing is known to have significant advantages in solving certain computational tasks, such as simulating quantum systems [3, 5–8], machine learning [15–18], solving optimization problems [19–21], cryptography [22, 23], and several others. Recent advancements in quantum technologies have already shown that quantum computers can outperform currently existing classical computers [24].

Quantum adiabatic algorithms (QAA) [25–28] are one of the leading candidates for solving optimization problems [29–31]. In adiabatic quantum computation (AdQC), we start with a simple Hamiltonian whose ground state can be easily prepared and evolve the system adiabatically to the ground state of the final Hamiltonian, which encodes the solution of the optimization problem. This is embodied by the well-known method of quantum annealing [32]. Quantum annealers, such as the D-Wave machine [33], provide the test-bed for adiabatic algorithms [34]. Despite its applications, quantum annealers have certain limitations, such as difficulty in implementing non-stoquastic Hamiltonian, limited qubit connectivity and noise. Although AdQC is equivalent to the standard circuit model [35], the advantage of digital quantum computation (DQC) over quantum annealers is that the circuit model offers more flexibility to construct arbitrary interactions, and it is consistent with error correction. The recent work by R. Barends et al. [36] combines the advantage of

AdQC and the circuit model, termed as digitized adiabatic quantum computation (DAdQC), has been presented and implemented on a superconducting system.

QAs are generally governed by the quantum adiabatic theorem that restricts a system to evolve along a specific eigenstate, i.e., from the ground state of an initial Hamiltonian \hat{H}_i to the ground state of a final Hamiltonian \hat{H}_f , while the evolution is considerably slow. The computation time for the QAA depends on the minimum energy gap between the successive eigenstates during the evolution. When the system size increases, this poses a significant disadvantage for the implementation of QAA as the energy gap decreases with increasing system size, which ends up in transition between various instantaneous eigenstates. One has to increase the adiabatic evolution time to circumvent such an issue. However, in practice, evolution time for QAA is significantly larger than the coherence time of the current quantum computers, leading to the loss of fidelity of the evolution.

The techniques of “Shortcut to adiabaticity” (STA) [37, 38] have been developed during the past decade and proved to be extremely useful for accelerating quantum adiabatic processes in general [39]. Various techniques like counter diabatic (CD) driving (equivalently transitionless quantum algorithm) [40–42], invariant based inverse engineering [43, 44], fast-forward approach [45, 46] are rigorously explored and implemented in several studies [47–49]. Among these works, studies related to quantum spin systems such as Ising and Heisenberg spin models are of particular interest due to their relevance to the applicability and ease of implementation in the development of modern-day quantum algorithms [50]. In particular, the CD driving has been useful for studying fast dynamics [51–55], preparation of entangled states [56–59], quantum annealing [60–62] and, others.

In this chapter, we explore the STA techniques to enhance the performance of the DAdQC using Ising spin systems. Starting from a single spin, we extend our study to many spins with nearest-neighbor interactions using the CD driving. We find out that the CD interactions in the QAA improve the fidelity remarkably compared to the previous studies. Due to the difficulty in the implementation of the exact CD term for a many-body system, we opt to find local CD terms that can drive smaller systems precisely and able to achieve the target state in very few time steps. By considering approximate CD terms using the nested commutator, we study the non-integrable Ising-model and extend this idea for the preparation of Bell state and GHZ state in larger systems.

3.2 Single spin system

We begin our heuristic discussions with a single spin in the presence of time-dependent external magnetic-field $\mathbf{h}(t)$, represented by a two-level Hamiltonian, given by

$$\hat{H}_0^{(1)}(t) = \mathbf{h}(t) \cdot \hat{\boldsymbol{\sigma}}, \quad (3.1)$$

where $\hat{\boldsymbol{\sigma}}$ represents the Pauli matrices, and the superscript 1 represents the number of spin. Following the general method for AdQC, also that of quantum annealing, we express this Hamiltonian as a combination of two time-independent parts,

$$\hat{H}_0^{(1)}(t) = (1 - \lambda(t))\hat{H}_i + \lambda(t)\hat{H}_f, \quad (3.2)$$

\hat{H}_i and \hat{H}_f are time-independent with ground states $|\psi_i\rangle$ and $|\psi_f\rangle$, respectively. The time dependence of the system is introduced through the parameter $\lambda(t)$. The initial Hamiltonian is chosen as $\hat{H}_i = h_x\sigma_x$, and the final Hamiltonian as $\hat{H}_f = h_z\sigma_z$, where h_x and h_z being the magnetic field strength along respective directions. Such a choice leads to express the magnetic field effectively as $\mathbf{h}(t) = [h_x(1 - \lambda(t)) \quad 0 \quad h_z\lambda(t)]^T$. AdQC, in its rudimentary approach, allows $\lambda(t)$ to be any function that varies from 0 to 1 and drives the system from $|\psi_i\rangle$ to $|\psi_f\rangle$. Although, the most general way to choose it as a linear function, here to begin with, it is considered as $\lambda(t) = \sin^2(\omega t)$, where $\omega = \pi/2T$ with T being the total evolution time. Although $\hat{H}_0(t)$ is extremely elementary and can easily be implemented in the circuit model [63], there are hints that the evolution can be improved significantly using the STA [52]. In this case, one should be tempted to find out the CD term, which is somewhat straightforward to calculate using the methods in reference [42],

$$\hat{H}_{cd}^1(t) = \frac{1}{2|\mathbf{h}(t)|^2} (\mathbf{h}(t) \times \dot{\mathbf{h}}(t)) \cdot \hat{\boldsymbol{\sigma}}. \quad (3.3)$$

The latter yields the explicit form as follows,

$$\hat{H}_{cd}^{(1)}(t) = F^{(1)}(t)\sigma_y = \frac{-h_x h_z \partial_t(1 - \lambda(t))}{2[h_x^2(1 - \lambda(t))^2 + h_z^2\lambda^2(t)]} \sigma_y. \quad (3.4)$$

Therefore, the total Hamiltonian assisted with CD term becomes

$$\hat{H}^{(1)}(t) = (1 - \lambda(t))h_x\sigma_x + \lambda(t)h_z\sigma_z + F^{(1)}(t)\sigma_y. \quad (3.5)$$

Note that the introduction of the CD term should not affect the initial and final states, since $F^1(t)$ should always satisfy the boundary conditions, $F^{(1)}(t=0) = F^{(1)}(t=T) = 0$. Also,

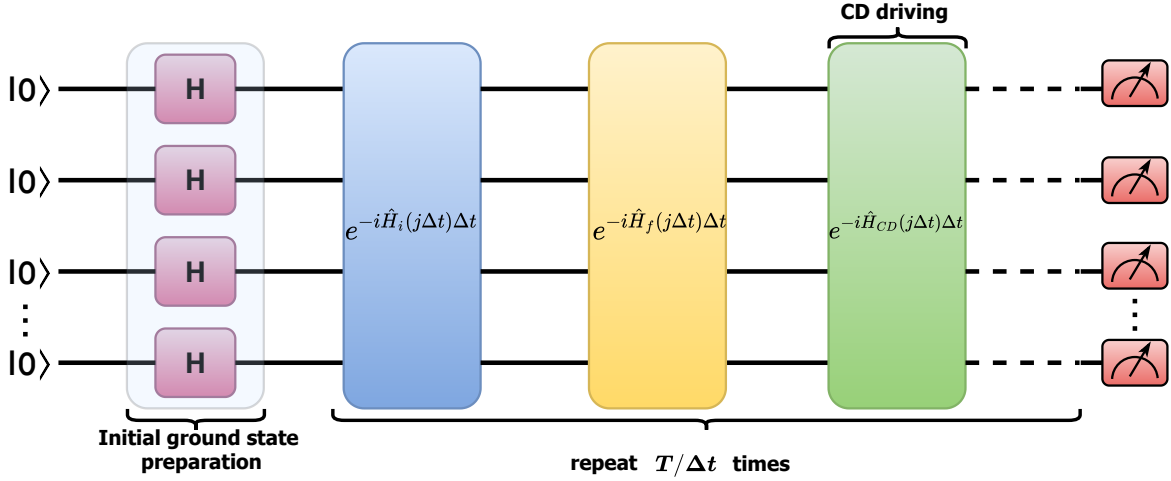


图 3.1 Circuit implementation for the digitized adiabatic evolution using CD driving, where T is the total evolution time, and Δt is the step size. The circuit is repeated $n = T/\Delta t$ times, where the Hamiltonian's satisfy the condition $\hat{H}_f(0) = \hat{H}_{CD}(0) = \hat{H}_{CD}(T) = \hat{H}_i(T) = 0$.

the STA methods generally follow the inverse engineering approach of quantum control, i.e., designing the interaction for achieving the desired eigenstates. Therefore the notion of the eigenstate, although not that essential in traditional AdQC, turns out to be extremely important in the present case. Here, the initial state of \hat{H}_i is chosen in the computational basis, i.e., $\{|0\rangle, |1\rangle\}$, as $|\psi_i\rangle = |+\rangle$ and the final state is, $|\psi_f\rangle = |1\rangle$. It should be noted that $|+\rangle = (|0\rangle + |1\rangle)/\sqrt{2}$ and $|1\rangle$ are the natural ground states of \hat{H}_i and \hat{H}_f , respectively, but these choices are not restricted to the ground states only. However, such a choice restrains the qubit in the ground state, minimizing the effect of the decoherence. To implement the evolution using one qubit, we used first-order Trotter-Suzuki formula. The time evolution is digitized with n number of small time steps Δt (see Eq (3.33)). Ideally, the discretized version of AdQC approaches the actual adiabatic evolution for $n = T/\Delta t \rightarrow \infty$, ($\Delta t \rightarrow 0$). Although, in real situations, n is finite and it has to be a relatively small number since each trotter step is being implemented by three rotation gates (see Appendix 3.7). The error associated with the first-order trotterization is $\mathcal{O}(\Delta t^2)$ [64].

To perform the simulation, we used publicly available five-qubit superconducting quantum computer of IBM Quantum Experience [65]. For the single spin experiment we use qubit Q_0 on *ibmq_essex*. Since the single qubit gate error of the device is of the order of 10^{-4} , the initial state is prepared with very high fidelity. Also a significant error in this simulation comes from the readout error ($\sim 4\%$), for that we used the error mitigation technique using matrix inversion method described in Appendix 3.9.

In the simulation, time evolution takes place between $|+\rangle$ to $|1\rangle$ and measured in the computational basis, which restricts the variation of the probability between 0.5 to 1, see

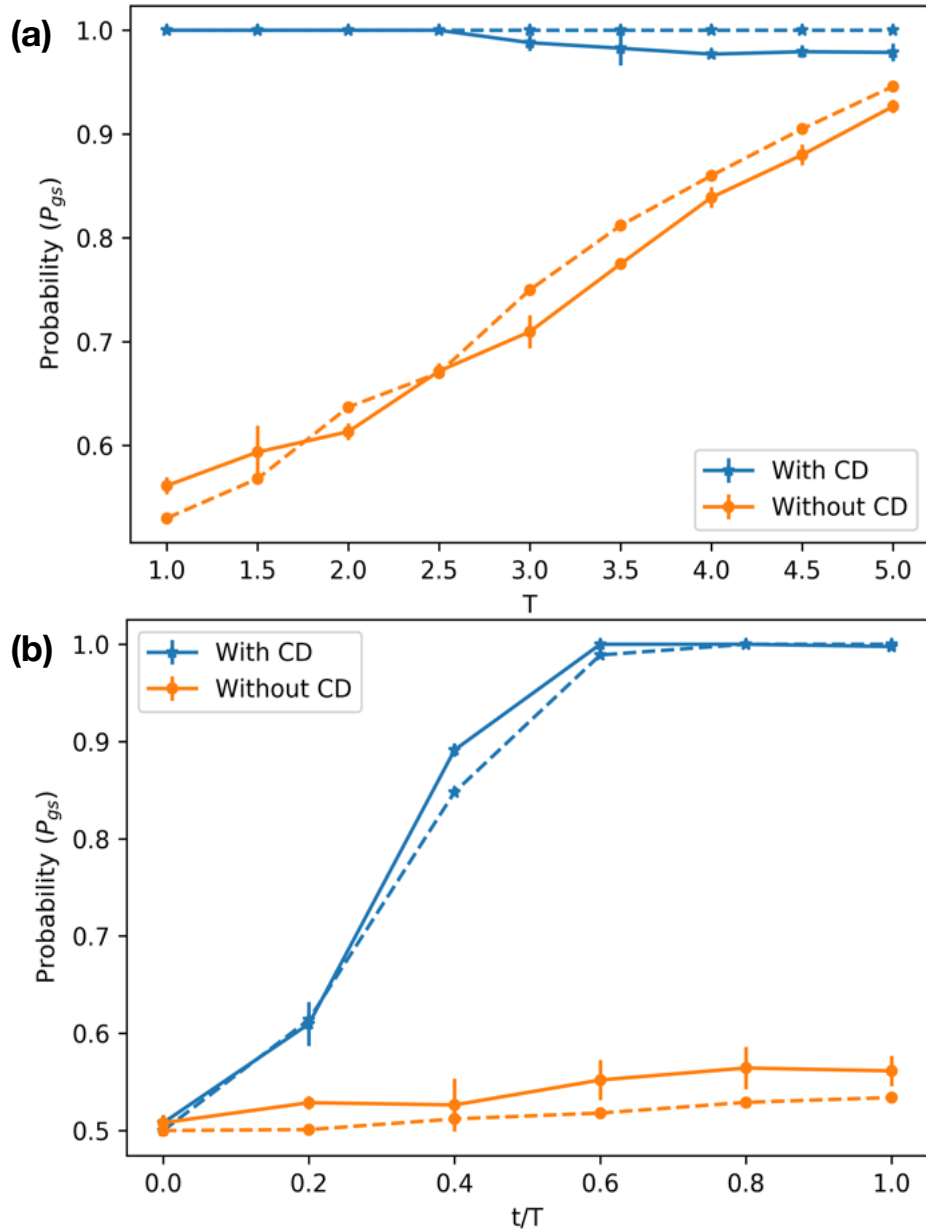


图 3.2 (a) The final ground state probability P_{gs} versus the simulation time for a single qubit using CD driving on `ibmq_essex` quantum computer (solid blue) compared to the ideal simulator (dashed blue). The simulation without CD driving in real device (solid brown) and ideal simulator (dotted brown). (b) Time evolution using DAdQC and STA methods for $T = 1$. Parameters are following: $\Delta t = 0.2$, $h_x = -1$, $h_z = 1$, and number of shots $N_{shots} = 1024$.

Fig. 3.2. Since the trotter error is of the order $\mathcal{O}(\Delta t^2)$, we choose, $\Delta t = 0.2$, and $T = 1$ for the comparison of the evolution using DAdQC and STA assisted DAdQC. To study the probability of final ground state $P_{gs} = |\langle \psi(t) | 1 | \psi(t) | 1 \rangle|^2$, where $|\psi(t)\rangle$ denotes the time evolved state of $\hat{H}_0(t)$, measurement is performed at each progressing time step. Fig. 3.2(b) shows a single evolution of the qubit governed by both Eq. (3.2) and Eq. (3.5), using both simulation and experiment on a real quantum device. With the application of CD driving $F^{(1)}(t)$, the probability of getting the state $|1\rangle$ from the experiment comes out to be around 0.997. Whereas, when the CD driving is zero, i.e., for the adiabatic evolution, the final state probability is around 0.561 only. However, if the evolution is extended for a larger T , we could obtain a much higher probability, even without $F^{(1)}(t)$, a signature of the typical adiabatic process. This is evident in Fig. 3.2(a), where the fidelity of the evolution (in the computational basis) for different T is shown. Even when $T = 1$ ($\Delta t = 0.02$) using the STA method, the final ground state is reached with nearly unit fidelity. We observe that fidelity for the STA method for large T maintains its value at around 0.978. However, for the adiabatic case, fidelity gradually increases with increasing simulation time and the average fidelity will be around 0.927 for $T = 5$. Notice that in Fig. 3.2(a), the experimental values differ slightly from the exact simulation values, and the difference is slightly larger for the STA assisted case. As T increases, the circuit depth becomes larger, which results in ramping up the gate errors, affecting STA more than the adiabatic case as it requires more gates for implementation.

3.3 Local counterdiabatic driving

The results in Sec. 3.2 establishes the fact that STA assisted DAdQC shows significant improvement over the DAdQC, at least when a single qubit is considered. However, such implementation becomes far more interesting when multiple qubits are considered. The simplest choice is a system of N interacting spins in one-dimensional lattice, coupled by a time-dependent exchange interaction $J(t)$ with a rotating magnetic field acting upon it. Here we consider $J(t)$ to constitute $\sigma_z\sigma_z$ type interaction with J_0 being the coupling amplitude. The spins are initially aligned along the transverse magnetic field, h_x , while an Ising Hamiltonian represents the system's final state. The total Hamiltonian is expressed as

$$\hat{H}_0^{(N)}(t) = (1 - \lambda(t)) \sum_{j=1}^N h_x \sigma_x^j + \lambda(t) \sum_{j=1}^N (h_z^j \sigma_z^j + J_0 \sigma_z^j \sigma_z^{j+1}). \quad (3.6)$$

The scheduling $\lambda(t)$ is chosen similarly, as in Eq. (3.2). The traditional approaches to finding the CD driving are predominantly limited to two and three-level systems and become more complex for higher dimensional many-body systems. However, for interacting many spin systems, as in the preceding section, a local CD driving could be more useful. Instead of acting on the whole system, a set of approximated interactions could be designed to control the spins individually. Such type of local CD driving is more general and can be extended to a larger number of spins.

3.3.1 Local CD from Berry's algorithm

To realize such CD driving, it is intuitive to approximate the system to a non-interacting one. Using mean-field approximation, this can be achieved effectively for an infinite-range Ising model [66]. However, this is problematic for DAdQC, as it requires self-consistent feedback $\langle \sigma_j | \sigma_j \rangle$ after every step. Instead, we consider a more direct approach. Since, at $t = 0$, the spins have no mutual interaction and are dictated by the transverse magnetic field, it can be assumed that, during the evolution, the magnitude of h_z^j and J_0 grows gradually from zero to some maximum value while the system evolves gradually from \hat{H}_i to \hat{H}_f . Therefore, we approximate that those spins are governed by a local effective magnetic field, given by $h(t) = [h_x(1 - \lambda(t)) \quad 0 \quad \tilde{h}_z^j \lambda(t)]^T$, where $\tilde{h}_z^j = h_z^j + J_0$. Subsequently, the local CD driving is calculated and summed over for each spin using Eq. (3.3),

$$\hat{H}_{CD}^{(N)}(t) = \sum_{j=1}^N F_j^{(N)}(t) \sigma_y^j = \sum_{j=1}^N \frac{-h_x \tilde{h}_z^j \partial_t (1 - \lambda(t))}{2 \left[h_x^2 (1 - \lambda(t))^2 + (\tilde{h}_z^j)^2 \lambda^2(t) \right]} \sigma_y^j. \quad (3.7)$$

Therefore, the modified Hamiltonian that governs the evolution can be expressed as

$$\hat{H}^{(N)}(t) = \hat{H}_0^{(N)}(t) + \sum_{j=1}^N F_j^{(N)}(t) \sigma_y^j. \quad (3.8)$$

As an example, we consider interacting two-qubit system, where the time evolution for $\hat{H}^{(2)}(t)$ can be easily implemented by two-qubit entangling gates and single-qubit rotation gates. The general circuit for implementing the evolution using CD driving is shown in Fig. 3.1. The initial and the target states chosen for the evolution are $|++\rangle$ and $|11\rangle$, respectively, which is inferred directly from the following parameters: $h_0 = -1$, $h_1 = h_2 = 1$ and $J_0 = -0.1$. The time evolution for STA-assisted DAdQC and DAdQC for two qubits are shown in Fig. 3.3. Again, like the single qubit case, one can achieve a high fidelity for the target state preparation. The result obtained from the ideal digital simulator, in Fig. 3.3(a),

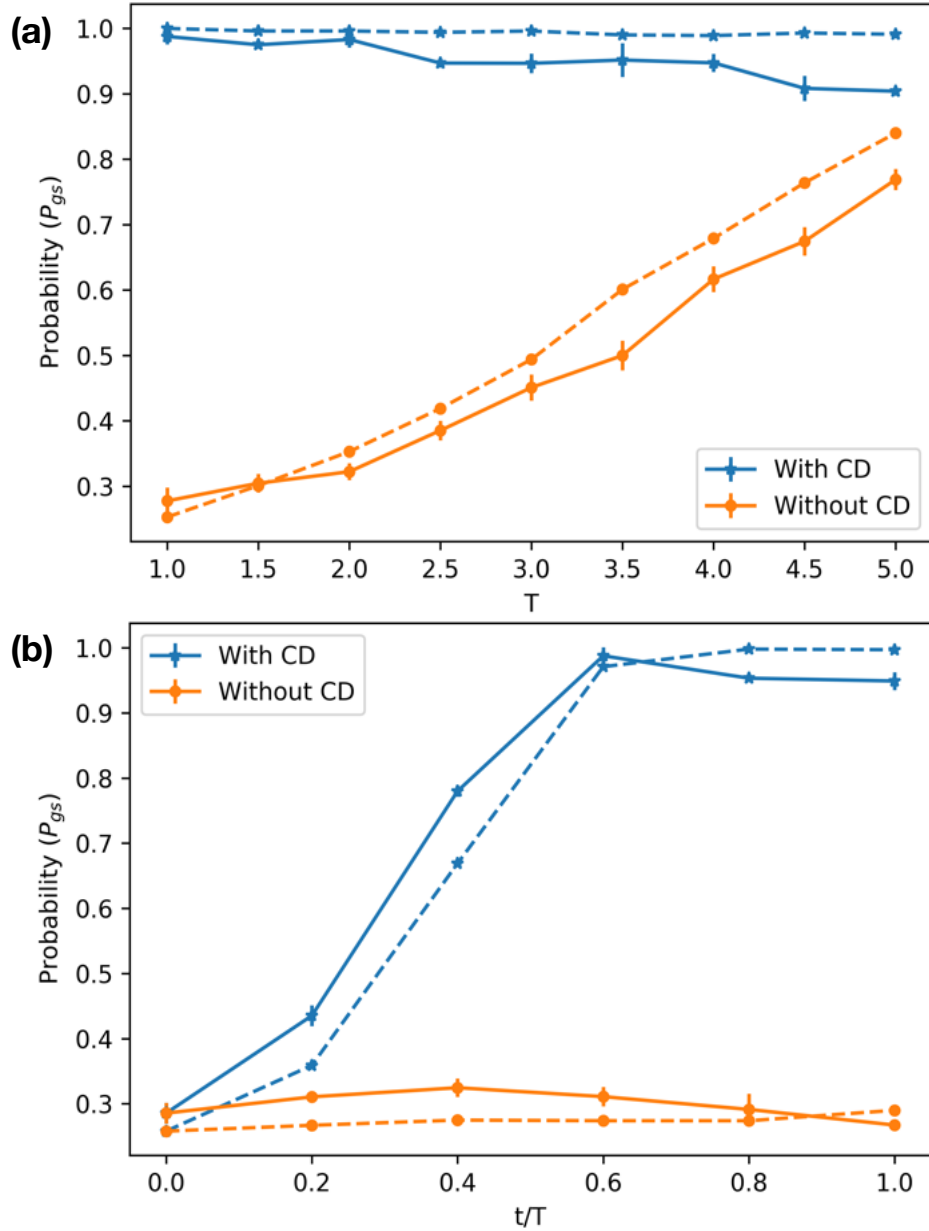


图 3.3 (a) The final ground state probability P_{gs} versus the simulation time for the two interacting spin system ($\Delta t = 0.5$). The red solid curve represents the time evolution using STA method, the solid blue curve represents the DAdQC on `ibmq_london` 5-qubit quantum processor. As the evolution time increases, the gate error starts to dominate, which is clearly inferred from the figure. (b) Implementation of the time evolution for two spin system without CD term (solid blue) and including CD term (solid red). Parameters are following: simulation time $T = 1$, $\Delta t = 0.2$, $h_x = -1$, $h_z^1 = h_z^2 = 1$, $J_0 = -0.1$, and $N_{shots} = 1024$. Both the curves are showing the expected profile.

shows that, when the additional term $\hat{F}_j^{(2)}(t)$ is considered, the target state can be achieved with almost unit fidelity. Furthermore, when a single evolution is considered, as depicted in Fig. 3.3(b), the target state can be achieved substantially faster than adiabatic evolution. However, when implemented in the real experiment, fidelity around 0.93 is achieved with the application of the CD term, where the fidelity in the computational basis is calculated as $|\langle \psi_i(n\Delta t) | \psi_f | \psi_i(n\Delta t) | \psi_f \rangle|^2$. The application of the CD term is more suitable when the evolution time T is small. In principle, the fidelity should remain the same even if we increase the number of time steps. Nevertheless, due to limited coherence time and the increasing number of gates required to implement the CD term, fidelity gradually decreases as depicted in Fig. 3.3(a).

3.3.2 Local CD from variational approach

A recently proposed method by Sels and Polkovnikov [13], based on the variational approach, also provides an alternative to calculate the approximate CD Hamiltonian with only local terms. The method for this calculation is to choose an appropriate adiabatic gauge potential \hat{A}_λ^* [67] and minimizing the action $S = \text{Tr} [\hat{G}_\lambda^2]$, where the operator \hat{G}_λ is defined by $\hat{G}_\lambda = \partial_\lambda \hat{H} + i[\hat{A}_\lambda^*, \hat{H}]$ (see Appendix 3.8). The CD driving using this method is expressed as $\hat{H}_{CD}^{(N)} = \dot{\lambda} \hat{A}_\lambda^*$. Since the Hamiltonian contains only real values in the z -basis, the simplest ansatz is to choose $\hat{A}_\lambda^* = \sum_j \alpha_j(t) \sigma_y^j$, i.e., applying an additional magnetic field along the y -direction for each spin. By minimizing the action S with respect to α_j , the variational coefficient $\alpha_j(t)$ is analytically calculated, which takes the general form, for Eq. (3.6) [13],

$$\alpha_j(t) = \frac{1}{2} \frac{h_x h_z^j}{[h_x^2(1 - \lambda(t))^2 + (h_z^j + 2J_0)^2 \lambda^2(t)]}. \quad (3.9)$$

The expression for $\hat{H}_{CD}^{(N)} = \sum_j \dot{\lambda} \alpha_j(t) \sigma_y^j$ is similar to that of Eq. (3.7) except for a few modifications. In Fig. 3.4(a), the probabilities of obtaining the ground state, from both the ideal simulator and the experimentally implemented data from `ibmqx2` are shown for up to 5 qubits. Like the previous case, the final ground state $|11..1\rangle$ can be prepared using the additional $\hat{H}_{CD}^{(N)}$ with high fidelity. The ideal simulator data shows that the final probability, $|\langle \psi(T) | 11..1 | \psi(T) | 11..1 \rangle|^2$ reaches almost unity for $T = 1$ in five trotter steps, especially when $|J_0|$ is small. However, the implemented value differs from the simulator due to the device errors. It should be noted that, in the above discussion, the interaction strength J_0 is kept sufficiently small compared to the external magnetic field, $J_0 \ll h_z^j$. The

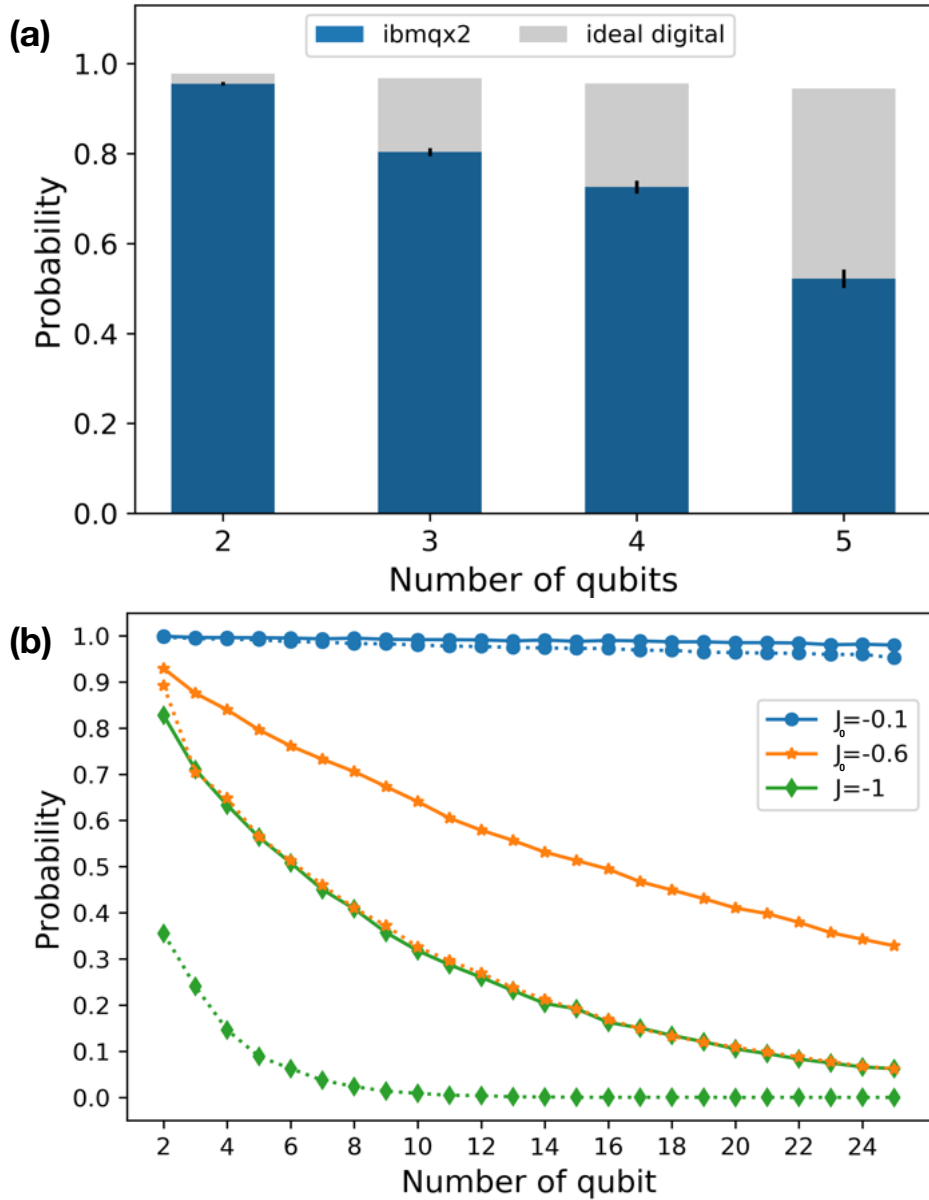


图 3.4 (a) For the non-integrable Ising model, the probability of obtaining the final ground state using local CD term calculated from variational method for up to 5 qubit system is depicted. The experiment is performed on 5 qubit `ibmqx2` processor. The experimental parameters are $J_0 = -0.1$, $h_x = h_z = 1$, $N_{shots} = 8192$. (b) The probability of obtaining the final ground state as a function of coupling strength using local CD driving for up to 25 qubits are shown. The solid line is for the local CD term from the variational approach, and the dotted line is for the local CD term from Berry formula, see Eq. (3.7). The parameters chosen are $h_x = -1$, $h_z^j = 1$, $dt = 0.1$, and $T = 1$. The simulation was performed on a `qasm_simulator`.

ground state of the final Hamiltonian is a ferromagnetic state, i.e., either $|00..0\rangle$ or $|11..1\rangle$, depending on the sign of h_z^j . In such scenario, the evolution assisted by the local CD terms in Eq. (3.7) and Eq. (3.9) produces the exact final ground state. Fig. 3.4(b) compares the probability of interacting multi-qubit system with ground state $|111\dots1\rangle$. For $J_0 \ll h_z^j$, the probability is around 98% in the ideal simulator for both the methods. When J_0 becomes higher, the probability using Eq. (3.4) decreases drastically and reduces to 35%, even for two qubits. Whereas, for the variational approach, the probability is significantly higher for large $|J_0|$ values. When the ground state is degenerate, the obtained result seems to differ from the actual ground state. For instance, when $J_0 = 2$, with the similar values of other parameters, the ground state becomes doubly degenerate, i.e., the states $|01\rangle$ and $|10\rangle$, the application of the CD term drives the system to one of the eigenstates. This comes out to be true for many spin systems also. Moreover, the calculation of the local CD term is based on the approximation that every spin is treated individually by considering an effective magnetic field acting upon each spin. The effects of the interaction J_0 are undermined while calculating the CD term. As a result, the CD term does not help the system evolve into the exact ground state when J_0 is comparable or stronger than that of the local magnetic field.

Subsequently, when $h_z^j = 0$, the final ground state becomes entangled, and one can deduce from Eq. (3.7) that for small J_0 , the CD term becomes small, i.e., $\hat{F}_j^{(N)}(t) \rightarrow 0$. In such cases, the final evolved state, in a short T , does not match the adiabatic one. For the variational approach, the CD term vanishes altogether and can not be applied using such form. Therefore, if we are to prepare a highly entangled state, the single qubit approximation for the CD term is not a good choice. This drawback occurs as CD driving is calculated using the σ_y terms, which refers to driving a single qubit with the external magnetic field only. In fact, the spin-spin interaction term decides the final state here and the driving for $\sigma_z\sigma_z$ coupling has to be incorporated. This enforces the fact that the direct approach from the first principle to find the local CD driving is not realistic and should contain other interactions such as $\sigma_y\sigma_z$ and $\sigma_z\sigma_x$ and others [60].

3.4 Approximate counterdiabatic protocol

Following the discussion in the preceding section, when complex many-body systems are considered, the calculation of the exact CD term becomes difficult. Also, the form of the CD term can be severely complicated with different non-local and many-body interaction terms. Besides, it becomes rather difficult to implement systems with such interactions

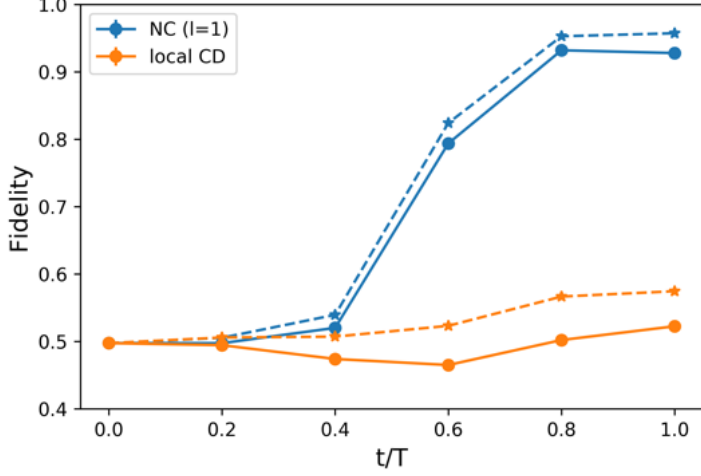


图 3.5 The fidelity of obtaining the final ground state $(|01\rangle + |10\rangle)/\sqrt{2}$ as a function of evolution time for local CD and NC ansatz ($l=1$) obtained from `ibmq_vigo`. The solid line represents the experimental result and the dashed line represents the result from ideal digital simulator. Parameters: $J_0 = 2$, $h_z = 0.6$, $T = 1$, $dt = 0.2$, and $N_{shots} = 8192$.

on current quantum computers. Although, the local terms, see Eq. (3.9), from variational approach gives an optimal solution, it is not that useful for preparing entangled states, especially when $h_z^{(j)} = 0$. The nature of the CD term from variational calculation depends on the choice of appropriate adiabatic gauge potential \hat{A}_λ^* . A recently proposed method gives a more general way to choose the gauge potential by using the nested commutator (NC) [14],

$$\hat{A}_\lambda^{(l)} = i \sum_{k=1}^l \alpha_k(t) \underbrace{[\hat{H}, [\hat{H}, \dots, [\hat{H}}_{2k-1}, \partial_\lambda \hat{H}]]], \quad (3.10)$$

where l determines the order of the expansion. Depending on the required accuracy, we can keep the number of variational coefficients small. If we consider only the first-order term, our ansatz will be $\hat{A}_\lambda^{(1)} = i\alpha_1(t)[\hat{H}, \partial_\lambda \hat{H}]$, and the effective Hamiltonian can be written as

$$\hat{H}_{eff}(t) = \hat{H}(\lambda) + \dot{\lambda} \hat{A}_\lambda^{(1)}, \quad (3.11)$$

where $\dot{\lambda} \hat{A}_\lambda^{(1)}$ is the relevant CD term. First of all, we apply this technique to non-integrable Ising spin model, described by the Hamiltonian in Eq. (3.6). Considering the two-qubit system ($N = 2$), we approximate CD term using first-order nested commutator,

$$\hat{H}_{CD}^{(2)} = 2\alpha_1(t)h_x [\sigma_y^1(\sigma_y^1 + \sigma_y^2) + J_0(\sigma_y^1\sigma_z^2 + \sigma_z^1\sigma_y^2)], \quad (3.12)$$

with

$$\alpha_1(t) = \frac{1}{4} \frac{h_z^2 + J_0^2}{\lambda^2(h_z^4 J_0^4 + 3h_z^2 J_0^2) + (1 - \lambda)^2 h_x^2(h_z^2 + 4J_0^2)}. \quad (3.13)$$

The second-order term ($l = 2$) can give the exact gauge potential [14]. However, for the experimental demonstration, we only consider the first-order term and implement the time evolution on a quantum processor. The circuit implementation for the CD driving is shown in Appendix 3.7. Using this method, the final ground state is achieved with very few trotter steps compared to digitized adiabatic evolution, which drastically reduces the number of gates required as well as the total simulation time. In Fig. 3.5, we depicted the fidelity as a function of evolution time using first-order nested commutator method when the final ground state is degenerate and compared the result with the local CD term from Eq. (3.9). The fidelity is much better compared to the local CD case for degenerate state and thereby it justifies our argument in the preceding section.

Secondly, we shall check the reliability and validity as well as the extent of the variational approach in the many body regime. To this aim, we apply this technique to prepare the GHZ state in Ising spin chain with many spins, described by the Hamiltonian,

$$\hat{H}(\lambda(t)) = (1 - \lambda(t)) \sum_j^N h_x \sigma_x^j + \lambda(t) J_0 \sum_j^N \sigma_z^j \sigma_z^{j+1}, \quad (3.14)$$

with N being the number of spins. Here, the periodic boundary condition $\sigma^{N+1} = \sigma^0$ is assumed. Following the procedure described in Sec. 3.4, by considering only the first-order expansion, we calculate the approximate gauge potential as

$$\hat{A}_\lambda^{(1)} = 2\alpha_1^N(t) J_0 h_x \sum_j^N (\sigma_z^j \sigma_y^{j+1} + \sigma_y^j \sigma_z^{j+1}). \quad (3.15)$$

The variational coefficient, $\alpha_1^N(t)$ is calculated by minimizing the action S . For the experimental demonstration on a quantum processor, we choose a small system with two and three qubits to prepare a Bell state and GHZ state. For the bell state, $(|00\rangle + |11\rangle)/\sqrt{2}$, governed by the Hamiltonian in Eq. (3.14), the variational coefficient is calculated as $\alpha_1(t) = -J_0 h_x / [2(J_0^2 \lambda^2 + 4(1 - \lambda)^2 h_x^2)]$. Here we have noticed that, for two spins, the first order commutator is proportional to the higher-order terms. The resulting CD driving from the approximate gauge is exact and produces unit fidelity in ideal situations [14]. The same procedure can be followed in case of more qubits to prepare a GHZ state $|GHZ\rangle = (|0\rangle^{\otimes N} + |1\rangle^{\otimes N})/\sqrt{2}$ starting from the N qubit ground

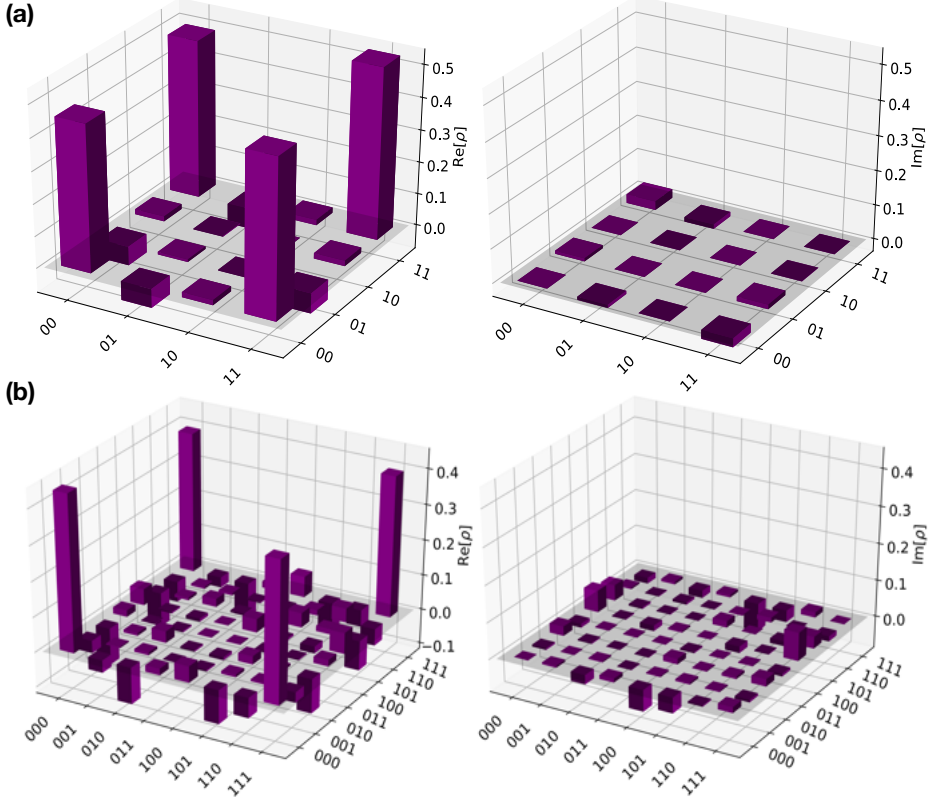


图 3.6 The density matrix representation of the final ground state obtained from state tomography. (a) Bell-state from `ibmq_ourense` and (b) GHZ-state from `ibmq_vigo`.

state $|+\rangle^{\otimes N}$. Specifically, the variational coefficient for a three-qubit case is given by $\alpha_1(t) = -J_0 h_x / [5J_0^2 \lambda^2 + 8(1 - \lambda)^2 h_x^2]$.

The simulation was performed on a five qubit quantum processor `ibmq_ourense`. A similar trotterization, as in Eq. (3.35), is used to study the evolution with digitized time step $dt = 0.01$. Using the CD driving, with only three trotter steps, the desired bell state is obtained with experimental fidelity 0.984. The ideal digital simulation gives almost unit fidelity ($F = 0.999$). The fidelity is calculated as, $F(\rho_1, \rho_2) = \langle \psi_1 | \rho_2 | \psi_1 \rangle \langle \psi_1 | \rho_2 | \psi_1 \rangle$, where the exact bell state is represented by, $\rho_1 = |\psi_1\rangle\langle\psi_1|$. Similarly, for the three-qubit system, the ideal digital evolution gives the fidelity 0.935 with the exact GHZ state, and the corresponding experimental fidelity is 0.819. The density matrix representation of the final state (ρ_2) is obtained by performing quantum state tomography for both Bell and GHZ states and is depicted in Fig. 3.6. Whereas, Fig. 3.7, shows how the fidelity varies with increasing system size on a ideal digital simulator with six trotter steps. The first-order approximation of the CD term provides high fidelity for small system size. As we increase N , the probability of obtaining the final ground state decreases gradually. This can be overcome by considering the higher-order commutators while calculating the approximate

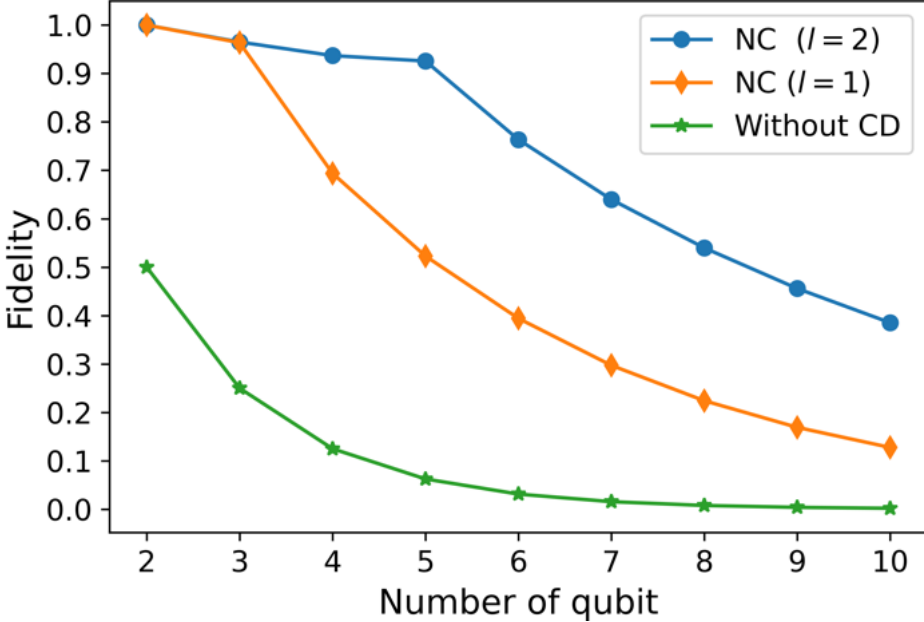


图 3.7 Fidelity to prepare the GHZ state as a function of system size on an ideal digital simulator with CD term from nested commutator (NC) ansatz with different orders and the naive approach without CD term. Where the parameters are $T = 0.006$ and $\Delta t = 0.001$.

CD term. As the variational method tends to provide exact CD driving for larger l -values, which in principle, can give a better fidelity in many-body systems.

3.5 Preparation of topological order

We consider the problem of adiabatic preparation of topologically ordered states, especially the toric code model. It was shown that, the time required for preparing the state scales as $\mathcal{O}(\sqrt{n})$, where $n \sim L^2$ is the number of spins. The Hamiltonian for the toric code model is given by

$$H_{\text{TC}} = - \sum_s A_s - \sum_p B_p, \quad (3.16)$$

where A_s and B_p are the star and plaquette operators, respectively,

$$A_s = \prod_{j \in \text{star}(s)} \sigma_j^x, \quad B_p = \prod_{j \in \text{plaq}(p)} \sigma_j^z. \quad (3.17)$$

Here, $[A_s, B_p] = 0$, so that the system is exactly solvable. For preparing the ground state of the toric code model, we follow the adiabatic theorem, by starting with a trivial ground state corresponding to the initial Hamiltonian H_i and evolve the state adiabatically by slowly turning on the interactions corresponding to the final Hamiltonian H_{TC} . The total

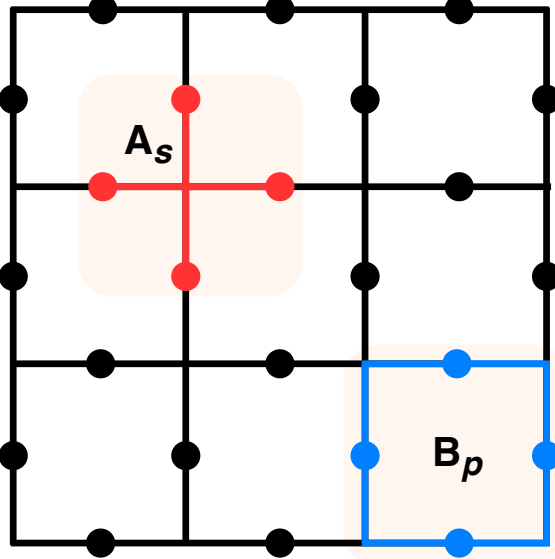


图 3.8 Visualization of the toric code Hamiltonian on a 2D lattice, where the shaded circles represents the qubits. $A_s = \sigma_i^x \sigma_j^x \sigma_k^x \sigma_l^x$, and $B_p = \sigma_i^z \sigma_j^z \sigma_k^z \sigma_l^z$ represents the star and the plaquette operators, respectively.

Hamiltonian corresponding to the adiabatic evolution is given by

$$H_{\text{ad}}(t) = (1 - \lambda(t)) \sum_j -\sigma_j^z - \lambda(t) \sum_s A_s - \lambda(t) \sum_p B_p, \quad (3.18)$$

where the scheduling parameter $\lambda = \sin^2 \left[\frac{\pi}{2} \sin^2 \left(\frac{\pi t}{2T} \right) \right]$, and T is the total evolution time such that, $\dot{\lambda}(t=0) = \dot{\lambda}(t=T) = 0$. We have chosen the initial Hamiltonian as $H_i = - \sum_j \sigma_j^z$, and the corresponding ground state is $|0\rangle^{\otimes n}$. The time required for the evolution is decided by the minimum energy gap between the ground state and the first excited state during the evolution. In practice, this time will be much larger than the coherence time of a current quantum computers, which results in the accumulation of decoherence errors. Here, we apply CD driving techniques to prepare the ground state of the toric code model, which has its importance in topological quantum computation and is also useful for quantum error correction.

We begin by considering the toric code model on a 2×2 lattice, given by the Hamiltonian

$$H_{\text{TC}} = - \sum_s \sigma_1^x \sigma_2^x \sigma_3^x \sigma_4^x - \sum_p \sigma_1^z \sigma_2^z \sigma_3^z \sigma_4^z. \quad (3.19)$$

The ground state of this Hamiltonian is four fold degenerate, given by

$$\begin{aligned} |\psi_{g,1}\rangle &= \frac{1}{\sqrt{2}}(|0000\rangle + |1111\rangle), & |\psi_{g,2}\rangle &= \frac{1}{\sqrt{2}}(|0011\rangle + |1100\rangle), \\ |\psi_{g,3}\rangle &= \frac{1}{\sqrt{2}}(|1010\rangle + |0101\rangle), & |\psi_{g,4}\rangle &= \frac{1}{\sqrt{2}}(|1001\rangle + |0110\rangle) \end{aligned} . \quad (3.20)$$

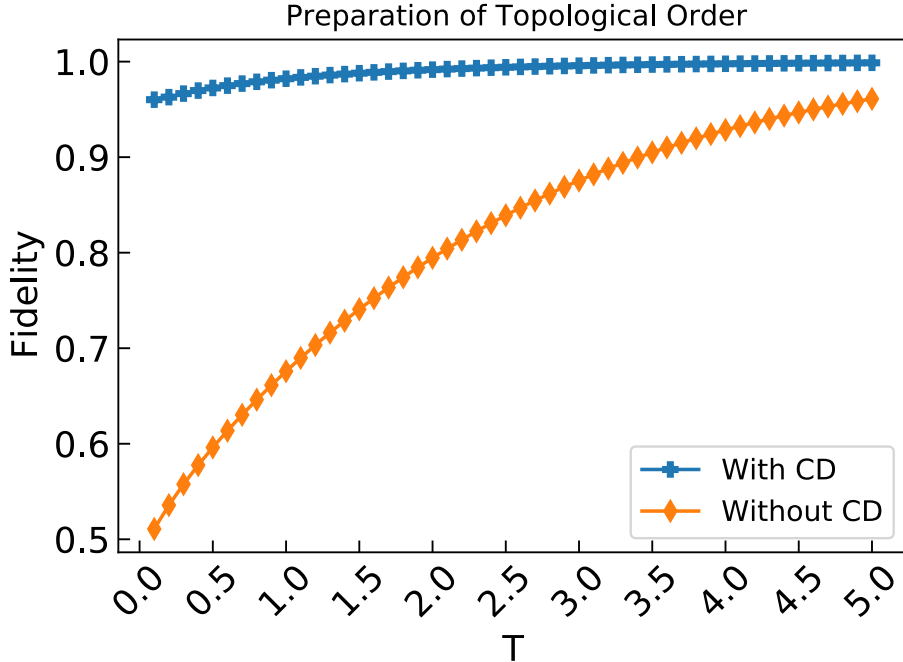


图 3.9 Fidelity as a function of evolution time for the ground state preparation of toric code model on a 2×2 square lattice. We compared the fidelity by including the CD term and without the CD term. For a short time, we can see a huge improvement in the fidelity with approximate CD driving obtained from first-order ($l=1$) NC ansatz.

In order to prepare this ground state, we follow the adiabatic evolution described in Eq. (3.18). To obtain the CD term corresponding this Hamiltonian, we consider the nested commutator (NC) method (3.10), which gives a general approach for obtaining the approximate CD term. The NC ansatz takes the form,

$$A_\lambda^{(l)} = i \sum_{k=1}^l \alpha_k \underbrace{[H_{ad}, [H_{ad}, \dots [H_{ad},]}_{2k-1} [\partial_\lambda H_{ad}]], \quad (3.21)$$

where A_λ is known as adiabatic gauge potential, the corresponding CD term is given by $H_{CD} = \dot{\lambda} A_\lambda$. By considering the first order approximation, we obtain

$$\begin{aligned} A_\lambda^{(1)} = & -2\alpha_1(t) (\sigma_1^y \sigma_2^x \sigma_3^x \sigma_4^x + \sigma_1^x \sigma_2^y \sigma_3^x \sigma_4^x \\ & + \sigma_1^x \sigma_2^x \sigma_3^y \sigma_4^x + \sigma_1^x \sigma_2^x \sigma_3^x \sigma_4^y). \end{aligned} \quad (3.22)$$

The CD coefficient $\alpha_1(t)$ is calculated by minimising the action $S = \text{Tr}[G_\lambda^2]$, where $G_\lambda = \partial_\lambda H + i[A_\lambda^1, H]$,

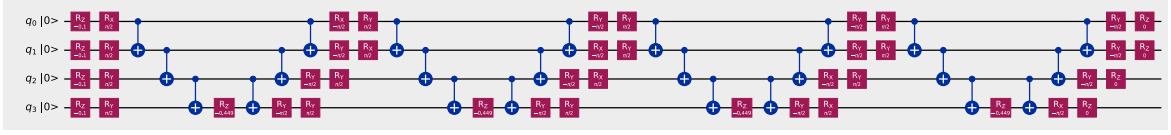


图 3.10 Quantum circuit for the preparation of the ground state of toric code model. Two trotter steps are shown. The time chosen for the evolution is very small ($T = 0.02$), hence only the CD terms are significant, and the interactions corresponding to the Hamiltonian H_{TC} can be neglected.

$$\alpha_1(t) = -\frac{1}{40 - 80\lambda(t) + 44\lambda(t)^2}. \quad (3.23)$$

The total Hamiltonian by including the CD term is $H(t) = H_{ad}(t) + \dot{\lambda}(t)A_\lambda^1$. For preparing the ground state of toric code model using CD driving, we consider two trotter steps of size $\delta = 0.01$, and the total evolution time $T = 0.02$. Since, for the fast evolution, the CD term is the dominant term, we can neglect the term H_{TC} . Starting with the initial ground state $|0\rangle^{\otimes n}$, by time evolving the system we obtain the final state $|\psi_{g,1}\rangle$, which is one of the ground state among the four degenerate state in Eq. (3.20). The circuit corresponding to the digitized-adiabatic evolution for two trotter steps are shown in Fig. 3.10. In Fig. 3.11, the final ground state fidelity as a function of total evolution time obtained from the ideal quantum simulator is depicted, which shows that even for a very small evolution time, one can obtain the final ground state with high fidelity by adding the CD term. The cost of implementing the adiabatic algorithm can be quantified by

$$\text{cost} = T \max_{\lambda} \|H(\lambda)\|. \quad (3.24)$$

In the circuit model, the total evolution time T corresponds to the circuit depth and the total cost in Eq. (3.24) corresponds to the total gate counts.

3.6 Ground state of hydrogen molecule (H_2)

In the first quantization notation with Born-Oppenheimer approximation, the Hamiltonian of H_2 is given by

$$H \left(\vec{r}_1, \vec{r}_2 \mid \vec{R}_1, \vec{R}_2 \right) = \mathcal{E}_{\text{nuc}}(R) + \sum_{i=1,2} \frac{\vec{p}_i^2}{2m} - \sum_{i,j=1,2} \frac{e^2}{4\pi\varepsilon_0 |\vec{r}_i - \vec{R}_j|} + \frac{e^2}{4\pi\varepsilon_0 |\vec{r}_1 - \vec{r}_2|}, \quad (3.25)$$

where $\mathcal{E}_{\text{nuc}}(R)$ corresponds to the nuclear term (which is considered as a constant term under the Born-Oppenheimer approximation) and it depends on the inter nuclear distance

$R = |\vec{R}_1 - \vec{R}_2|$. The second term represents the kinetic energy of the electrons with momentum \vec{p}_i . The last two terms are for the potential energy corresponding to the Coulomb attraction and repulsion between nuclei-electrons and electron-electron, where \vec{r}_i and \vec{R}_i denotes the coordinates of electrons and nuclei, respectively. In the second quantized notation the above Hamiltonian can be written as

$$H = \mathcal{E}_{\text{nuc}} + \sum h_{ij} a_i^+ a_j + \sum h_{ijkl} a_i^+ a_j^+ a_k a_l, \quad (3.26)$$

where h_{ij} and h_{ijkl} denotes the one and two-electron integrals. And, the creation (a_i^+) and annihilation (a_i) operators follow the fermionic anti-commutation relations, i.e., $[a_i, a_j^+]_+ = \delta_{i,j}$ and $[a_i, a_j]_+ = 0$. To convert the fermionic operators to Pauli operators we follow the Bravyi-Kitaev transformation which result in a simplified two qubit Hamiltonian given by

$$H_p = k_0 + k\sigma_1^z + k\sigma_2^z + k_{12}\sigma_1^y\sigma_2^y, \quad (3.27)$$

where the parameters $\{k_0, k, k_{12}\}$ are function of inter-nuclear distance R . As an example we consider $R = 0.04 \text{ \AA}$, and the parameters are given by $\{k_0 = 10.08E_h, k = -1.055E_h, k_{12} = 0.1557E_h\}$, where $E_h \approx 27.2 \text{ eV}$. To find the ground state of Hamiltonian (3.27), we follow the digitized-counterdiabatic protocol. We choose the initial Hamiltonian as $H_i = -\sum_i^n h^x \sigma_i^x$. The corresponding CD term is calculated from the first order nested commutator, i.e., $H_{CD} = \dot{\lambda} A_\lambda^1$.

$$A_\lambda^1 = \alpha_1(t) [0.3114(\sigma_1^z\sigma_2^y) + \sigma_1^y\sigma_2^z + 2.11(\sigma_1^y + \sigma_2^y)], \quad \alpha_1(t) = -\frac{0.1124}{\lambda^2 - 0.9564\lambda + 0.4782}.$$

The digitized time evolution operator for the total Hamiltonian $H(t) = (1 - \lambda)H_i + \lambda H_p + (\lambda)A_\lambda$ is approximated using Trotter-Suzuki formula as similar to Eq. (7.10),

$$U_{\text{dig}}(0, T) = U_{\text{dig}}((M - 1)\Delta t, M\Delta t) \dots U_{\text{dig}}(\Delta t, 2\Delta t) U_{\text{dig}}(0, \Delta t) |++\rangle. \quad (3.28)$$

For one Trotter step, the unitary operator takes the form,

$$\hat{U}(0, \Delta t) \approx \prod_{j=1}^2 \{e^{-i\theta_x(\Delta t)\sigma_j^x\Delta t} e^{-i\theta_z(\Delta t)\sigma_j^z\Delta t} e^{-i\theta_{yy}(\Delta t)\sigma_j^y\sigma_{j+1}^y\Delta t} e^{-i\theta_y(\Delta t)\sigma_j^y} e^{-i\theta_{zy}(\Delta t)\sigma_j^z\sigma_{j+1}^y\Delta t} e^{-i\theta_{yz}(\Delta t)\sigma_j^y\sigma_{j+1}^z\Delta t}\}. \quad (3.29)$$

Here, the angles $\theta_x(\Delta t) = (\lambda(\Delta t) - 1)$, $\theta_z(\Delta t) = k\lambda(\Delta t)$, $\theta_{yy}(\Delta t) = k_{12}\lambda(\Delta t)$, $\theta_y(\Delta t) = 2k\dot{\lambda}(\Delta t)\alpha_1(\Delta t)$, $\theta_{zy}(\Delta t) = \theta_{yz}(\Delta t) = 2k_{12}\dot{\lambda}(\Delta t)\alpha_1(\Delta t)$. The

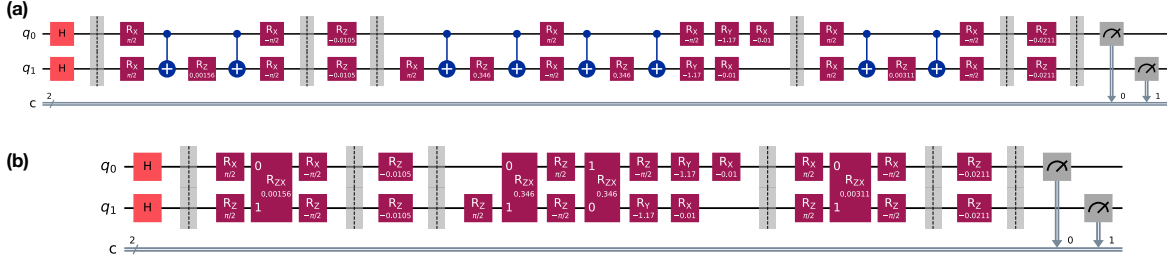


图 3.11 Circuit implementation for the digitized-counterdiabatic evolution with two Trotter steps.
(a) circuit decomposition using standard gate set (b) circuit decomposition using the native CR gate.

product of matrix exponentials in the above equation can be decomposed using single-qubit rotation gates and CNOT gates. We target a transmon-based quantum processor with fixed-frequency superconducting qubits for the experimental implementation of the problem. These devices support parametrized Cross-Resonance (CR) gates. Instead of using the standard quantum logic gates, we use the native CR gate for efficient hardware implementation. This CR gate implements a parametric 2-qubit $Z \otimes X$ interaction, and the corresponding unitary matrix is given by

$$R_{ZX}(\theta) = \exp\left(-i\frac{\theta}{2}Z \otimes X\right) = \begin{pmatrix} \cos\left(\frac{\theta}{2}\right) & -i\sin\left(\frac{\theta}{2}\right) & 0 & 0 \\ -i\sin\left(\frac{\theta}{2}\right) & \cos\left(\frac{\theta}{2}\right) & 0 & 0 \\ 0 & 0 & \cos\left(\frac{\theta}{2}\right) & i\sin\left(\frac{\theta}{2}\right) \\ 0 & 0 & i\sin\left(\frac{\theta}{2}\right) & \cos\left(\frac{\theta}{2}\right) \end{pmatrix}. \quad (3.30)$$

In Fig. 3.11 the quantum circuit implementing the digitized-counterdiabatic evolution for one trotter step is shown. In Fig. 3.11 (a) depicts the circuit decomposition using standard quantum logic gates, and Fig. 3.11 (b) shows the same using native CR gate. We notice that implementing each 2-local operator corresponding to the system's time evolution requires two CNOTs and rotation gates using standard decomposition. However, the same operation can be done with a single CR gate and rotation gates. We conclude that using the native gates reduces the total schedule duration by a factor of two and also helps to reduce the gate error.

3.7 Method of digitization

The circuit model can efficiently simulate the adiabatic quantum computing by using the digitization of continuous adiabatic evolution. The time-dependent Hamiltonians, considered here, can be represented as a sum of M k -local terms that act on at most k -qubits.

This can be represented as

$$\hat{H}(t) = \sum_{m=1}^M C_m(t) \hat{H}_m. \quad (3.31)$$

The continuous time evolution operator of $\hat{H}(t)$ is given by,

$$\hat{U}(0, T) = \mathcal{T} \exp \left[-i \int_0^T dt \hat{H}(t) \right], \quad (3.32)$$

where \mathcal{T} is the time ordering operator. The discretization is done using the first-order Trotter-Suzuki formula,

$$\hat{U}(0, T) \rightarrow \hat{U}(0, T)_{dig} = \prod_{j=1}^n \prod_{m=1}^M \exp \left\{ -i \Delta t C_m(j \Delta t) \hat{H}_m \right\}. \quad (3.33)$$

Here the total evolution time T is divided into n equal steps of width Δt i.e., $n = T/\Delta t$. In this case, the error would be of the order $\mathcal{O}(\Delta t^2)$ [64]. One can also consider higher-order decomposition, which can give better approximation by minimizing the error further [68]. However, an interesting observation from our simulation is that the digital adiabatic evolution using CD driving is independent of the simulation time T , and depends only on the number of Trotter steps. So, by fixing the total time steps, we can choose an arbitrarily small value for T and Δt so that we can achieve arbitrary precision even with the first-order trotterization. We ignore the time variation of the Hamiltonian $\hat{H}(t)$ on time scale lower than Δt , which contributes to an extra error $\sim \|\partial \hat{H}/\partial t\| \Delta t$ per each step. When the Hamiltonian fluctuation is very fast, it is possible to suppress this additional error, which is discussed in [69]. From Eq. (3.33), the digital unitary evolution can be designed for the different Hamiltonians chosen in this chapter. For instance, one single step of TS decomposition for Eq. (3.5) will look like

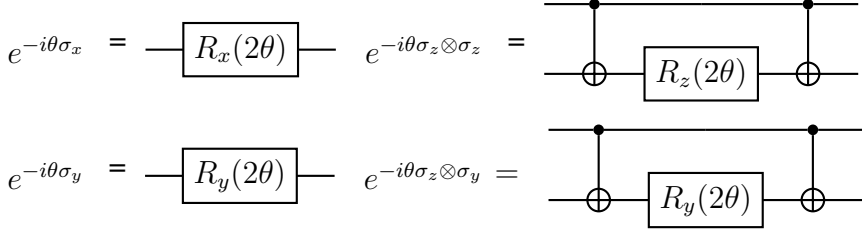
$$\hat{U}(0, \Delta t) = e^{-i\hat{H}(t)\Delta t} \approx e^{-i\theta_x(\Delta t)\sigma_x\Delta t} e^{-i\theta_z(\Delta t)\sigma_z\Delta t} e^{-i\theta_y(\Delta t)\sigma_y\Delta t}, \quad (3.34)$$

where $\theta_x(\Delta t) = (1 - \lambda(\Delta t))$, $\theta_z(\Delta t) = \lambda(\Delta t)$ and $\theta_y(\Delta t) = F^{(1)}(\Delta t)$, are the variables that represent the change in the Hamiltonian in each step. Similarly, for Eq. (3.8), four variables are required for each spin in each step, i.e.,

$$\hat{U}(0, \Delta t) \approx \prod_{j=1}^2 e^{-i\theta_x(\Delta t)\sigma_x^j\Delta t} e^{-i\theta_z(\Delta t)\sigma_z^j\Delta t} e^{-i\theta_{zz}(\Delta t)\sigma_z^j\sigma_z^{j+1}\Delta t} e^{-i\theta_y(\Delta t)\sigma_y^j}. \quad (3.35)$$

These unitary operators are implemented in the circuit model. According to the Solovay-Kitaev theorem [70], any k-body unitary operation can be decomposed into a combination

of single-qubit and two-qubit gate operations. Following are some example of the implementations, corresponding to the unitary operators used in this study.



3.8 Approximate CD term using variational method

The main idea of counter-diabatic driving is to add an auxiliary term to the original Hamiltonian and evolve the system according to an effective Hamiltonian,

$$\hat{H}(t) = \hat{H}_0(t) + \dot{\lambda}\hat{A}_\lambda, \quad (3.36)$$

where \hat{H}_0 is the original Hamiltonian, $\dot{\lambda}$ is the control parameter, and \hat{A}_λ is the exact adiabatic gauge potential responsible for the diabatic transitions. For the spin model considered in our simulation, the calculation of exact gauge potential results in non-local m-body interaction terms. Even though it is possible to implement these interactions using a basic set of quantum gates, the required gates will be huge and increase rapidly with the system size. Instead, for the practical purpose, we consider approximate gauge potential \hat{A}_λ^* , which satisfies the equation

$$\left[i\partial_\lambda \hat{H}_0 - \left[\hat{A}_\lambda^*, \hat{H}_0 \right], \hat{H}_0 \right] = 0. \quad (3.37)$$

For the optimal solution, we have to minimize the operator distance between the exact gauge potential and the approximate gauge potential, which is equivalent to minimizing the action

$$S_\lambda \left(\hat{A}_\lambda^* \right) = \text{Tr} \left[\hat{G}_\lambda^2 \left(\hat{A}_\lambda^* \right) \right], \quad (3.38)$$

where the Hilbert-Schmidt norm \hat{G}_λ is given by

$$\hat{G}_\lambda \left(\hat{A}_\lambda^* \right) = \partial_\lambda \hat{H}_0 + i \left[\hat{A}_\lambda^*, \hat{H}_0 \right]. \quad (3.39)$$

A simple ansatz for \hat{A}_λ^* for the Hamiltonian in Eq. (3.6) from the main-text is, $\hat{A}_\lambda^* = \sum_j \alpha_j(t) \sigma_y^j$. This single qubit approximation works very well even for many-body systems. However, when the spin interaction terms become the leading term of the adiabatic gauge

potential, this ansatz fails. So, we consider a general way to choose the ansatz using sequence of nested commutators proposed in [14], that is

$$\hat{A}_\lambda^{(l)} = i \sum_{k=1}^l \alpha_k(t) \underbrace{[\hat{H}, [\hat{H}, \dots, [\hat{H}, \partial_\lambda \hat{H}]]]}_{2k-1}, \quad (3.40)$$

from which, when $l \rightarrow \infty$, we will get the exact gauge potential.

As an example, we explicitly calculate the CD term using first-order nested commutator for the Hamiltonian to prepare the Bell state,

$$\hat{H}(\lambda) = (1 - \lambda)h_0(\sigma_x^1 + \sigma_x^2) + \lambda J_0\sigma_z^1\sigma_z^2. \quad (3.41)$$

Here $\lambda = \lambda(t)$ contains the time dependence of the Hamiltonian. We choose the approximate adiabatic gauge potential as

$$\hat{A}_\lambda^1 = i\alpha_1(t)[\hat{H}, \partial_\lambda \hat{H}] = 2\alpha_1 h_0 J_0(\sigma_y^1\sigma_z^2 + \sigma_z^1\sigma_y^2). \quad (3.42)$$

Now $\hat{G}_\lambda = \partial_\lambda \hat{H} - i[\hat{H}, \hat{A}_\lambda^1]$ is calculated as

$$\hat{G}_\lambda = -h_0(1 + 4\alpha_1\lambda J_0^2)(\sigma_x^1 + \sigma_x^2) + J_0(1 + 8\alpha_1(1 - \lambda)h_0^2)\sigma_z^1\sigma_z^2 - 8\alpha_1 h_0^2 J_0(1 - \lambda)\sigma_y^1\sigma_y^2,$$

with

$$[\hat{H}, \hat{A}_\lambda^1] = i\alpha_1[\hat{H}, [\hat{H}, \partial_\lambda \hat{H}]] = 2\alpha_1 h_0^2 J_0(1 - \lambda)[4i(\sigma_z^1\sigma_z^2 - \sigma_y^1\sigma_y^2)] + 2\alpha_1 \lambda h_0 J_0^2[-2i(\sigma_x^1 + \sigma_x^2)]. \quad (3.43)$$

The action can be defined as $S_\lambda = Tr[\hat{G}_\lambda^2]$, yielding

$$S_\lambda = 2h_0^2(1 + 4\alpha_1\lambda J_0^2)^2 + J_0^2(1 + 8\alpha_1(1 - \lambda)h_0^2)^2 + 64\alpha_1^2 h_0^4 J_0^2(1 - \lambda)^2. \quad (3.44)$$

Minimizing the action $\partial S_\lambda / \partial \hat{A}_\lambda^1 = 0$, we finally obtain the CD coefficient

$$\alpha_1 = -\frac{1}{4(4(-1 + \lambda)^2 h_0^2 + \lambda^2 J_0^2)} \implies \hat{A}_\lambda^1 = -\frac{J_0 h_0 (\sigma_y^1 \sigma_z^2 + \sigma_z^1 \sigma_y^2)}{2(J_0^2 \lambda^2 + 4h_0^2(1 - \lambda)^2)}. \quad (3.45)$$

3.9 Error Analysis

Various errors significantly impact the outcomes of the experiments. The sources of errors can be divided into three main categories. (i) *Discretization error* arises due to the choice of Δt in the trotterization process, (ii) *Cumulative gate error* is a combination of

表 3.1 The state fidelity and the gate counts after circuit optimization is depicted.

Circuit optimization	Fidelity		Gate Count		Expected gate error
	Ideal	Experiment	Rotation	CNOT	
Bell state preparation					
Optimized	0.999	0.9835	8	2	0.01927
Not optimized		0.8021	19	14	0.11834
GHZ state preparation (3 qubit)					
Optimized	0.9325	0.8198	20	7	0.07063
Not optimized		0.7370	23	15	0.14276

single qubit gate errors and CNOT errors and increases linearly with the circuit depth and (iii) *Measurement error* arises due to the measurements at the end of the time evolution. Also if the system evolves for a long time, as in the adiabatic case, the energy relaxation and dephasing also has to be considered. The cross-talks between the qubits and other environmental effects can also disturb our simulation, but these effects have not been considered in our simulations. In digital quantum simulation the main source of error arises from the discretization of the continuous time evolution of a Hamiltonian and decomposing this evolution into a sequence of quantum gates. The discretization can be performed using various methods, but the Trotter-Suzuki (TS) formula is the most widely used method among all because of its simplicity. In our simulation, we consider first order TS formula, where the error is of the order $\mathcal{O}(\Delta t^2)$. For a given total time T , we can choose an arbitrarily small value for Δt to decrease the Trotter error. However, with small Δt , we need more Trotter steps to reach the final time, which will increase the total gate count and eventually leads to accumulation of gate error. One possible solution for this problem is to consider a higher-order TS formula using extra gates [68]. Since the gate error is comparatively larger than the Trotter error, we restrict ourselves to a first-order approximation.

3.9.1 Gate error

While implementing the time evolution of a system, gate error plays a crucial role. With increasing trotter steps, the gate error also increases linearly. The average fidelity of a single qubit and a CNOT gate of the IBM quantum computer in our simulation is 99.95% and 98.5%, respectively. For the experimental implementation on a noisy device, it's necessary to optimize the quantum circuit before sending it to the hardware to get the desired result. In our simulation, to decrease the gate error, we used the transpilation function

表 3.2 We compare the number of quantum gates required for the successful implementation of adiabatic evolution on a digital quantum computer by including the CD term and excluding the CD term.

System	Trotter step	Rotation gates	CNOT gates	Fidelity
With CD				
Single spin system	2	7	-	0.995
Non-integrable Ising model (5-qubit, $J_0 = -0.1$)	4	70	40	0.993
Bell-state preparation	3	27	14	0.999
GHZ state (3 qubit)	4	111	60	0.966
Without CD				
Single spin system	20	39	-	0.996
Non-integrable ising model (5-qubit, $J_0 = -0.1$)	30	445	300	0.985
Bell-state preparation	24	70	48	0.998
GHZ state (3 qubit)	18	105	108	0.962

available in Qiskit Terra for circuit optimization. Table 3.1 shows the experimental fidelity for the preparation of Bell-state and GHZ state with circuit optimization and without circuit optimization. The gate count and the expected gate error is calculated in both cases. In Table 3.2, the gate counts for the successful implementation of the adiabatic evolution for different systems on a digital quantum computer is illustrated. From the data, it is conclusive that the inclusion of the CD term can improve fidelity and reduce the total gate count.

3.9.2 Measurement error mitigation

One of the main sources of error in our simulation is the readout error of the device. In the following, we briefly discuss how to mitigate measurement error on a small system using the matrix inversion method. For that, we have to find out the response matrix M_R for the given device. To measure M_R , we consider a set of 2^n calibration circuits using only X-gate. Let P_{noisy} be the probability distribution for each possible 2^n states obtained from the quantum processor after measuring at the end. P_{actual} be the probability distribution without readout noise. Then we can obtain $P_{mitigated}$ which is approximately equal to the P_{actual} by applying the matrix inversion M_R^{-1} on the obtained result, *i.e.*

$$M_R^{-1} P_{noisy} = P_{mitigated}. \quad (3.46)$$

This method works only when the measurement error is much larger than the single qubit gate error used for initial state preparation. This is true for IBMQ devices, where the average single qubit gate error is of the order of 10^{-4} and the measurement error is of the order 10^{-2} . During the simulation, we use the tool provided by qiskit ignis [71] for performing the measurement error mitigation. More advanced methods can be found in [72].

3.10 Conclusion

In conclusion, we have demonstrated the implementation of digitalized STA on a superconducting quantum processor. The problem Hamiltonian, chosen for the simulation, emulates the one-dimensional Ising spin chain. The STA is realized by means of the local and approximate CD driving, which is obtained using mainly two methods: the long-established Berry's algorithm and the newly proposed variational approach. The CD term in our simulation is non-stoquastic in nature. Therefore it can't be simulated efficiently on a classical computer. The effective Hamiltonian is implemented using the available quantum gates, and the time evolution of the system is studied to achieve the ground state of the problem Hamiltonian. We have shown that the time steps required to reach the target state are minimal compared to the DAdQC method, leading to minimal loss due to the decoherences and accumulated gate errors. The local CD driving proved to be very effective for weakly interacting spin chains; however, is not useful in case of strong interaction and fails to produce degenerate target states. To remedy this situation, the approximate CD driving is useful, which can be calculated using the nested commutator method. We applied the first-order approximate CD term to prepare Bell and GHZ state with high fidelity for a few qubit systems. Furthermore, for the many qubit systems, the fidelity can be further improved with higher-order terms at the cost of gate numbers.

In this chapter, we provided the evidence that significant enhancement of the DAdQC approach can be achieved using the STA methods by decreasing the total computational cost and hence achieving the desired results within the coherence time of the device. In the next chapter, we show the application of the approximate CD terms as a non-stoquastic catalyst to speed up adiabatic quantum optimization.

第四章 Digitized-Counterdiabatic Quantum Optimization

In this chapter, we propose a novel method called digitized-counterdiabatic quantum optimization (DCQO) to achieve polynomial enhancement over adiabatic quantum optimization for the general Ising spin-glass model, which includes the whole class of combinatorial optimization problems. This is accomplished via the digitization of adiabatic quantum algorithms that are catalyzed by the addition of non-stoquastic counterdiabatic terms. The latter is suitably chosen, not only for escaping classical simulability but also for speeding up the performance. Finding the ground state of a general Ising spin-glass Hamiltonian is used to illustrate that the inclusion of k-local non-stoquastic counterdiabatic terms can always outperform the traditional adiabatic quantum optimization with stoquastic Hamiltonians. In particular, we show that a polynomial enhancement in the ground-state success probability can be achieved for a finite-time evolution, even with the simplest 2-local counterdiabatic terms. Furthermore, the considered digitization process within the gate-based quantum computing paradigm provides the flexibility to introduce arbitrary non-stoquastic interactions. As an experimental test, we study the performance of the DCQO algorithm on cloud-based IBM's superconducting and Quantinuum's ion-trap quantum processors with up to 8 qubits. Along these lines, quantum speed-up may be reached using our proposed paradigm on current NISQ computers to find approximate solutions for NP-complete and NP-hard optimization problems. We expect DCQO to become a fast-lane paradigm toward quantum advantage in the NISQ era.

4.1 Introduction

Many important optimization problems in science and industry can be formulated as solving combinatorial optimization problems [73]. In general, these problems are known to be NP-hard, so that no classical or quantum computers are expected to solve them efficiently. However, there is a hope that quantum computers might give some polynomial speed-up, which helps reduce the resources and hence the cost of solving many practical problems of interest. Especially, adiabatic quantum optimization (AQO) algorithms are developed to tackle such problems [25, 32, 74]. Here, the solution to the optimization problem is encoded in the ground state of an Ising spin-glass Hamiltonian [50]. The adiabatic theorem states that the system will remain in the instantaneous ground state if the evolution from the

ground state of an initial Hamiltonian to the final Hamiltonian is sufficiently slow enough. The corresponding time-dependent Hamiltonian is given by

$$H_{ad}(\lambda) = \lambda(t) \left[\sum_{i < j} J_{ij} \sigma_i^z \sigma_j^z + \sum_i h_i \sigma_i^z \right] - (1 - \lambda(t)) \left[\sum_i \sigma_i^x \right], \quad (4.1)$$

where σ^z and σ^x are the Pauli operators. And, $\lambda(t) \in [0, 1]$ is a scheduling function that represents the interpolation from the initial Hamiltonian to the final Hamiltonian. In Eq. (4.1), the first term corresponds to the Ising spin-glass Hamiltonian with all-to-all interactions, finding its ground state in the worst-case scenario is NP-hard [75]. The second term with a transverse field represents the initial Hamiltonian, corresponding to quantum fluctuation.

The Hamiltonian $H_{ad}(\lambda)$ has off-diagonal matrix elements that are real and non-positive in the computational basis, in other words, stoquastic and quantum Monte Carlo simulations can tackle such problems without facing any sign problem. It is believed that adiabatic quantum optimization or quantum annealing with stoquastic Hamiltonian might not give significant enhancement over classical algorithms, but some counterexamples have recently been found [76–78]. The adiabatic quantum computation with non-stoquastic Hamiltonians is known to be universal [35]. However, the role of non-stoquastic catalysts to speed-up adiabatic quantum optimization problems is an unresolved problem. There are some problems where the non-stoquastic catalysts are advantageous [79–86], and others are known to worsen the performance compared to their stoquastic counterparts [87]. The main reason for this ambiguity is that the non-stoquastic terms are chosen randomly in all the previous works.

The counterdiabatic (CD) technique, borrowing from shortcuts to adiabaticity (STA) [88, 89], was introduced to speed up adiabatic evolutions by adding Hamiltonian terms to suppress the non-adiabatic transitions [90–93]. Recently, a number of developments have shown the advantage of CD techniques in digitized-adiabatic quantum computing [94–97], quantum annealing [54, 98–101], and quantum approximate optimization algorithms (QAOA) [102–104]. In this chapter, we propose digitized-counterdiabatic quantum optimization (DCQO) as a novel paradigm to solve the general class of combinatorial optimization problems with quantum speed-up. We show that the suitably designed CD terms appearing during the non-adiabatic evolution act as non-stoquastic catalysts. This provides us with a guaranteed enhancement over traditional adiabatic quantum optimization with stoquastic Hamiltonians while solving the long-range Ising spin-glass problem. More-

over, we consider approximate local CD terms that can be obtained without knowing any prior detail of the Hamiltonian spectra [14, 105, 106]. We remark that we derive a general analytical expression for the CD coefficients so that one does not have to calculate them explicitly for each case. Finally, we follow the gate-model approach for the digitized-adiabatic quantum evolution [36, 94], allowing the digital implementation of arbitrary non-stoquastic CD terms in current noisy intermediate-scale quantum (NISQ) computers. Consequently, the proposed DCQO paradigm will be useful in solving the general class of combinatorial optimization problems with quantum speed-up in the NISQ era.

4.2 Counterdiabatic driving as a non-stoquastic catalyst

The concept of STA was originally proposed last decade [88], and was found to have wide applications in many fields, ranging from quantum physics, classical physics to stochastic physics [89]. Among all techniques of STA, CD driving, also called transitionless driving, provided the possibility of tailoring the Hamiltonian of quantum many-body systems [14, 105] to speed up the adiabatic process. Here, the source adiabatic Hamiltonian is added by a CD term that takes the form

$$H(\lambda) = (1 - \lambda(t))H_i + \lambda(t)H_f + f(\lambda)H_{cd}. \quad (4.2)$$

Here, H_i and H_f are the initial and the problem Hamiltonians connected by $\lambda(t)$, satisfying $\lambda(0) = 0$ and $\lambda(T) = 1$, and H_{cd} is the CD term with scheduling $f(\lambda)$, which vanishes at the beginning and end of the protocol. In principle, introducing the exact CD term help to follow the instantaneous ground state of the original Hamiltonian $H_{ad}(\lambda)$ at all times during the evolution. This motivates us to define the CD term as $H_{cd}(\lambda) = \dot{\lambda}A_\lambda$. We can notice that when the evolution is very fast, H_{cd} increases dramatically, and in the adiabatic limit, i.e., $|\dot{\lambda}| \rightarrow 0$, the CD term vanishes. Here, $A_\lambda = i \sum_m (1 - |m(\lambda)\rangle \langle m(\lambda)|) |\partial m(\lambda)\rangle \langle m(\lambda)|$ is known as adiabatic gauge potential corresponding to the non-adiabatic transitions between the eigenstates $|m(\lambda)\rangle$ [67], which satisfies the condition $[i\partial_\lambda H_{ad} - [A_\lambda, H_{ad}], H_{ad}] = 0$. Obtaining the exact A_λ for a many-body system is challenging. Its implementation is not optimal because, in many cases, A_λ can contain exponentially many terms with non-local many-body interactions. An alternative approach is to consider the approximate form of the adiabatic gauge potential [105, 106] that can be obtained from a nested commutator (NC)

[14]

$$A_{\lambda}^{(l)} = i \sum_{k=1}^l \alpha_k(t) \underbrace{[H_{ad}, [H_{ad}, \dots, [H_{ad}, \partial_{\lambda} H_{ad}]]]}_{2k-1}. \quad (4.3)$$

Here, $\alpha_k(t)$ is the CD coefficient, obtained by minimizing the operator distance between the exact gauge potential and the approximate gauge potential. This is similar to minimizing the action $S = \text{tr}[G_{\lambda}^2]$, where the Hilbert-Schmidt operator $G_{\lambda} = \partial_{\lambda} H_{ad} + i[A_{\lambda}^{(l)}, H_{ad}]$. For the real-valued Hamiltonian in Eq. (4.1), the adiabatic gauge potential is always imaginary, so the terms appearing in the NC expansion always contain an odd number of Pauli- y terms. So, by restricting to lower-order terms obtained from Eq. (4.3) and post-selecting only one-spin and two-spin interaction terms, one can construct the general 2-local CD term as

$$H_{cd}(\lambda) = \sum_i \alpha_i(\lambda) \sigma_i^y + \sum_{i \neq j} \beta_{ij}(\lambda) \sigma_i^z \sigma_j^y + \gamma_{ij}(\lambda) \sigma_i^x \sigma_j^y, \quad (4.4)$$

where the CD coefficients α_i , β_{ij} , and γ_{ij} is obtained by variational minimization [105, 107]. We can notice that, by construction, the approximate CD terms have imaginary numbers as the off-diagonal matrix elements, which makes it non-stoquastic. So, the NC ansatz in Eq. (4.3) serves as a prescription for choosing the non-stoquastic catalyst. However, not all the terms in the NC ansatz give significant enhancement. Therefore, preselecting the correct operators can help reduce the cost of implementation. Besides, by introducing more control parameters, the use of machine learning techniques and quantum variational algorithms for obtaining optimal values might further enhance the performance [102, 107–110].

We start with a simple local adiabatic gauge potential, which takes the form $\tilde{A}_{\lambda} = \sum_i^N \beta_i(t) \sigma_i^y$, where the general expression for the CD coefficient $\beta_i(t)$ is calculated as $\beta_i(t) = h_i/2 [(\lambda - 1)^2 + \lambda^2 (h_i^2 + \sum_i J_{ij}^2)]$. Even though the off-diagonal matrix elements for \tilde{A}_{λ} contains complex values, with a simple change of basis, one can make it stoquastic. Also, from the first-order expansion of the NC ansatz, we obtain the 2-local CD term as

$$H_{cd}^{(1)}(\lambda) = -2\dot{\lambda}\alpha_1(t) \left[\sum_i h_i \sigma_i^y + \sum_{i < j} J_{ij} (\sigma_i^y \sigma_j^z + \sigma_i^z \sigma_j^y) \right]. \quad (4.5)$$

Here, the CD coefficient $\alpha_1(t) = -\frac{1}{4} \left[\sum_i h_i^2 + 2 \sum_{i < j} J_{ij}^2 \right] / R(t)$, where $R(t)$ is given by

$$R(t) = (1 - 2\lambda(t)) \left[\sum_i h_i^2 + 8 \sum_{i < j} J_{ij}^2 \right] + \lambda(t)^2 \left[\sum_i h_i^2 + \sum_i h_i^4 \right]$$

$$+8 \sum_{i < j} J_{ij}^2 + 2 \sum_{i < j} J_{ij}^4 + 6 \sum_{i \neq j} h_i^2 J_{ij}^2 + 6 \sum_{i < j} \sum_{k < l} J_{ij}^2 J_{kl}^2 \Big]. \quad (4.6)$$

In the last term of Eq. (4.6), we have the following additional constraints: $i = k$ or $j = l$, and equivalently $i = l$ or $j = k$. In Eq. (4.5), we only have a single variational parameter $\alpha_1(t)$. For better performance, one can also consider the CD term in Eq. (4.4), which requires optimizing N^2 parameters considering $\beta_{ij} = \beta_{ji}$, and $\gamma_{ij} = \gamma_{ji}$. For convenience, we use the shorthand notation, $Y = \dot{\lambda} \sum_i^N \beta_i(t) \sigma_i^y$, and $Y|ZY = H_{cd}^{(1)}(\lambda)$.

4.3 Digitized counterdiabatic driving

For adiabatic quantum optimization problems, the CD terms are non-stoquastic, making it challenging to realize such Hamiltonian on existing quantum annealers [83, 111]. Also, for obtaining a higher success probability in many-body systems, it is essential to consider higher-order k-local CD terms. This is a challenging task for analog quantum computers and quantum annealers. Along with that, the lack of flexibility in realizing arbitrary interactions is one of the main drawbacks of analog quantum computers and quantum annealers. To overcome all these problems, we used digitized-adiabatic quantum computing techniques [36, 94], which provides the flexibility to introduce arbitrary multi-qubit and non-stoquastic interactions. The model is also consistent with error correction [112], and error mitigation techniques are being developed for NISQ computers [113].

For the time-dependent Hamiltonian in Eq. (4.2), the evolved state is given by $|\psi(T)\rangle = \mathcal{T}e^{-i \int_0^T H(\lambda) dt} |\psi(0)\rangle$, where $|\psi(0)\rangle = \frac{1}{\sqrt{2}}(|0\rangle + |1\rangle)^{\otimes N}$, and \mathcal{T} is the time ordering operator. The total Hamiltonian can be decomposed into sum of local terms, *i.e.*, $H(\lambda) = \sum_j \gamma_j(t) H_j$. We discretize the total time T into many small intervals of size δt . Using the first-order Trotter-Suzuki formula, we obtained the approximate time evolution operator given by

$$U_{\text{dig}}(0, T) = \prod_{k=1}^M \prod_j \exp \{-i\delta t \gamma_j(k\delta t) H_j\}, \quad (4.7)$$

where M corresponds to the number of Trotter steps. For a better approximation, one can also consider the recently proposed commutator product formulas [114]. In Fig. 4.1, the quantum circuit for implementing the digitized-counterdiabatic quantum evolution is shown. For the evolution of a time-dependent Hamiltonian, the Trotter step size δt should be less than the fluctuation time scale of the Hamiltonian [69], *i.e.*, $\delta t \ll \|\partial H / \partial t\|^{-1}$. However, recently, it has been shown that the digitized-adiabatic quantum evolution is robust against

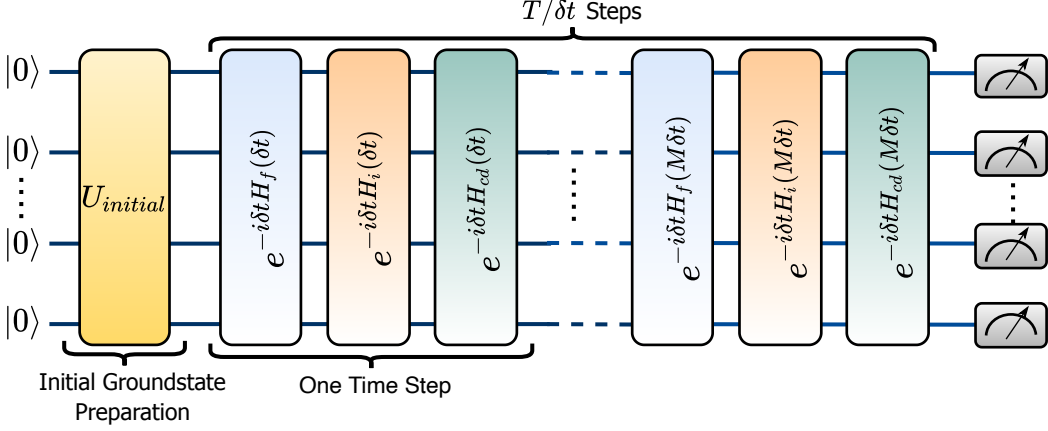


图 4.1 Schematic of the quantum circuit implementation of digitized-counterdiabatic evolution using the first-order Trotter-Suzuki formula in Eq. (7.10).

discretization error [115]. This loosens the restrictions on δt . The cost associated with the digitized-counterdiabatic quantum evolution is given by $\text{Cost} = T \max_\lambda \|H(\lambda(t))\|$, which corresponds to the total gate count, while the number of Trotter steps decide the circuit depth. For the fully-connected Ising spin-glass problem, total $N(N - 1)/2$ entangling operations are needed for each Trotter step, and the inclusion of the 2-local CD terms increases it by a constant factor. Recently, it has been shown that implementing such fully connected Ising spin-glass problems on current quantum annealers, and also on parity quantum computers, results in huge time overhead because of the embedding schemes [116]. In this regard, it is argued that gate-model quantum computing on a 2-D grid has an advantage compared to other architectures. In this sense, trapped-ion systems with all-to-all connectivity would be an ideal choice but they are not strictly necessary.

In our simulation, we fix the total time $T = 1$, and the step size $\delta t = 0.05$. The scheduling function is chosen as $\lambda(t) = \sin^2 \left[\frac{\pi}{2} \sin^2 \left(\frac{\pi t}{2T} \right) \right]$, so that CD terms vanish at the beginning and the end of the evolution. Each matrix exponential term in Eq. (7.10) is implemented using standard two-qubit CNOT gates and single-qubit rotations. For all the cases, the number of shots is chosen between 10000-100000 depending on the system size. By measuring the qubits in the computational basis, we obtain the success probability given by $P_s = |\langle \psi_g | \psi_f(\lambda = 1) | \psi_g | \psi_f(\lambda = 1) \rangle|^2$. Here, $|\psi_g\rangle$ is the actual ground state, and $|\psi_f(\lambda = 1)\rangle$ is the time evolved state at $t = T$. For the Hamiltonian in Eq. (4.1), the coupling terms J_{ij} and the local fields h_i are chosen randomly from a continuous Gaussian distribution with unit variance and zero mean. For estimating the fraction of instances where the inclusion of the CD term gives an enhancement, we define a metric called enhancement ratio, given by $R_{enh} = L^{cd}/L$. Here, L^{cd} is the number of instances with

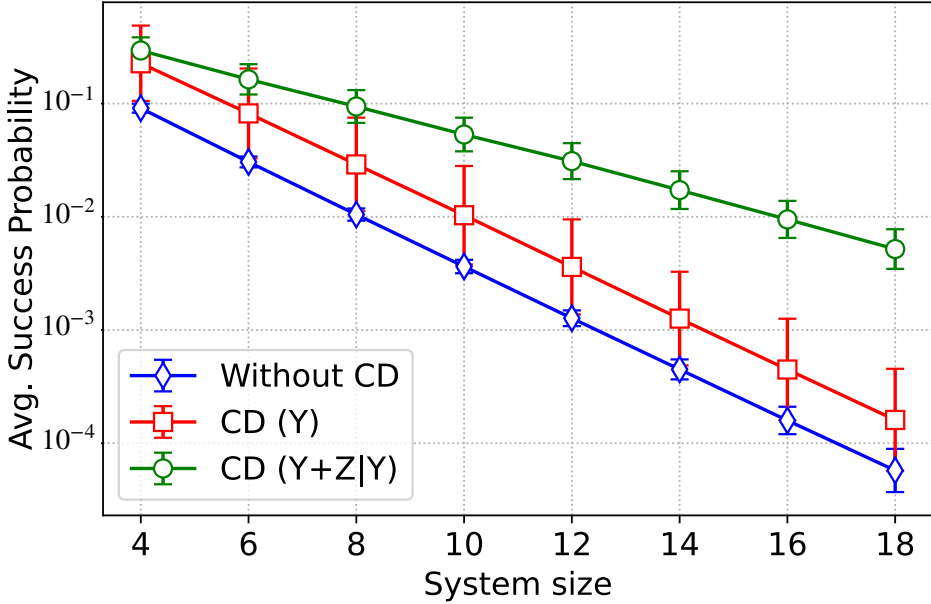


图 4.2 The Average success probability of obtaining the ground state as a function of number of spins in the Ising spin-glass Hamiltonian is depicted. Here, we fix the total evolution time $T = 1$ and the number of Trotter steps to 20, *i.e.* $\delta t = 0.05$. The interaction strengths and the local fields are chosen randomly from a Gaussian distribution for 1000 random instances. The blue curve corresponds to the evolution without the CD term, the red curve is with the local single qubit CD term, and the green curve is for the 2-local CD term in Eq. (4.5). In the latter case, a polynomial enhancement in the success probability can be observed.

enhanced performance by including the CD term, and L is the total number of instances, where we set $L = 1000$. In order to quantify the improvement in the success probability, we define a quantity called success probability enhancement, given by $P_{enh} = P_s^{cd}/P_s^{ad}$. Here, P_s^{cd} and P_s^{ad} are the success probability with and without the CD terms, respectively. In Fig. 4.2, the average ground-state success probabilities for the naive stoquastic Hamiltonian with only a transverse field in Eq. (4.1), including the local CD term Y , and 2-local CD term obtained from NC ansatz $Y|ZY$ are depicted for system sizes up to 18 qubits. We see that the success probability decreases rapidly with increasing system size for the naive non-adiabatic approach, the inclusion of the 2-local CD term $H_{CD}^{(1)}$ gives a polynomial enhancement, and the local single-spin CD gives a constant enhancement. In Fig. 4.4, the histogram shows the ground-state success probability distribution for evolution with and without including the CD term for 1000 random instances of the Ising spin-glass problem for various system sizes. The top panel of Fig. 4.3 shows the average success probability enhancement (P_{enh}^{Avg}) by including the CD terms Y and $Y|ZY$. As the system size grows, P_{enh}^{Avg} increases polynomially for the CD term obtained from the first-order NC ansatz. With the single spin CD term Y , we obtained an enhancement by a factor of ≈ 3 , irrespective of the system size. The bottom

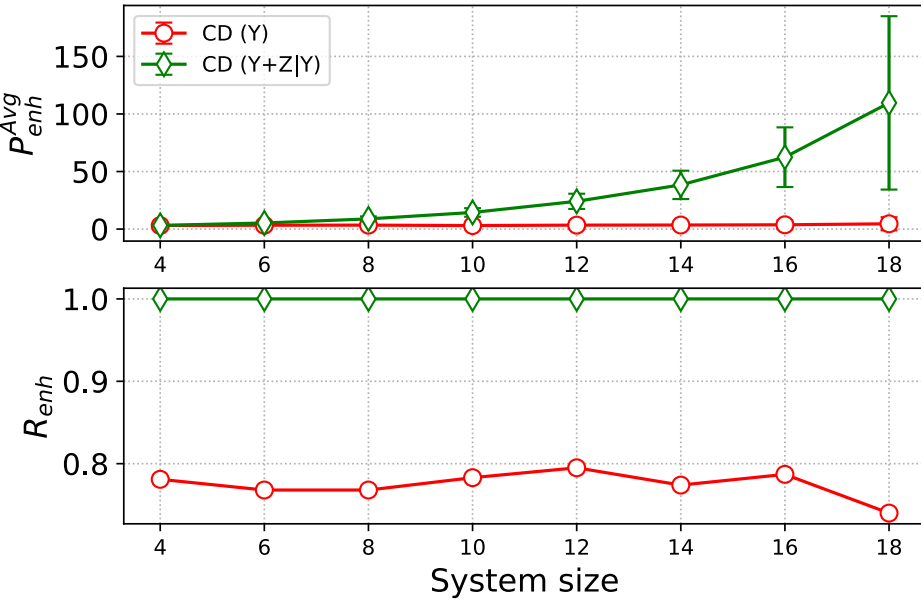


图 4.3 The average success probability enhancement (P_{enh}^{Avg}) and probability enhancement ratio (R_{enh}) as a function of system size for the Ising spin-glass problem is depicted. For the 2-local CD term from the first order NC ansatz, P_{enh}^{Avg} increases with the system size. Whereas for the local CD term (Y), a constant enhancement by a factor of 3 is observed. In the bottom panel, we see that the 2-local CD term always gives enhancement for all 1000 random instances, whereas the local CD has an average enhancement ratio of 0.756.

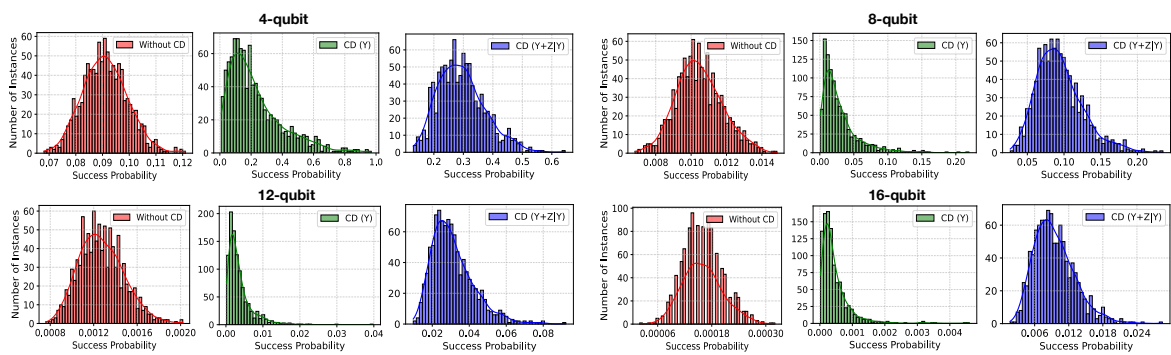


图 4.4 The distribution of ground-state success probability for 1000 randomly chosen instances is illustrated. The red plot corresponds to the traditional stoquastic adiabatic Hamiltonian in Eq. (4.1), the green plot is for the local single-spin CD term, and the blue plot is for the non-stoquastic 2-local CD term in Eq. (4.5).

panel of Fig. 4.3 depicts the fraction of instances where the inclusion of the CD term gives enhancement. For the local CD Y , we obtained $R_{enh} \approx 75.6\%$, while the CD term $Y|ZY$ gives the enhancement ratio $R_{enh} \approx 100\%$, indicating that the 2-local CD term gives a guaranteed enhancement for all the random instances. In general, the inclusion of CD terms does not help reduce the minimum gap, and its enhancement is explained by the fact that the additional terms help suppress the matrix elements responsible for the excitations between the eigenstates. However, to analyze the effect of non-stoquastic CD terms on the minimum gap Δ_{min} , we study the instantaneous energy spectrum as a function of time. Surprisingly, we noticed that the inclusion of approximate CD terms obtained from the NC ansatz increases the minimum energy gap between the ground state and the first excited state during the evolution. This increased gap helps to reduce the excitations, resulting in increased success probability. In Fig. 4.5, the energy gap between the ground state and the first excited state ($|E_1 - E_0|$) as a function time is plotted for four randomly chosen instances with system size $N = 10$. Also, in Fig. 4.6, success probability versus minimum gap (Δ_{min}) is plotted for 250 random instances. We can observe that the inclusion of the 2-local CD term will result in increased success probability as well as the minimum gap.

4.4 Experimental implementation

In order to demonstrate the potential of DCQO on current NISQ devices, we use IBM's cloud-based superconducting quantum processor `ibmq_montreal` with 27-qubits and Quantinuum's fully connected ion-trap processor with 10-qubits. The system we study consists of $N = \{5, 6, 7, 8\}$ spins, and the interaction between the spins J_{ij} and local fields h_i are chosen randomly. The CD term is considered as in Eq. 4.5. For the trotterized evolution, we set the total evolution time $T = 0.1$ and the step size $\delta t = 0.05$, with only two Trotter steps. In Fig. 4.7, the quantum circuit implementing the time evolution operator with two Trotter steps is depicted for the 5-spin system. The CD term H_{cd} is dominant for this fast evolution, and we can neglect H_{ad} while implementing on the hardware. We prepare the qubits in the initial ground state $|+\rangle^{\otimes N}$ by using Hadamard gates and apply the time evolution unitary operator using the available basis set of gates. We obtain the result by measuring the qubits in the computational basis with a number of shots $N_{shots} = 8192$ and $N_{shots} = 500$ from the superconducting and trapped-ion systems, respectively. In Fig. 4.5, the probability distribution obtained from the different hardware and ideal simulators with and without including the CD terms are compared. For all the cases we studied, the result

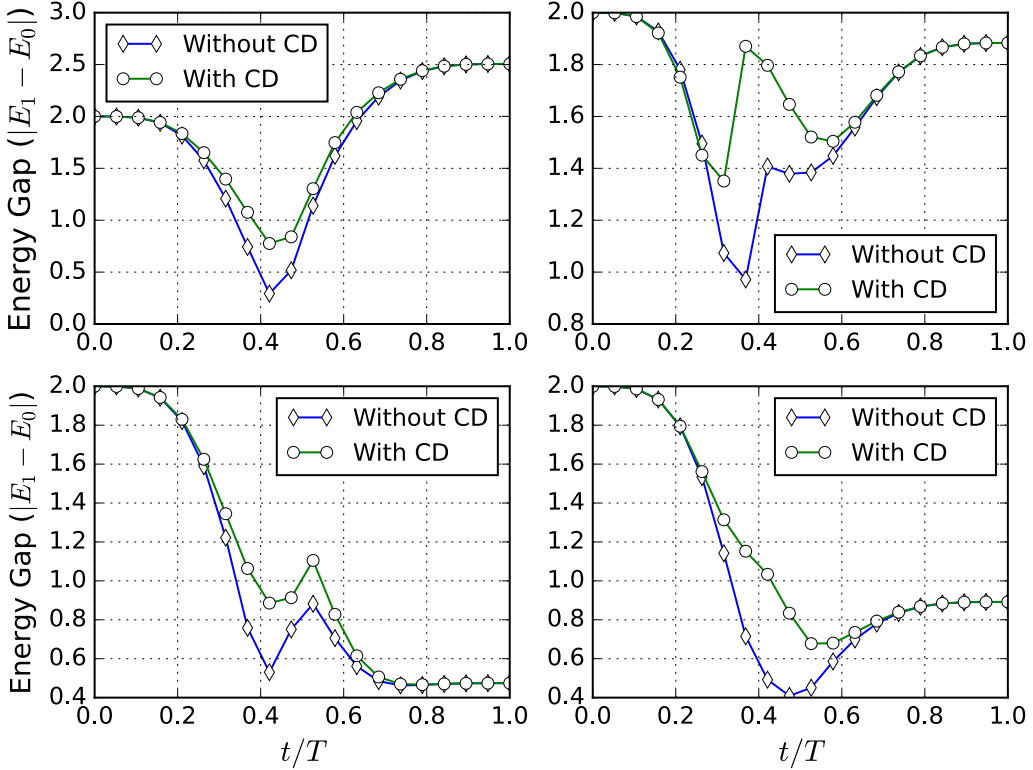


图 4.5 The energy gap between the ground state and the first excited state is plotted as a function of time for a system size $N = 10$. The blue curve corresponds to the stoquastic Hamiltonian in Eq. (4.1), while the green curve corresponds to the non-stoquastic Hamiltonian by including the 2-local CD term in Eq. 4.5.

obtained from DCQO has a large overlap with the exact ground state even with just two Trotter steps. To compare the success rate of the ideal result with the experimental results, we compute the Hellinger distance using $F(P_{\text{exp}}, P_{\text{ideal}}) = [\sum_i \sqrt{P_{i,\text{ideal}} P_{i,\text{exp}}}]^2$, where $P_{i,\text{ideal}}$ and $P_{i,\text{exp}}$ are the state occupations and i runs over the computational basis. The success rate for the ideal DCQO with the results from the trapped-ion system is 0.966, 0.956, 0.887, and 0.845 for system sizes 5 to 8 qubits, respectively. And for the superconducting quantum processor, we restricted our experiment to only five spins due to limited qubit connectivity and obtained a success rate of 0.835.

4.5 Discussion and conclusion

In this chapter, we studied a long-debated problem in adiabatic quantum optimization, i.e., the speed-up role of non-stoquastic catalysts. We showed that cleverly chosen non-stoquastic counterdiabatic Hamiltonians achieve enhanced performance compared to traditional stoquastic adiabatic methods. We considered the general Ising-spin glass Hamil-

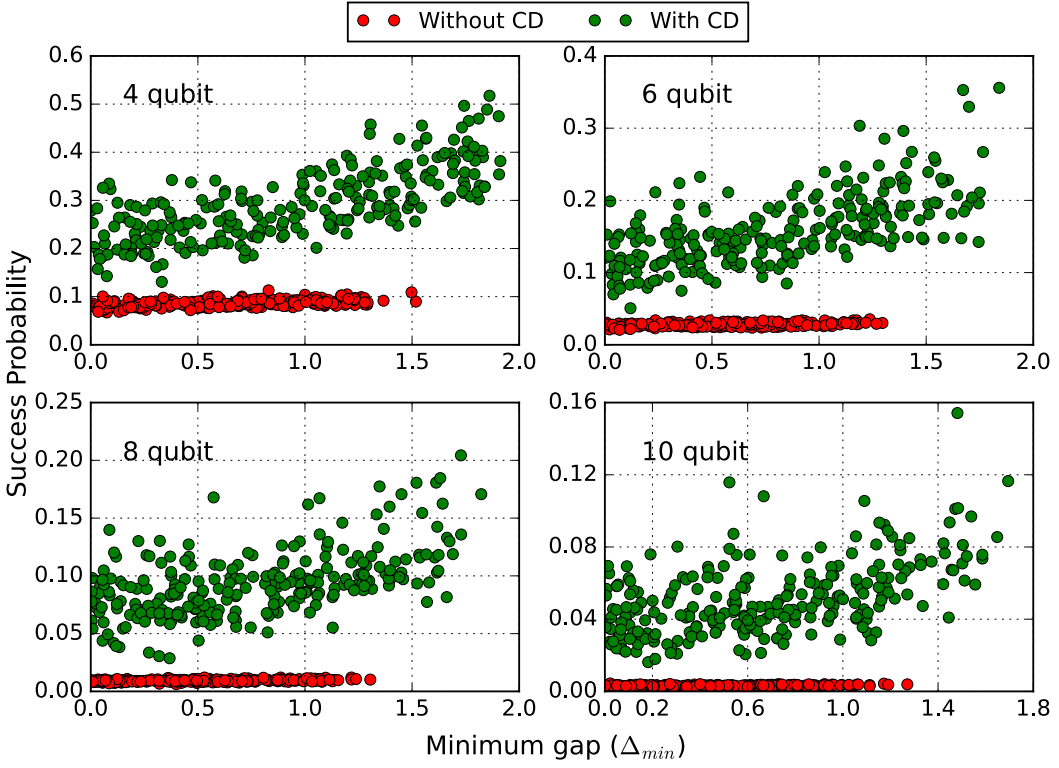


图 4.6 The plot shows success probability versus minimum gap for 250 random instances of the Ising spin glass problem with and without including the CD term. We can observe that adding the CD term will result in an increase in success probability and minimum gap. The parameters are $T = 1$, $\delta t = 0.05$.

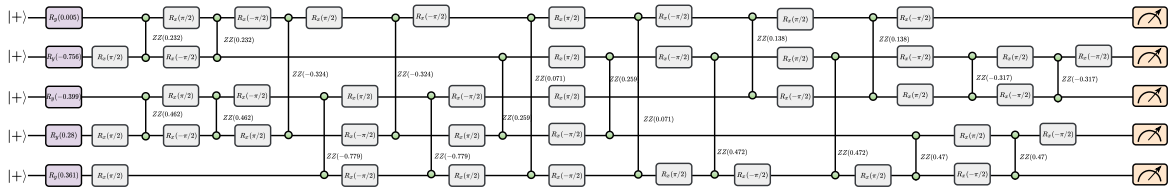


图 4.7 Circuit implementation for the digitized-counterdiabatic evolution for 2 Trotter steps. The time chosen for the evolution is very small ($T = 0.1$); hence only the CD terms are significant, and the terms in H_{ad} are neglected.

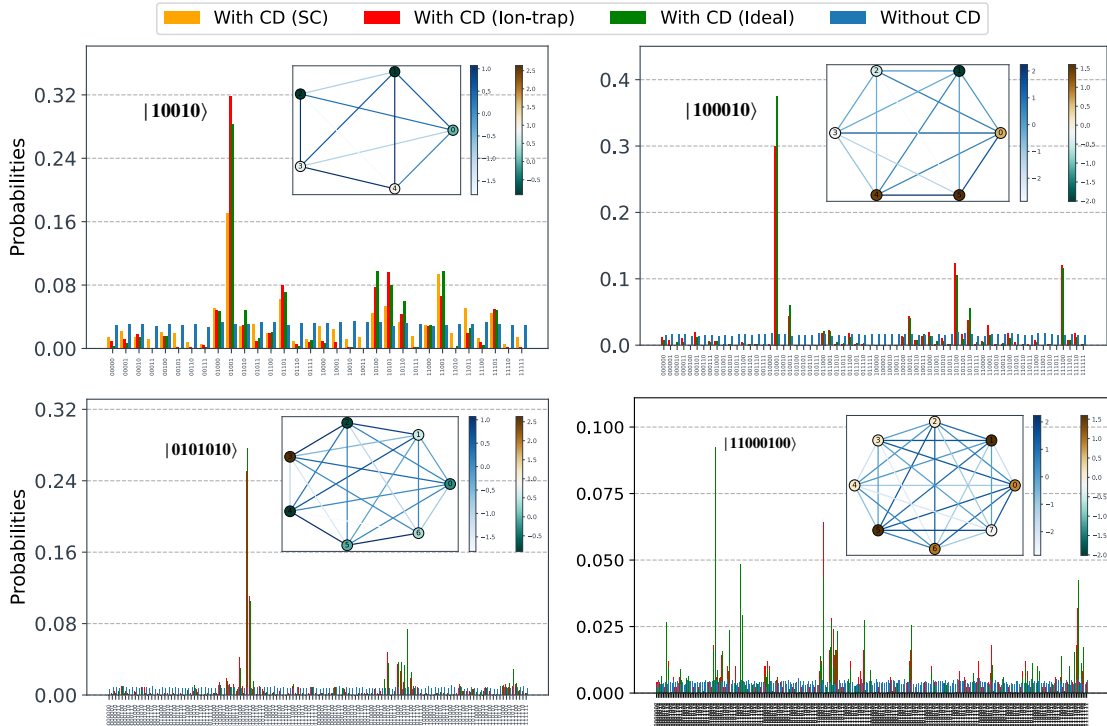


图 4.8 Probability distribution obtained from digitized-counterdiabatic quantum evolution of Ising spin glass Hamiltonian is depicted. We considered random instances of all-to-all connected Ising spin-glass Hamiltonian with 5 to 8 spins. The system is evolved using Trotter–Suzuki approximation with and without including the CD terms given in Eq. (4.5). The experimental results are obtained from IBM’s transmon-based superconducting quantum processor `ibmq_montreal` and Quantinuum’s ion-trap quantum processor. The ground state success probability obtained after two Trotter steps are compared for the digitized-counterdiabatic quantum evolution with the non-adiabatic one. We observed that the experimental and ideal simulations using the DCQO approach have a large overlap with the exact ground state highlighted in the figure. The inset depicts the graph representation of the problem instance with coupling terms, and local field strengths are shown in color bars.

tonian with all-to-all connectivity to show that a polynomial enhancement in the ground-state success probability can be obtained, even with 2-local non-stoquastic CD terms stemming from the NC ansatz. As an outlook, considering higher-order k-local CD terms may further enhance the already observed quantum speed-up of the DCQO paradigm. We also provided a general analytical expression for scheduling these CD terms, whose calculation does not require any prior knowledge of the Hamiltonian spectra or the structure of the eigenstates. Finally, we implemented the DCQO algorithm on two different quantum hardware, i.e., a transmon-based superconducting quantum processor and a trapped-ion system. In conclusion, we proved that the proposed digitized counterdiabatic quantum optimization (DCQO) paradigm involving suitable non-stoquastic CD terms is superior to the traditional adiabatic quantum optimization (AQO) using stoquastic Hamiltonians. In this sense, DCQO might help to achieve quantum advantage for obtaining approximate solutions to combinatorial optimization problems on noisy intermediate-scale quantum (NISQ) computers from hundreds to a few thousand qubits.

第五章 Digitized-Counterdiabatic Quantum Approximate Optimization Algorithm

The quantum approximate optimization algorithm (QAOA) has proved to be an effective classical-quantum algorithm serving multiple purposes, from solving combinatorial optimization problems to finding the ground state of many-body quantum systems. Since QAOA is an ansatz-dependent algorithm, there is always a need to design ansatze for better optimization. To this end, in this chapter, we propose a digitized version of QAOA enhanced via the use of shortcuts to adiabaticity. Specifically, we use a counterdiabatic (CD) driving term to design a better ansatz, along with the Hamiltonian and mixing terms, enhancing the global performance. We apply our digitized-counterdiabatic QAOA to Ising models, classical optimization problems, and the P -spin model, demonstrating that it outperforms standard QAOA in all cases we study.

5.1 Introduction

Hybrid classical-quantum algorithms have the potential to unleash a broad set of applications in the quantum computing realm. The challenges involved in realizing fault-tolerant quantum computer have promoted the study of such hybrid algorithms, which proved to be relevant to modern noisy intermediate-scale quantum (NISQ) devices [117, 118] with few hundred qubits and limited coherence time. One notable example is that of variational quantum algorithms (VQA), which is implemented by designing variational quantum circuits to minimize the expectation value for a given problem Hamiltonian. VQA is advantageous given the fact that preparing a tunable circuit ansatz is found to be difficult on a classical computer. It has already been widely applied in quantum chemistry [119–124], condensed matter physics [125–127], solving linear system of equations [128], combinatorial optimization problems [129, 130] and several others [131, 132]. Remarkably, one of the early implementations of the VQA was performed using photonic quantum processors [133], which prompted further theoretical progress [134–139]. VQA has been demonstrated in superconducting qubits [119, 122, 134] and trapped ions [124, 140, 141].

One compelling outcome of VQA is the development of the quantum approximate optimization algorithm (QAOA) [142], which provides an alternative for solving combinatorial optimization problems using shallow quantum circuits with classically optimized param-

ters. In the past few years, there has been a rapid development in QAOA-based techniques that have been applied not only for solving conventional optimization problems like MaxCut but also for solving ground state problems in different physical systems [141, 143, 144]. Improved versions of QAOA, like ADAPT-QAOA [145] and Digital-Analog QAOA [146] have also been reported recently. Like any combinatorial optimization problem, QAOA depends on optimizing a cost function to obtain the desired optimal state corresponding to a p -level parametrized quantum circuit. In addition, the choice of the approximate trial state, from which the cost function is obtained, is crucial to the success of the QAOA algorithm. Generally, this is done by using quantum adiabatic algorithms (QAA) which produce near-optimal results for large p which is not suitable for current NISQ devices. Moreover, due to the requirement of large p , the cost of classical optimization increases and the algorithms suffer from the problem of vanishing gradients and local minima [147–149].

Several studies have been reported in past few years showing that high fidelity quantum states can be prepared by assisting QAA with additional driving interaction [150]. These studies establish that for certain problems, the inclusion of additional driving terms can reduce the computational complexity, and with it the circuit depth. These driving terms are usually calculated using methods developed under the umbrella of so-called shortcuts to adiabaticity [37, 38], which have been introduced to improve the traditional quantum adiabatic processes, removing the requirement for slow driving [39]. Instances of these methods include counterdiabatic (CD) driving [40–42], fast-forward approach [45, 46], and invariant-based inverse engineering [43, 44]. Among them, CD driving is interesting and has been used to study fast dynamics [51–53, 55, 151], preparation of entangled states [57–59, 152], adiabatic quantum computing [150, 153] and quantum annealing [60–62].

In the context of QAOA, the advantage of the introduction of CD driving is twofold. The CD driving decreases the circuit depth, while reducing the number of optimization parameters. On the other hand, it provides a better approximate trial state which is beneficial for finding the optimal target state. In this chapter, we propose a novel algorithm, digitized-counterdiabatic quantum approximate optimization algorithm (DC-QAOA), which improves the performance of the conventional QAOA using CD driving. In this context, it is worthwhile to mention the work of Ref. [154], also inspired by CD driving techniques.

This chapter is organized as follows. In Sec. 5.2, we introduce DC-QAOA algorithm and explain it in detail, comparing it with the quantum adiabatic evolution and QAOA. In the following sections we present a comparative study of the proposed DC-QAOA and the conventional QAOA method in the context of various physical systems. In Sec. 5.3, we

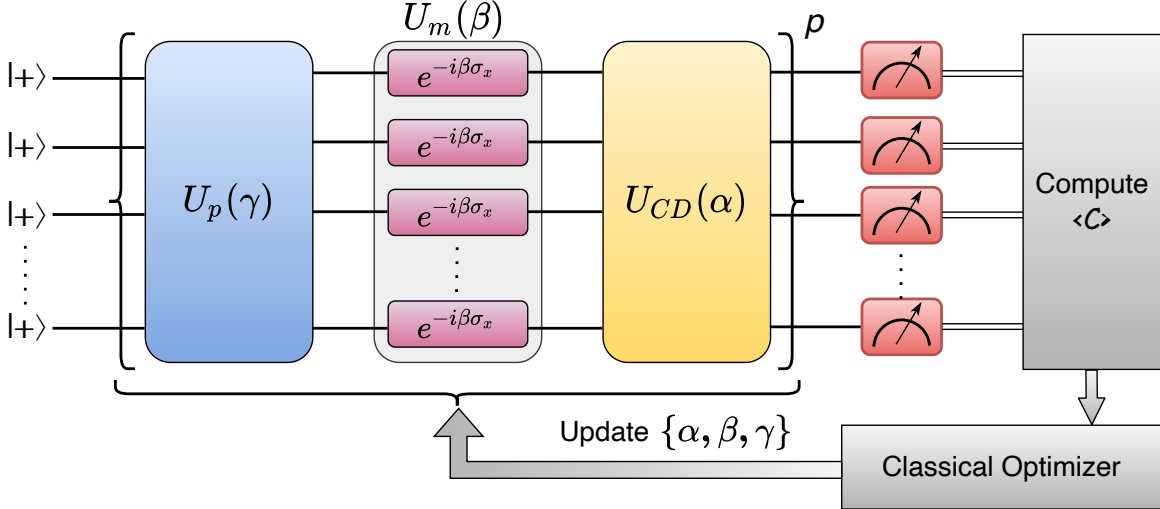


图 5.1 Schematic diagram with circuit used for DC-QAOA having additional CD term along with the Hamiltonian and mixing terms.

prepared the ground state of three different types of 1D Ising spin models, namely, the Longitudinal field Ising model (LFIM), the transverse field Ising model (TFIM), and the GHZ state. In Sec. 5.4, we studied classical optimization problems such as the MaxCut problem and the Sherrington-Kirkpatrick model, while in Sec. 5.5, different variants of P -spin model are considered. In doing so, we establish, by comparing the approximation ratios, that the DC-QAOA is advantageous compared to the QAOA for shallow quantum circuits. We conclude with a discussion in Sec. 5.6.

5.2 Digitized-counterdiabatic quantum approximate optimization algorithm

The conventional QAOA method can be viewed as a combination of two distinct parts: the quantum part consists of a parameterized circuit ansatz, which is in turn complemented by a classical optimization algorithm to determine the parameters that minimize (maximize) a predefined cost function. The circuit ansatz for the quantum part is governed by an annealing Hamiltonian,

$$H_a(t) = (1 - \lambda(t))H_{mixer} + \lambda(t)H_{prob}, \quad (5.1)$$

where $\lambda(t) \in [0, 1]$ is the annealing schedule for $t \in [0, T]$. $H_{mixer} = \sum_i h_i \sigma_i^x$ is the mixing Hamiltonian that produces an equal (weighted) superposition state in the computational basis to begin with, whereas the desired final state is the ground state (or an eigenstate) of H_{prob} . In continuous annealing, the system evolves from the eigenstate of H_{mixer} to the

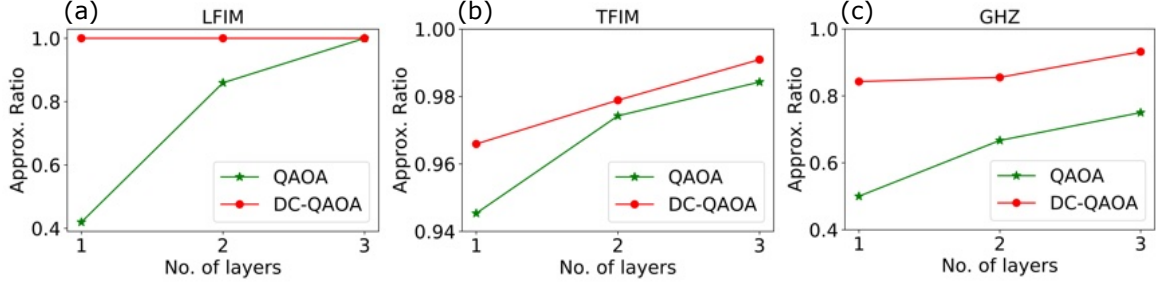


图 5.2 Comparison of approximation ratios (\mathcal{R}) as a function of number of layers (p) for three representative cases of Ising spin model. Green lines show results of QAOA whereas red lines show results of DC-QAOA. (a) shows \mathcal{R} variation of LFIM where $J_{ij} = 1$, $h_i = 1$, and $k_i = 0$. (b) depicts TFIM where $J_{ij} = 1$, $h_i = 0$, and $k_i = 1$, and (c) shows preparation of GHZ state where $J_{ij} = 1$, $h_i = 0$, and $k_i = 0$. System size for all the cases was kept to $L = 12$ qubits.

eigenstate of H_{prob} through adiabatic evolution. The corresponding digital adiabatic circuit ansatz can be designed using the trotterized time evolution operator [64, 69]

$$U(0, T) \approx \prod_{j=1}^p \prod_{m=1}^M \exp \{-iH_m(j\Delta t)\Delta t\}, \quad (5.2)$$

where we consider that $H_a(t)$ can be decomposed into M k -local terms, i.e., into terms $H_m(t)$ which have k -body interactions at most. Note that the $U(0, T)$ is a product of p sub-unitaries, each corresponding to an infinitesimal propagation step Δt . An adiabatic evolution using $U(0, T)$ can always produce an exact target state at the cost of resorting to a large value of p . This can be translated to the language of QAOA if one parameterizes $U(0, T)$ as

$$U(\boldsymbol{\gamma}, \boldsymbol{\beta}) = U_m(\beta_p)U_p(\gamma_p)U_m(\beta_{p-1})U_p(\gamma_{p-1}) \dots U_m(\beta_1)U_p(\gamma_1), \quad (5.3)$$

where the evolution operators are given by $U_m(\beta_p) = \exp\{(-i\beta_p H_{mixer})\}$ and $U_p(\gamma_p) = \exp\{(-i\gamma_p H_{prob})\}$. Here, the annealing schedule is characterized by the discrete set of parameters $\{\beta_p, \beta_{p-1}, \dots, \beta_1\}$ and $\{\gamma_p, \gamma_{p-1}, \dots, \gamma_1\}$. $(\boldsymbol{\gamma}, \boldsymbol{\beta})$ defines a $2p$ parameter space that corresponds to the depth of the circuit ansatz and the cost function $F(\boldsymbol{\gamma}, \boldsymbol{\beta})$ is optimized classically to obtain an optimal parameter set $(\boldsymbol{\gamma}^*, \boldsymbol{\beta}^*)$, which produces the desired target state, i.e., $|\psi(\boldsymbol{\gamma}^*, \boldsymbol{\beta}^*)\rangle$. Note that in most cases this target state is chosen to be the ground state of H_{prob} .

As the case of adiabatic evolution, QAOA requires large p to obtain a near-optimal trial state, even with the assistance of the classical optimizer. In addition, the realization of $U(\boldsymbol{\beta}, \boldsymbol{\gamma})$ for an interacting many-body system for large p becomes inefficient due to the large number of gates involved. In DC-QAOA, we focus on improving the quantum part of

QAOA, by adding a variational parameter in each step, i.e.,

$$U(\gamma, \beta) \rightarrow U(\gamma, \beta, \alpha), \quad F(\gamma, \beta) \rightarrow F(\gamma, \beta, \alpha), \quad (5.4)$$

The application of another parameter decreases the size of p drastically. This additional parameter can be quantified as the inclusion of the CD driving term in the problem Hamiltonian. The resulting circuit ansatz is shown in Fig. 5.1.

In general, CD driving amounts to using an additional control Hamiltonian in Eq. (5.1), required for suppressing non-adiabatic transitions [40–42, 93]. This is especially effective for many-body systems with tightly spaced eigenstates. CD driving comes at a cost, as it generally involves nonlocal many-body interactions, and their exact specification of the CD Hamiltonian term requires access to the spectral properties of the driven system [40, 42, 51]. As a way out, variational approximations have been proposed to obtain the CD terms [13, 152, 155]. In this context, one can use the adiabatic gauge potential for finding an approximate CD driving without spectral information of the system [13, 156].

In the following sections, a pool of CD operators is defined using the nested commutator approach of the adiabatic gauge potential, provided by Claeys et al. [14],

$$A_\lambda^{(l)} = i \sum_{k=1}^l \alpha_k(t) \underbrace{[H_a, [H_a, \dots, [H_a, \partial_\lambda H_a]]]}_{2k-1}. \quad (5.5)$$

Here, we considered up to the second order in the expansion of the nested commutator, $l = 2$, which gives rise to an operator pool $A = \{\sigma^y, \sigma^z\sigma^y, \sigma^y\sigma^z, \sigma^x\sigma^y, \sigma^y\sigma^x\}$, including solely local and two-body interactions. Note that the choice of this operator pool depends on $H_a(t)$ and may contain other operators depending on the problem Hamiltonian. However, A contains every possible CD operator that can be derived from the problem Hamiltonians, used in the present study. We chose the CD term as a combination of these operators for each system based on the success probability of the algorithm. For instance, the local CD driving term provides better success probability in the case of the transverse-field Ising model and P -spin model, however not suitable for solving the MaxCut Hamiltonian. The CD coefficients α_k are transformed into the additional variational parameter associated with the CD driving. The addition of such a new free parameter increases the degrees of freedom, making it possible to reach broader parts of the Hilbert space of the Hamiltonian with a lower circuit depth than in QAOA. Furthermore, as DC-QAOA only requires the operator form of the CD driving combined with the additional set of parameters α , it eliminates the requirement of complex calculation of the CD coefficients. DC-QAOA is also more

flexible in regards to the boundary conditions compared to the CD evolution which permits the application of the driving term even for one step only. Moreover, the operators can be chosen heuristically and according to the requirement of the system which is being studied.

Although there are several ways to define the cost function, we opt for the most convenient one which is the energy expectation value of the problem Hamiltonian calculated for the trial wave function

$$F(\boldsymbol{\gamma}, \boldsymbol{\beta}, \boldsymbol{\alpha}) = \langle \psi(\boldsymbol{\gamma}, \boldsymbol{\beta}, \boldsymbol{\alpha}) | H_{prob} | \psi(\boldsymbol{\gamma}, \boldsymbol{\beta}, \boldsymbol{\alpha}) \rangle, \quad (5.6)$$

where $\psi(\boldsymbol{\gamma}, \boldsymbol{\beta}, \boldsymbol{\alpha})$ represents the approximate trial state produced by the digitized CD ansatz. The efficiency of our algorithm can be measured in terms of the approximation ratio, given by

$$\mathcal{R} = \frac{F(\boldsymbol{\gamma}, \boldsymbol{\beta}, \boldsymbol{\alpha})}{E_0}, \quad (5.7)$$

where E_0 is the ground state energy of the system.

Classical optimization techniques are an integral part of variational algorithms, which helps to find the optimal parameters that minimize the cost function. Our study mainly considers two optimization techniques, namely Momentum Optimizer and Adagrad Optimizer, which are specific examples of stochastic gradient descent (SGD) algorithms. Momentum Optimizer is a variant of SGD in which a momentum term is added along with the gradient descent. The prime purpose of the momentum term is to increase the parameter update rate when gradients are in the same direction and decrease the update rate when gradients point in a different direction [157]. On the other hand, Adagrad Optimizer's main purpose is to change the update rate based on the past descent results [158]. Adagrad has shown great improvements in the robustness of SGD [159]. These two classical optimization techniques work pretty well for the cases we consider. This is because these optimization routines have proven faster convergence than gradient descent. Moreover, some of the cases we study involve a large Hilbert space, which may lead to local minima in the energy landscape. In the presence of steep gradients, the use of these techniques proves beneficial. This problem dependence of the performance is shared with other optimization routines such as Nesterov Momentum, Adam, and AdaMax. An overview and comparison about challenges faced by the different types of gradient descent optimization, can be found in Ref. [160].

5.3 Ising spin models

1D quantum Ising spin chains are the manifestation of the simplest many-body systems that are widely studied in existing quantum processors. Numerous computational problems can be mapped to finding the ground state of the Ising-like Hamiltonians, which makes it suitable for benchmarking various quantum algorithms. The general form of the Hamiltonian of 1D Ising spin model is given by

$$H_{prob}(\sigma) = - \sum_{\langle i,j \rangle} J_{ij} \sigma_i^z \sigma_j^z - \sum_i h_i \sigma_i^z - \sum_i k_i \sigma_i^x, \quad (5.8)$$

where σ_i^δ denotes the Pauli matrices at the i th site, and $\langle i, j \rangle$ corresponds to the nearest-neighbor interaction with strength J_{ij} . The on-site interaction terms h_i and k_i represent the longitudinal and transverse fields, respectively. We consider the periodic boundary conditions so that our model describes a ring of interacting spins [161–163]. Note that three special cases can be retrieved from Eq. (5.8): i) longitudinal field Ising model (LFIM) when $k_i = 0$, ii) transverse field Ising model (TFIM) when $h_i = 0$, and iii) a special case when both $k_i = 0$ and $h_i = 0$, for which the resulting ground state of H_{prob} is the highly entangled Greenberger-Horne-Zeilinger (GHZ) state [164–167]. For simplicity, we choose the system to be homogeneous i.e., $J_{ij} = J$ as well as $h_i = h_z$ and $k_i = h_x$. To prepare an equal superposition of the qubits, as a input of the circuit ansatz, the mixing Hamiltonian is chosen as $H_{mixer} = \sum_i \sigma_i^x$. To implement DC-QAOA, as mentioned in Sec. 5.2, along with the problem and mixer Hamiltonian, we include the CD term to define the circuit ansatz. The CD operator is chosen heuristically from the operator pool A . For instance, in the case of LFIM, the ground state is ferromagnetic and constitutes a large energy gap with the first excited state for the chosen interaction strengths. In such cases, the local driving term $A_t = \sum_i \sigma_i^y$ can produce the ground state. On the other hand, the ground state of TFIM is closely spaced with the nearby excited states, which makes the local driving term insufficient. Similarly, the local driving term is also not suitable for GHZ state [93]. Instead, the second-order term $A_t = \sum_i \sigma_i^z \sigma_{i+1}^y$ is more likely to produce a better result. The unitary operator that represents the CD part of the circuit ansatz is given by

$$U_{CD}(\alpha) = \prod_{j=1}^L e^{-i\alpha A_t^q}, \quad (5.9)$$

where A_t^q represents the respective q -local CD operator chosen from the CD pool A . For instance, if $q = 1$ then $A_t^q = \{A_t\}_j$ and if $q = 2$, then $A_t^q = \{A_t\}_{j,j+1}$. The circuit is designed using the gate model of quantum computing whereas the classical optimization

is the stochastic gradient descent method. Fig. 5.2 depicts the improvement obtained by DC-QAOA over traditional QAOA. In the simulation, we study a 12-qubit system, for which we compute \mathcal{R} for different p values. For LFIM, as shown in Fig. 5.2a, $\mathcal{R} = 1$ even for $p = 1$ with DC-QAOA which constitutes considerable improvement over QAOA, that requires $p = 3$ to achieve unit \mathcal{R} . Hence, for Fig. 5.2a, the number of variational parameters required to achieve unit $\mathcal{R} = 1$ for DC-QAOA is $3p = 3$ whereas for QAOA it is $2p = 6$. We also see that, for a lower number of layers i.e., $p = 1, 2, 3$, DC-QAOA converges faster to the unit \mathcal{R} compared to QAOA. Furthermore, while DC-QAOA shows better convergence at lower depths, for the TFIM and the GHZ states, the exact ground state can only be achieved with $p \geq L/2$ layers. This effect can be attributed to the Lieb-Robinson bound [168, 169] which forces the circuits for TFIM and GHZ state to scale linearly with the system size in order to achieve unit \mathcal{R} .

To compare the resource requirements, both classical and quantum, one can inspect two crucial elements of these methods. In the case of systems with nearest-neighbor interactions, the increase in circuit depth per layer by adding a CD term will be constant, and it depends on the CD term chosen. The circuit depth can be quantified as $d \times p$, and the CD driving increases it to $(d + d_{cd}) \times p$, where d_{cd} represents the increment in depth per layer. For LFIM, the CD term σ_y gives $d_{cd} = 1$, whereas for TFIM $d_{cd} = 4$ for $\sigma_z\sigma_y$. On the other hand, the increase in parameter space due to the CD term is always from $2p$ to $3p$, making DC-QAOA advantageous specifically for low p values. In the limit of large p , the performance of QAOA and DC-QAOA becomes comparable for fixed system size.

5.4 Classical optimization problems

Thus far, we have discussed the applications of DC-QAOA for finding the ground state of the Ising model and preparing entangled states. Combinatorial optimization problems are another set of problems that can be encoded in the ground state of a quantum Hamiltonian, diagonal in the computational basis. Here we discuss the application of DC-QAOA for solving combinatorial optimization problems, where the main objective is to find the optimal solution for a given classical cost function. MaxCut is one fundamental combinatorial optimization problem that has been solved using QAOA.

For the MaxCut problem, let us consider a graph $G = (V, E)$, where V and E being the vertex set and edge set respectively. We consider a classical cost function $C(z)$ defined on binary strings $z = (z_1, z_2, \dots, z_n)$, and aim at separating the vertices into two sets so that

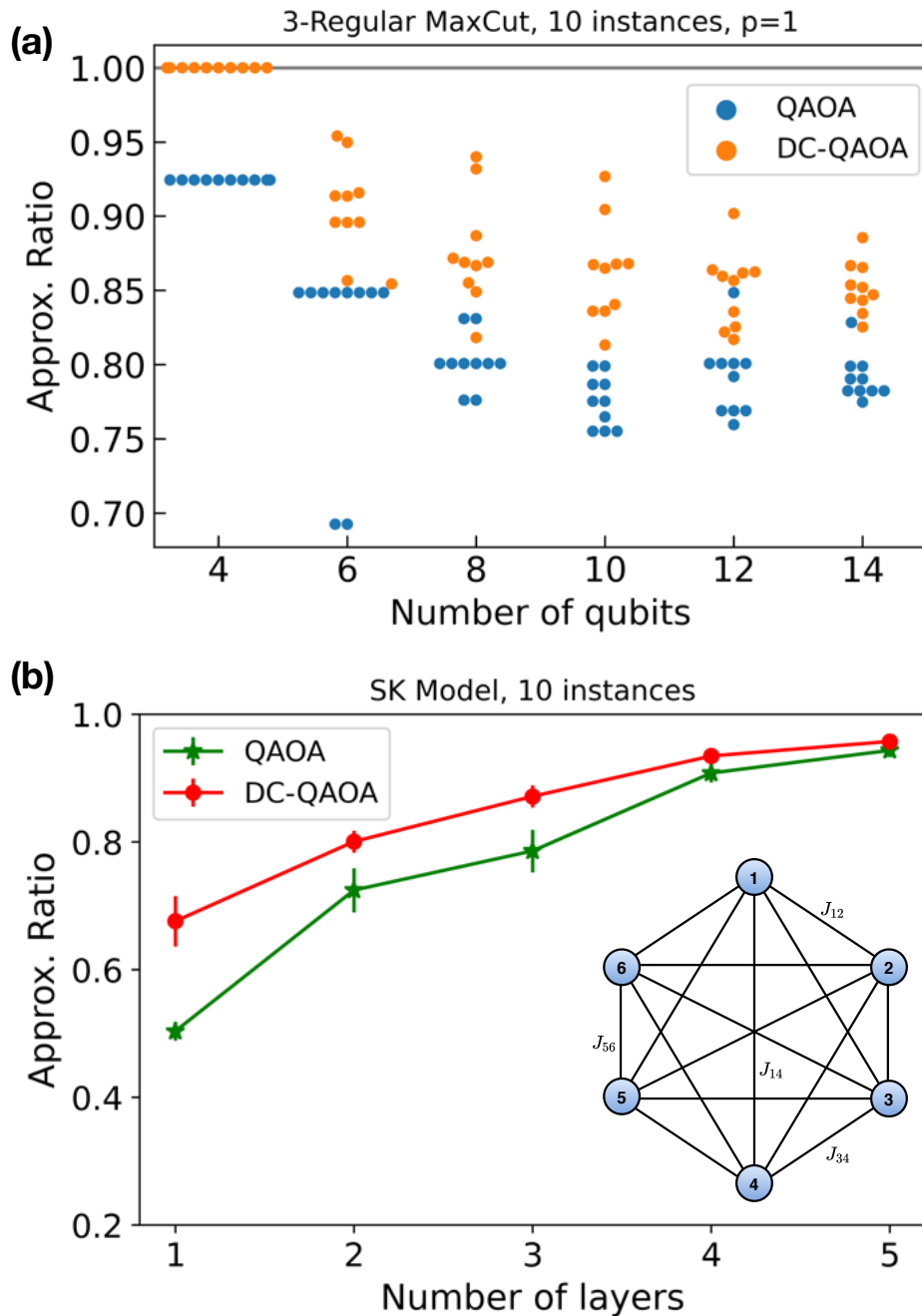


图 5.3 Comparison of approximation ratios obtained for different graph size using DC-QAOA and QAOA. (a) Unweighted 3-regular MaxCut for a randomly chosen 10 instances. (b) Approximation ratio vs number of layers (p) for SK model with 6-qubits (vertices) is depicted. Green line and red line show the values of QAOA and DC-QAOA respectively. On the right-bottom, a graph of 6 qubits with all-to-all connectivity is also shown. The results were obtained by considering 10 different randomly chosen instances of J_{ij} values. Error bars represents the standard error.

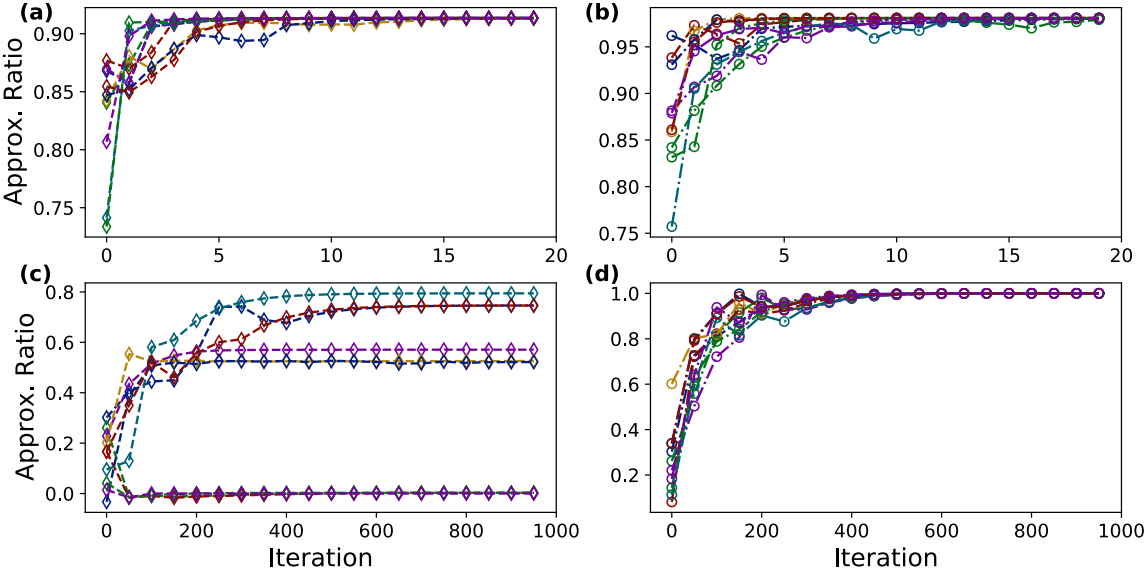


图 5.4 Comparison of approximation ratio (\mathcal{R}) with respect to number of iterations for $P = 4$ and $p = 1$. Panels (a) and (b) show the QAOA and DC-QAOA results for $h = 1$, respectively. The case with $h = 0$ is shown in panels (c) and (d) for QAOA and DC-QAOA results, respectively. The system size is $L = 6$. Each of the 10 random initial parameters chosen is represented by a color line.

the number of edges cut by $C(z)$ is *maximized*. This maximizes the classical cost function

$$C(z) = \frac{1}{2} \sum_{(i,j) \in E} w_{ij}(1 - z_i z_j), \quad (5.10)$$

where w_{ij} represents the edge weight between vertices i and j . Depending on the sets that the vertices of each edge are in after the cut, binary values (either 0 or 1) are assigned to variables z_i and z_j corresponding to respective vertices. This situation can be encoded in the ground state of the problem Hamiltonian by mapping the binary variables to Pauli operators

$$H(\sigma) = \sum_{(i,j) \in E} J_{ij} \sigma_i^z \sigma_j^z. \quad (5.11)$$

Note that Eq. (5.11) also belongs to the Ising class and is equivalent to Eq. (5.8) for GHZ states if only nearest neighbor interaction is considered, which is the case of the 2-regular MaxCut. Here, to verify the performance of our algorithm, we consider unweighted ($w_{ij} = J_{ij} = 1$) 3-regular MaxCut problem, with each vertex connected to three other vertices. The CD operator pool can be obtained from the NC expansion and is given by $A = \{\sigma^z \sigma^y, \sigma^y \sigma^z\}$. In Fig. 5.3 (a), the approximation ratio \mathcal{R} for different graph sizes with up to 14 vertices (qubits) are shown for a single layer ($p = 1$). We notice that for small graph sizes, say 4 qubits), DC-QAOA is superior as it reaches unit \mathcal{R} . However, for a bigger graph \mathcal{R} decreases gradually while exceeding the performance of QAOA. Although this can be improved for

$p > 1$ but for large depth DC-QAOA, the number of parameters for each step scales as $3p$, so the landscape of the cost function most likely has a complicated form, and we expect to see the problem of vanishing gradients (Barren plateau). A detailed analysis is needed for $p > 1$ DC-QAOA, which we leave for future work.

Interestingly, if J_{ij} is chosen as random all-to-all two-body interactions, Eq. (5.11) represents the so-called Sherrington-Kirkpatrick (SK) model. SK model is a classical spin model proposed by Sherrington and Kirkpatrick [170, 171] where J_{ij} are interaction terms such that $J = \{\forall J_{ij}\}$ has zero mean and unit variance. For instance, they can be randomly chosen from the set $J = \{-1, 1\}$ with probability $1/2$. The SK model is interesting for DC-QAOA as it can be studied as a combinatorial search problem on a complete graph. QAOA on the SK model has been extensively studied recently [172, 173]. Here, ten different instances of J_{ij} values are considered in a system of $L = 6$ spins. Note that the couplings J_{ij} are non-uniform and the CD term depends on the choice of J_{ij} . As this model involves similar interactions to that in the MaxCut problem, we chose the CD term from the same operator pool, $A = \{\sigma^z\sigma^y, \sigma^y\sigma^z\}$, calculated from the nested commutator ansatz. In fact, the CD-term chosen for the SK model is $A_t = J_{ij}\sigma_i^z\sigma_j^y$, where the operators are applied to all the sites due to its all-to-all connectivity.

In Fig. 5.3b, the approximation ratio (\mathcal{R}) is shown with respect to a varying number of layers (p). We observe that \mathcal{R} is higher for DC-QAOA as compared to QAOA and that as the number of layers increases DC-QAOA and QAOA start to converge to the same value. This shows that DC-QAOA is efficient for instances where the circuit ansatz is low-layered. In fact, for low layers, although not giving the exact ground state DC-QAOA gives significantly enhanced \mathcal{R} . This could be advantageous as we can find optimal parameters which could be used as initial parameters for high-layered QAOA.

5.5 P -spin Model

As a final benchmark, we consider the P -spin model, which is a long-range exactly-solvable fully-connected model [174–177]. The system Hamiltonian reads

$$H = -\frac{1}{L^{P-1}} \left(\sum_{i=1}^L \sigma_i^z \right)^P - h \sum_{i=1}^L \sigma_i^x . \quad (5.12)$$

While the ground-state of Hamiltonian (5.12) is trivial, the presence of a quantum phase transition makes its preparation challenging by quantum annealing [174]. For $P = 2$ this Hamiltonian exhibits a second-order phase transition whereas a first-order phase transition

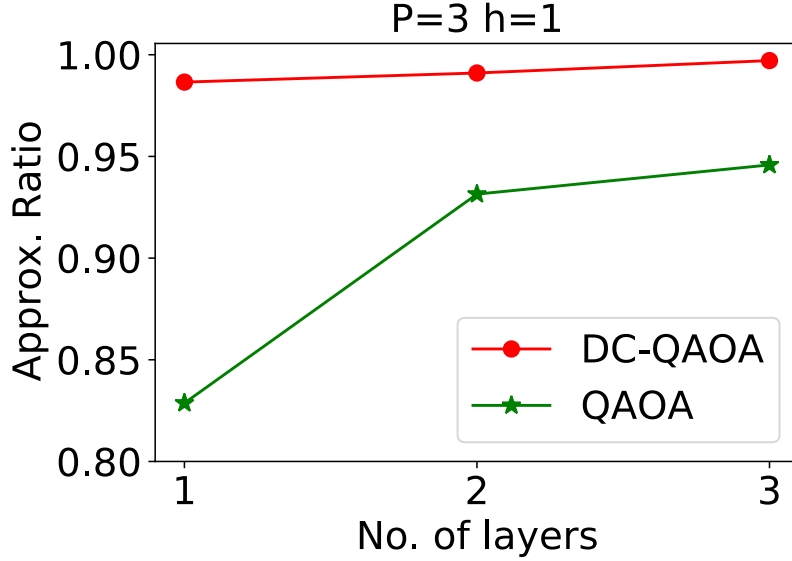


图 5.5 约束比 (\mathcal{R}) 作为层数 ($p = 1, 2, 3$) 的函数，对于 $P = 3$ 和 $h = 1$ 。绿色和红色线条显示了从 10 个随机参数初始化中获得的平均结果。标准偏差为 10^{-2} 。

occurs for $P \geq 3$, closing the energy gap exponentially with increasing system size. This has motivated proposals to change the first-order phase into second-order phase transition by making the Hamiltonian non-stoquastic [178, 179]. The nature of the ground state also depends on P . For odd P the ground state is non-degenerate, while for even P it has a two-fold degeneracy with Z_2 symmetry, which makes the choice of the CD operator difficult [62]. We study DC-QAOA in a 6 qubit P -spin model for the nontrivial case of $h \neq 0$ using local CD operator $A_t = \sum_i \sigma_i^y$. QAOA and DC-QAOA are compared for three different cases: $P = 3, h = 1$ and $P = 4, h = \{0, 1\}$ respectively. Fig. 5.4 and Fig. 5.5 shows the advantage obtained by DC-QAOA for $P = 4$ and $P = 3$ respectively. For $P = 4$, \mathcal{R} as a function of number of iterations is shown for $p = 1$ for 10 random parameter initialization. We observe that for a finite number of iterations, DC-QAOA shows higher \mathcal{R} values as compared to QAOA for both $h = 0$ and $h = 1$. It is evident that, in the case of $h = 0$, QAOA is highly dependent on the choice of initial parameters and lands into local minima in some instances. By contrast, DC-QAOA shows unit \mathcal{R} for every instance. For $P = 3, h = 1$, \mathcal{R} is shown as a function of number of layers ($p = 1, 2, 3$) for 10 random initial parameters. As expected, for DC-QAOA, \mathcal{R} values end up close to unity even for $p = 1$ and \mathcal{R} values increase as the number of layers increases. However, this is not surprising for $P = 3$ as the ground state is a product state making it favorable for the local CD operator. The more intriguing case is in Fig. 5.4b, where the approximation ratio reaches close to unity for $p = 1$ even when the ground state is degenerate. This occurs simply because the trial state converges to a

particular one of the two due to the local CD driving. This is in contrast with QAOA, which does not achieve the target state for $p = 1$ in any case.

5.6 Discussion and conclusion

In this chapter, we have introduced a quantum algorithm leveraging the strengths of shortcuts to adiabaticity for quantum approximate optimization algorithms. Specifically, we have formulated a variant of QAOA using CD driving, called DC-QAOA, and established its enhanced performance over QAOA in finding ground states of different models. We benchmark our algorithm by considering various examples, starting with Ising spin models, preparing entangled states, classical optimization problems like MaxCut and SK model and, the P-spin model. Including the CD term to the circuit ansatz, the performance of the QAOA algorithm is enhanced. Results reveal that for low-layered circuits, DC-QAOA converges to the ground state faster than state-of-the-art QAOA. Thus, adding a new free parameter in the form of a gate chosen from a predefined set (CD term) increases the performance of the algorithm for shorter circuit depths. Thus, DC-QAOA turns out to be a preferable algorithm for circuits of shorter depth.

In conclusion, DC-QAOA outperforms QAOA for all the models we have studied. For high-depth circuits, DC-QAOA can be applied for initial layers only to enhance the performance of the standard QAOA. An interesting prospect would be to use the resulting optimal parameters from low-depth DC-QAOA as the initial parameters of a high-depth QAOA in order to obtain the minima of the cost function efficiently. Our study shows that implementing principles of shortcuts-to-adiabaticity to enhance quantum algorithms has both fundamental and practical importance. The experimental realization of DC-QAOA on real hardware offers an exciting prospect for further progress.

第六章 Digitized-Counterdiabatic Quantum Factorization

Quantum integer factorization is a potential quantum computing solution that may revolutionize cryptography. Nevertheless, a scalable and efficient quantum algorithm for noisy intermediate-scale quantum computers looks far-fetched. We propose an alternative factorization method, within the digitized-adiabatic quantum computing paradigm, by digitizing an adiabatic quantum factorization algorithm enhanced by shortcuts to adiabaticity techniques. We find that this fast factorization algorithm is suitable for available gate-based quantum computers. We test our quantum algorithm in an IBM quantum computer with up to six qubits, surpassing the performance of the more commonly used factorization algorithms on the long way towards quantum advantage.

6.1 Introduction

Quantum computers have the potential to solve certain computational problems significantly faster compared to classical computers. One remarkable example is the integer factorization problem, where no classical algorithms are known to have a polynomial-time solution. In 1994, P. Shor proposed a quantum algorithm to solve the integer factorization problem in polynomial time on a universal gate-based quantum computer [4, 180]. However, we need a fault-tolerant quantum computer for reaching usefulness, which is far from the current noisy intermediate-scale quantum (NISQ) devices. Despite many demonstrations, the biggest number factored so far on an actual quantum computer using Shor’s algorithm does not go beyond two digits [181–184]. An alternative paradigm to implement factorization algorithms is adiabatic quantum computation (AdQC), which is polynomially equivalent to the gate-based model [35]. In this paradigm, we map the factorization problem to an optimization one [185], which has been implemented in several architectures [28, 186–189]. Nevertheless, due to low coherence time of quantum systems compared with the running time of algorithms in AdQC, its advantage is not clear [190]. In 2016, Barends *et al.* [36] used a digital quantum computer to implement a quantum adiabatic algorithm (QAA) by digitizing the adiabatic evolution. However, the large number of gates needed makes it still impractical for useful applications in NISQ devices.

In general, the efficiency of an algorithm is given by the run time to perform the computation. In the gate model, this run time depends on the number of quantum gates

required by the algorithm. According to the adiabatic theorem, for the digital implementation of QAA, the number of gates depends on the minimum gap in the Hamiltonian spectrum. Therefore, the circuit depth increases rapidly when the minimum energy gap decrease for the digital version of QAA. In such scenario, shortcuts to adiabaticity (STA) techniques [89, 93, 191, 192] can help us to mimic fast adiabatic evolution by suppressing the non-adiabatic transitions [40–42, 51]. In this context, counterdiabatic (CD) driving is one of the most general techniques of STA. Despite its advantages, the exact CD driving is hard to calculate, and its nonlocal nature makes it cumbersome for applications. Instead, one can consider approximate CD driving protocols [14, 105], which do not require the knowledge of the Hamiltonian spectrum for its calculation and can easily be implemented experimentally. It has been shown that, even with local CD terms, a drastic improvement in the fidelity can be obtained for many-body systems [62, 100, 155, 193, 194].

Recently, Hegade *et al.* [94] showed the advantage of considering CD terms in the digital version of QAA, which drastically decreases the circuit depth for implementing quantum algorithms. This new paradigm called digitized-adiabatic quantum computing (DAdQC) opens the door to implement efficient algorithms for the NISQ era. In this chapter, we propose an integer factorization algorithm in the DAdQC paradigm, obtaining a reduction in the number of quantum gates and improved performance, making it suitable for NISQ devices. We use two different approaches for the factorization problem: the direct optimization method and the binary multiplication table method combined with classical preprocessing. Moreover, we test our algorithm in the IBM quantum computer with up to six qubits, obtaining better fidelities in all the cases under study compared to the most popular factorization algorithms. This study shows the potential of DAdQC to advance the field towards the goal of quantum advantage for practical applications with current technology.

6.2 Approach 1: Direct optimization

Consider N to be an integer number with p and q being its prime factors, so that $N = pq = 0$. Now, we can define the cost function as

$$f(x, y) = (N - xy)^2, \quad (6.1)$$

with $x, y \in \mathbb{Z}^+$. As $f(x, y) \geq 0$, the minimum of the function ($f(x_s, y_s) = 0$) is reached only if $x_s y_s = N$, obtaining the solution of the factorization problem. Without losing generality, we will assume that N is an odd integer. It follows that the factors x and y must

also be odd numbers. To solve this problem in a quantum computer, we need to represent the factors x and y as a string of qubits. The exact length of the factors is previously unknown. However, the number of qubits sufficient to represent the prime factors in binary form requires $n_x = m\left(\lfloor \sqrt{N} \rfloor_o\right) - 1$, $n_y = m\left(\lfloor \frac{N}{3} \rfloor\right) - 1$ qubits [28]. Here, $\lfloor a \rfloor$ ($\lfloor a \rfloor_o$) denotes the greatest (odd) integer less than or equal to a , while $m(b)$ indicates the smallest number of bits required for representing b .

We encode the solution of the factorization problem in the ground state of a Hamiltonian,

$$H_f = \left[NI - \left(\sum_{l=1}^{n_x} 2^l \hat{x}_l + I \right) \left(\sum_{m=1}^{n_y} 2^m \hat{y}_m + I \right) \right]^2, \quad (6.2)$$

where $\hat{x}_l = \frac{I - \sigma_l^z}{2}$, and $\hat{y}_m = \frac{I - \sigma_m^z}{2}$. This Hamiltonian can be written in a general form as

$$\begin{aligned} H_f = & \sum_i \tilde{h}_i^z \sigma_i^z + \sum_{i < j} \tilde{J}_{ij} \sigma_i^z \sigma_j^z + \sum_{i < j < k} \tilde{K}_{ijk} \sigma_i^z \sigma_j^z \sigma_k^z \\ & + \sum_{i < j < k < l} \tilde{L}_{ijkl} \sigma_i^z \sigma_j^z \sigma_k^z \sigma_l^z, \end{aligned} \quad (6.3)$$

where \tilde{J}_{ij} , \tilde{K}_{ijk} and \tilde{L}_{ijkl} are the two, three, and four-body interaction terms, respectively. To find the ground state of this Hamiltonian, we initialize the system in the $|+\rangle^{\otimes n}$ state, which corresponds to the ground state of the initial Hamiltonian $H_i = \sum_i \tilde{h}_x \sigma_i^x$, and evolve the system adiabatically to the ground state of H_f . The total Hamiltonian thus for the adiabatic evolution can be expressed as

$$H_{ad}(t) = (1 - \lambda(t))H_i + \lambda(t)H_f, \quad (6.4)$$

where $\lambda(t) = \sin^2\left[\frac{\pi}{2} \sin^2\left(\frac{\pi t}{2T}\right)\right]$ is the scheduling function such that, $\dot{\lambda}(t)$ and $\ddot{\lambda}(t)$ vanishes at the beginning and end of the protocol. For finding the ground state of H_f , especially when the number of qubits required is large, the algorithm's run-time will be extensive. Subsequently, to perform the adiabatic evolution, the required computational cost is significantly higher which makes it rather unrealistic for implementation of factoring big numbers on a NISQ devices. These challenges can be overcome by using STA techniques by adding an auxiliary CD term $H_{CD} = \dot{\lambda}(t)A_\lambda$ to the Hamiltonian, which helps to achieve fast evolution by suppressing the non-adiabatic transitions. Here A_λ is known as adiabatic gauge potential [105, 106], and its calculation for a many-body system is a demanding task. Here, we follow the method proposed by Sels *et al.* [105] to calculate the approximate gauge potential using variational approach, where a local CD term has been introduced to enhance the performance of quantum annealing.

For the Hamiltonian in Eq. (6.4), the simplest form of the approximate CD term is an external magnetic field along the y-direction,

$$\tilde{A}_\lambda = \sum_j \alpha_j(t) \sigma_j^y. \quad (6.5)$$

Here, the local CD coefficient $\alpha_j(t)$ is calculated as

$$\alpha_j(t) = \frac{h_j^x(t)\dot{h}_j^z(t) - h_j^z(t)\dot{h}_j^x(t)}{R_j(t)}, \quad (6.6)$$

where, $R_j(t) = 2\dot{\lambda}(h_j^{x2} + h_j^{z2} + 2\sum_k J_{jk}^2 + 3\sum_{k < l} K_{jkl}^2 + 4\sum_{k < l < m} L_{jklm}^2)$. Note that, in Eq. (6.6), the scheduling function has been incorporated in the new set of parameters, $h_j^z(t) = \lambda(t)\tilde{h}_j^z$, $h_j^x(t) = \lambda(t)\tilde{h}_j^x$. The total Hamiltonian by including the CD term is $H(t) = H_{ad}(t) + \dot{\lambda}(t)\tilde{A}_\lambda$. This Hamiltonian can be written as sum of K terms with at most 4-local interactions, i.e., $H(t) = \sum_{k=1}^K H_k(t)$. For the time evolution of the system, we discretize the continuous evolution $U(0, T) = \mathcal{T} \exp\{-i \int_0^T H(t) dt\}$ using the product formula [69],

$$U(0, T) \approx \prod_{j=1}^M \prod_k \exp\{-iH_k(j\Delta t)\Delta t\}, \quad (6.7)$$

where M is the total number of discrete steps. Each term in the product can be efficiently implemented using a set of quantum gates. In Fig. 6.1, we compared the probability of obtaining the ground state measured in the computational basis for different evolution times T with and without CD driving. As in Fig. 6.1 (a), the ground state corresponding to factorization of 21 is $|111\rangle$, we can see that, even for very small total evolution time T , we can obtain $> 90\%$ success probability by adding the CD term. In Fig. 6.1 (b), the ground state corresponding to factorizing the number 91 is $|11011\rangle$, that represent the factors $q = (y_3y_2y_1) = (1101) = 13$, and $p = (x_2x_1) = (111) = 7$.

6.3 Approach 2: Binary multiplication table

For the Hamiltonian considered in Eq. (6.3), the main disadvantage is that the spectral range (ratio of largest and smallest eigenvalue) increases exponentially with the system size, which makes it inefficient in terms of resources required for the computation since the gate complexity for implementing the Hamiltonian scales with the integrated norm $\int_0^T dt \|H_{ad}(t)\|$ [195]. In order to reduce the complexity of the method, we consider the binary multiplication table to obtain the Hamiltonian using classical preprocessing [185, 186, 196, 197]. To

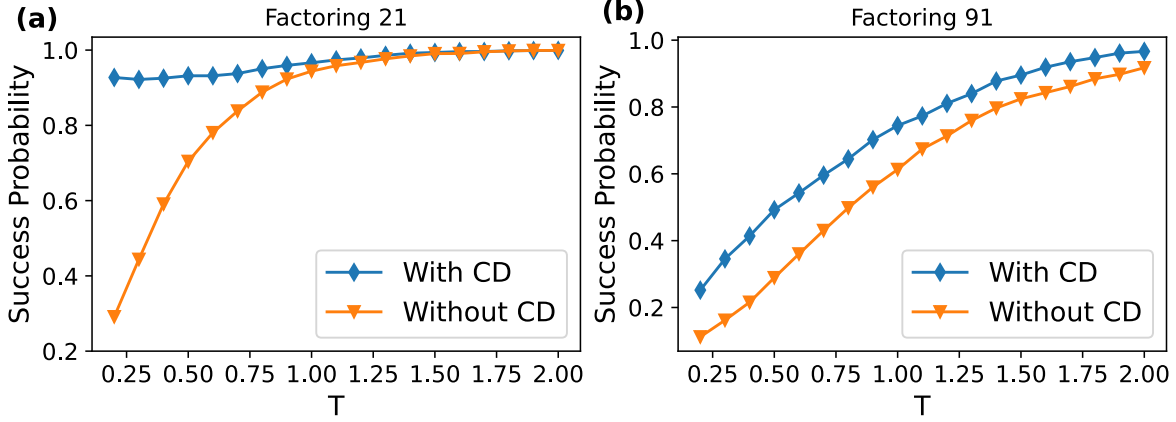


图 6.1 地态概率作为总演化时间的函数，用于因子化 21 和 91。蓝色线对应于带有局部 CD 驱动的演化，橙色线对应于不带 CD 驱动的演化。

为了说明这一点，我们考虑因子化数字 2479。因子 x 和 y 的位数 n_x 和 n_y 分别被选择为 7 和 6。由于质数是奇数，我们设置第一个和最后一个位为 1。表 I（在附录中）代表了因子化 2479 的乘法表。在这里，我们引入了二进制变量 c_{ij} 作为载体。通过添加表格中的每一列，我们获得了一组同时方程，称为因子化方程。我们进一步简化这些方程以减少总量子比特需求，通过基于二进制逻辑约束的古典预处理。该时间复杂度与简化程度成 $\mathcal{O}(n^3)$ ，即，多项式在被因子化的数字的位数上 [186]。在最终方程中变量的数量决定了所需的总量子比特数。已经观察到，在古典预处理后，所需的量子比特数与因子化规模成 $\mathcal{O}(n)$ [198, 199]，而未经任何简化则为 $\mathcal{O}(n \log n)$ [185]。最后，通过将变量映射到量子比特操作符 $q_i = (1 - \sigma_i^z)/2$ ，可以构建问题哈密顿量（见附录 A 中的详细计算）。因子化数字 2479 在古典预处理后的哈密顿量为

$$\begin{aligned}
H_f = & -2.5\sigma_1^z - 1.5\sigma_2^z + 0.75\sigma_3^z - 0.5\sigma_4^z + 0.25\sigma_1^z\sigma_2^z \\
& - 1.5\sigma_1^z\sigma_3^z - \sigma_1^z\sigma_4^z + 0.5\sigma_2^z\sigma_3^z + 1.5\sigma_2^z\sigma_4^z \\
& + 0.5\sigma_3^z\sigma_4^z + 0.75\sigma_1^z\sigma_2^z\sigma_3^z + 5.75 \mathbb{I}.
\end{aligned} \tag{6.8}$$

本地 CD 驱动方法，如前所述，通常给出更好的性能。然而，改进并不总是显著（见 Fig. 6.1b）。性能可以通过考虑 CD 哈密顿量中的更高阶项来进一步提高。最近，一种系统性方法用于构造近似 CD 驱动。

proposed by P. W. Claeys *et al.* [14], where the adiabatic gauge potential is chosen as

$$A_{\lambda}^{(l)} = i \sum_{k=1}^l \alpha_k(t) \underbrace{[H_{ad}, [H_{ad}, \dots, [H_{ad}, \partial_{\lambda} H_{ad}]]]}_{2k-1}. \quad (6.9)$$

Here, l corresponds to the expansion order, and when $l \rightarrow \infty$ we will get the exact gauge potential. By considering only the first-order expansion, we obtain the approximate CD term for the problem Hamiltonian in Eq. (6.8) as

$$\begin{aligned} A_{\lambda}^{(1)} = & 2\alpha_1(t)\tilde{h}_x \left[\sum_i \tilde{h}_i^z \sigma_i^y + \sum_{i < j} \tilde{J}_{ij} (\sigma_i^z \sigma_j^y + \sigma_i^y \sigma_j^z) \right. \\ & \left. + \sum_{i < j < k} \tilde{K}_{ijk} (\sigma_i^z \sigma_j^z \sigma_k^y + \sigma_i^z \sigma_j^y \sigma_k^z + \sigma_i^y \sigma_j^z \sigma_k^z) \right]. \end{aligned} \quad (6.10)$$

Using the variational method, we find the optimal CD coefficient $\alpha_1(t) = 0.0830/[h_x^2(1 - \lambda)^2 + 5.0112\lambda^2]$. Note that Eq. (6.10) represents a general form of the approximate CD term for an Ising spin chain that consists of a single CD coefficient. While this improves the success probability significantly, the performance can be enhanced further by introducing more coefficients that can be optimized using the variational method. In fact, we define an operator pool, restricted to only one and two spin terms that are obtained from the nested commutator (NC) expansion for $l = 1$ and $l = 2$ of Eq. (6.9), given by $\tilde{A}_{\lambda} = \{Y, Z|Y, X|Y\}$, where

$$\begin{aligned} Y &= \sum_i \alpha_i(t) \sigma_i^y, \quad Z|Y = \sum_{i < j} \beta_i(t) (\sigma_i^z \sigma_j^y + \sigma_i^y \sigma_j^z) \\ X|Y &= \sum_{i < j} \gamma_i(t) (\sigma_i^x \sigma_j^y + \sigma_i^y \sigma_j^x). \end{aligned} \quad (6.11)$$

We assume that $\alpha_i(t) = \tilde{h}_i^z \alpha(t)$, $\beta_i(t) = \tilde{J}_{ij} \beta(t)$, $\gamma_i(t) = \tilde{J}_{ij} \gamma(t)$. Fig. 6.2 shows the comparison of the success probability of obtaining the ground state using different CD terms, indicating that introducing more parameters will increase the success probability. Also, we observe that with only three trotter steps, one can obtain the prime factors of 2479 with a high probability (see the probability distribution in the appendix section A).

The cost of quantum adiabatic algorithm can be quantified by $C = T \max_{\lambda} \|H(\lambda(t))\|$ [74]. In DAdQC, the total evolution time T corresponds to the circuit depth, and the total cost corresponds to the total gate counts. Since the run time of the algorithm T depends on the minimum energy gap Δ_{min} , finding the time complexity of the adiabatic factorization algorithm with or without CD driving is a challenging task, and it is currently unknown. The

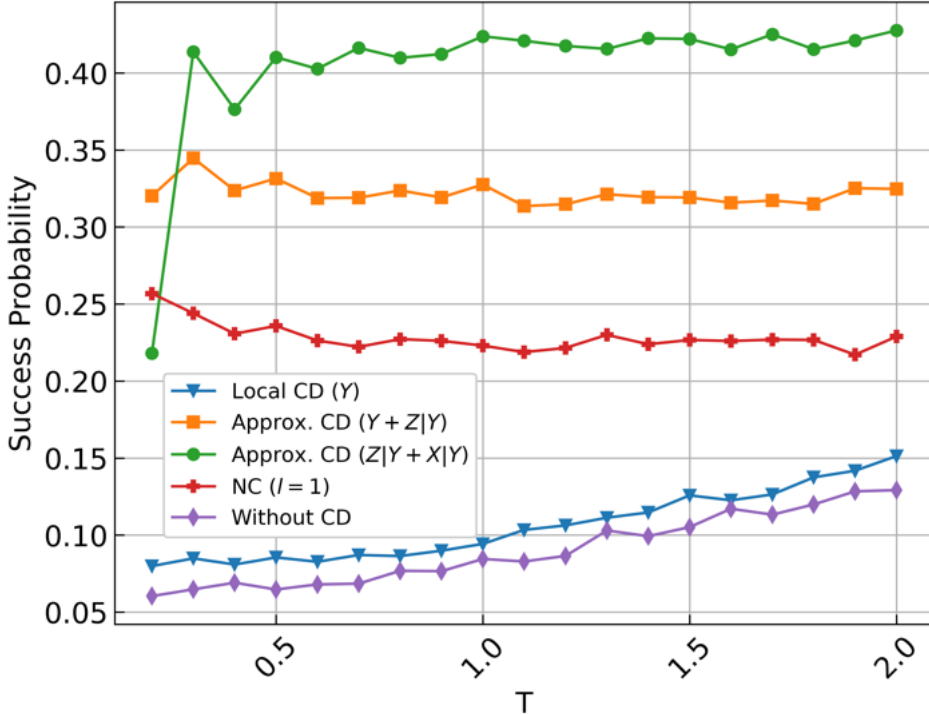


图 6.2 The success probability of obtaining the ground state ($|0100\rangle$) as a function of total evolution time for the Hamiltonian in Eq. (6.8) corresponding to factoring the number $2479 = 37 \times 67$ using the CD term with multiple parameters from Eq. (6.11) (green and orange), the CD term obtained from NC ansatz in Eq. (6.10) (red), the local CD in Eq. (6.5) (blue) and the corresponding adiabatic case (purple) by simulating on qasm simulator.

present study verifies the applicability of the proposed method for factoring small numbers with few qubits. However, some shreds of evidence support that the inclusion of the CD term can be advantageous for factoring large numbers as well since the variational CD driving has been used to study a number of many-body systems, yielding significant improvement [62, 94, 100, 105, 106, 194]. Moreover, the Hamiltonian corresponding to the factorization problem is stoquastic, and quantum Monte Carlo simulations can tackle such problems without facing any sign problem. It is believed that quantum adiabatic evolution or quantum annealing for stoquastic Hamiltonian might not give significant improvement over classical algorithms. However, the inclusion of the CD term makes the Hamiltonian non-stoquastic with imaginary entries at the off-diagonal terms, and no classical algorithms are known to implement such Hamiltonians efficiently. Also, there are several references showing that the inclusion of non-stoquastic drivers is advantageous [82, 83, 200], and for some systems, it can give exponential speedup [84]. Thus, the CD term can be considered as a type of non-stoquastic catalyst with the potential to lead to quantum speedups.

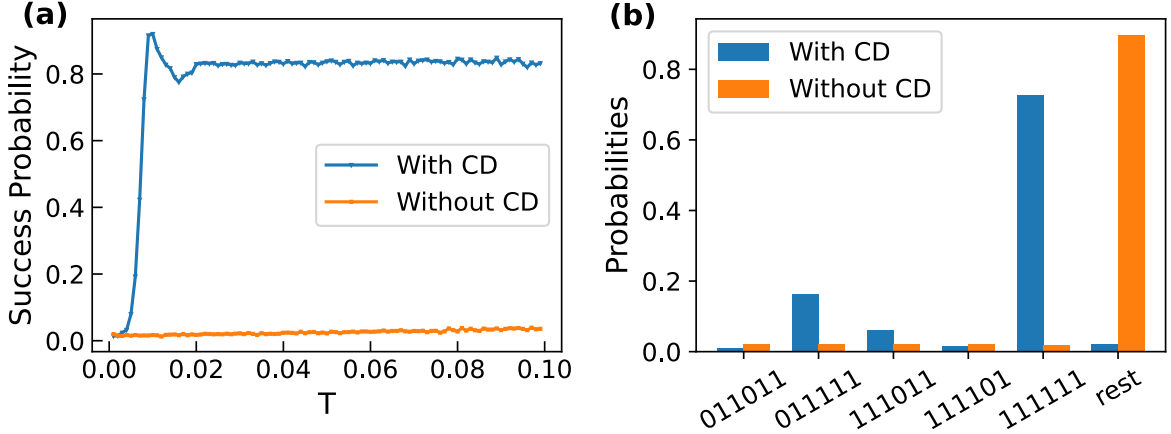


图 6.3 Factorization of $217 = 7 \times 31$: (a) The success probability as a function of total evolution time with and without CD driving using `qasm` simulator. (b) Probability distribution from 7-qubit quantum processor `ibmq_casablanca`. Parameters chosen are: $T = 0.01$, $\Delta t = 0.001$, $N_{shots} = 8192$.

6.4 Experimental analysis

For the experimental implementation of the algorithm, we consider IBM's cloud quantum computers `ibmq_vigo` and `ibmq_casablanca`, with 5-qubit and 7-qubit processors respectively. The first step in our simulation is to prepare the initial ground state $(|0\rangle + |1\rangle)^{\otimes n}/\sqrt{2}$. By applying the Hadamard gate on each qubit, we prepare this initial state with high fidelity (single qubit gate error $\sim 10^{-4}$). For the time evolution of the system, we adopt the DAdQC paradigm by discretizing the total evolution time T into a finite number of small steps of size $\Delta t = T/M$, where M is the number of time steps. Using the first-order Trotter-Suzuki formula, we approximate the evolution into a product of unitary operators corresponding to each time steps, that can be decomposed into a set of single-qubit and two-qubit gates. The corresponding digitized time evolution operator is given in Eq. (6.7). For the first-order trotterization the error is $\mathcal{O}(\Delta t^2)$ [64]. Also, since the Hamiltonian is time-dependent, the step size Δt must be smaller than the fluctuation time scale of the Hamiltonian, i.e., $\Delta t \ll \|\partial H/\partial t\|^{-1}$. An advantage of the gate model is that efficient circuit implementation for the digitized time evolution of a Hamiltonian with k-local interactions is well-known [201]. However, several sources of errors like gate error, readout error, and decoherence affect the outcome of the experiment. In order to obtain a better result, we consider readout error mitigation and circuit optimization techniques while implementing our algorithm on the actual hardware. In all our experiments, to obtain the probability distribution, we consider the number of shots, $N_{shots} = 8192$.

For the direct optimization method discussed earlier, we consider the factorization of

the number $N = 217 = 7 \times 31$, which requires at most $n = n_x + n_y - 2 = 6$ ($n_x = 3$, $n_y = 5$) qubits to represent the unknown factors. The Hamiltonian that encodes the solution of the problem in its ground state is given in the appendix section A. In Fig. 6.3 (a), we compare the ground state success probability for the evolution with local CD driving and the naive approach. Fig. 6.3 (b) is the result obtained from the quantum processor `ibmq_casablanca`. Here, we noticed that, although the original Hamiltonian contains several interaction terms, the local longitudinal fields are comparatively much stronger and dominate the evolution dynamics. Due to this, the local CD term can effectively suppress the transitions between the eigenstates. Subsequently, for the fast evolution, the CD terms become the dominant terms, and to avoid the device error, we neglected the interaction terms while implementing on the actual hardware.

For the second approach, we consider factorization of 35 and 235 using binary multiplication table. After classical preprocessing, we obtain the problem Hamiltonian, that requires 2 qubits for factoring 35 and 4 qubits for factoring 235. We consider first order NC method for obtaining the approximate CD term which contains up to two spin interaction terms. The factors corresponding to 35 have same bit length, due to exchange symmetry the ground state is a two-fold degenerate state, i.e., $(|01\rangle + |10\rangle)/\sqrt{2}$. Fig. 6.4 (a), depicts the fidelity versus evolution time for five trotter steps, where the blue line corresponds to the evolution with CD driving and orange line is for without CD driving. The solid line is for the experimentally obtained result from `ibmq_vigo`, and the dotted line is the ideal simulation result. Even though five trotter steps are depicted here, one can obtain the final ground state with experimental fidelity 0.982 with only two trotter steps, with $T = 0.002$ and $dt = 0.001$. In Fig. 6.4 (b), the probability distribution obtained from `ibmq_casablanca` for factoring the number 235 using two trotter steps are shown. Using CD driving, the final ground state $|0101\rangle$ obtained has the highest success probability. In contrast, the adiabatic case requires hundreds of steps.

6.5 Conclusions

In this chapter, we have proposed a method to speed up integer factorization using a digitized-adiabatic quantum algorithm, where the source adiabatic algorithm is enhanced via STA techniques with CD driving. We obtain a substantial improvement in the fidelities in a very short time, reducing the total gate required for the factorization problem compared to the conventional adiabatic evolution. We successfully factorized numbers bigger than

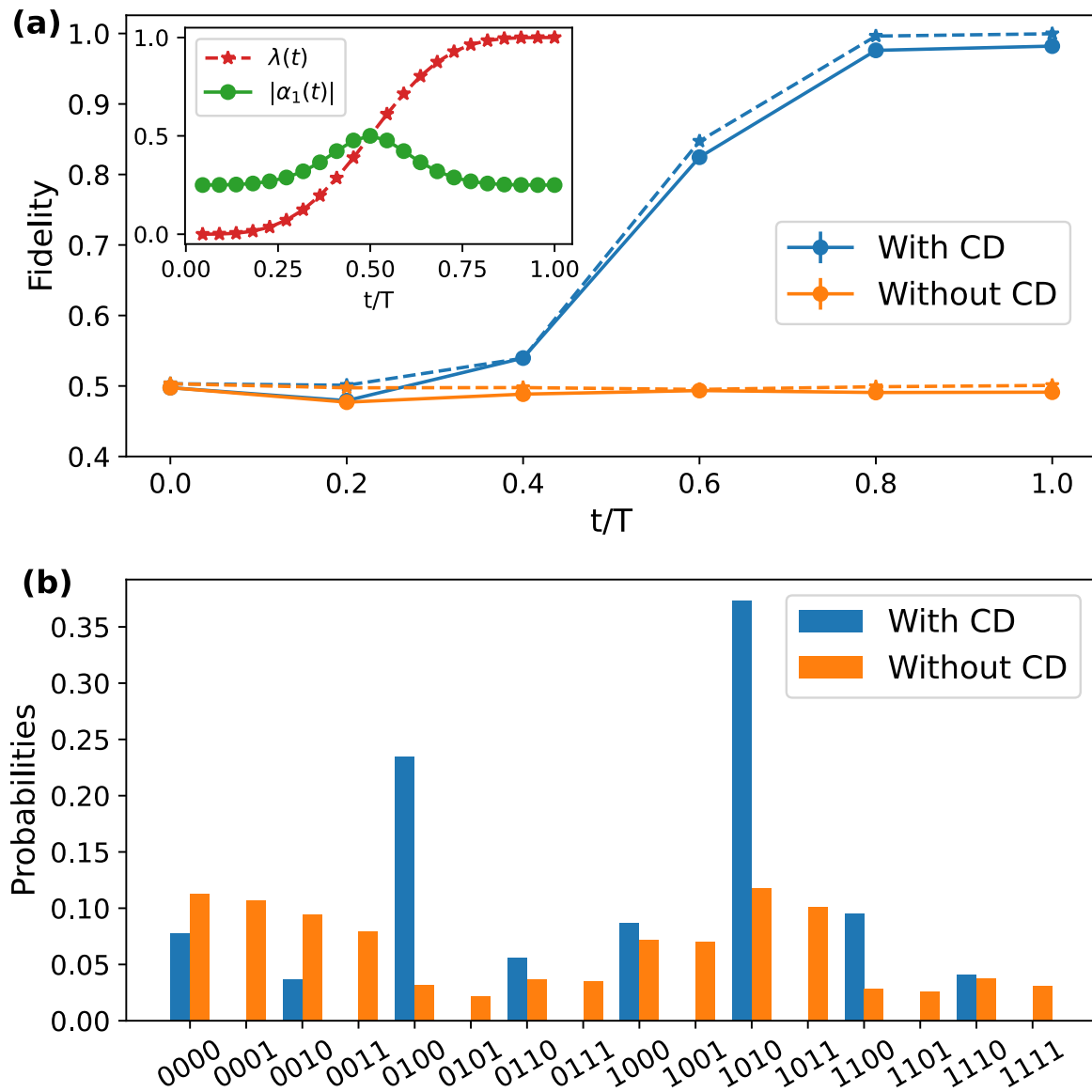


图 6.4 (a)The ground state fidelity as a function of evolution time for both with and without CD. Inset: scheduling parameter $\lambda(t)$ and the variational CD coefficient $\alpha_1(t)$ as a function of time. Experimental parameters: $T = 0.005$, $\Delta t = 0.001$, $h_x = -2$. (b) Probability distribution for factoring 235 using 4-qubits on `ibmq_casablanca` using only two trotter steps for $T = 0.02$, $\Delta t = 0.01$, $N_{shots} = 8192$.

those feasible using the Shor’s algorithm with the same number of qubits, which makes it more suitable for NISQ devices [184, 202]. Moreover, at variance with recent variational quantum factoring algorithm [198, 199], our method does not require classical optimization and, therefore, does not face the problem of local minima or barren plateaus. Furthermore, the optimal local CD coefficient can be easily calculated, and the classical preprocessing used to reduce the number of qubits requires only polynomial time.

We also show that by using more complex CD protocols, our results can be still improved. Therefore, a future direction is to go beyond current architectures with only nearest-neighbor interactions, in a co-design spirit, which can efficiently encode the problem Hamiltonian and the CD terms. In this context, recent works show an efficient alternative to implement k-local interactions [203–205], which could improve a variety of DAdQC protocols. Additionally, this chapter presents a technique to build efficient quantum algorithms that could lead to a quantum advantage when used on NISQ devices.

第七章 Portfolio Optimization with Digitized-Counterdiabatic Quantum Algorithms

In this chapter, we consider digitized-counterdiabatic quantum computing as an advanced paradigm to approach quantum advantage for industrial applications in the NISQ era. We apply this concept to investigate a discrete mean-variance portfolio optimization problem, showing its usefulness in a key finance application. Our analysis shows a drastic improvement in the success probabilities of the resulting digital quantum algorithm when approximate counterdiabatic techniques are introduced. Along these lines, we discuss the enhanced performance of our methods over variational quantum algorithms like QAOA and DC-QAOA.

7.1 Introduction

Optimization problems have been of significant interest due to their fundamental applications in many fields such as logistics, medicine, finance, among others. Nevertheless, due to their computational complexity, they cannot be solved efficiently using classical computers for industrial purposes. It is believed that a quantum computer might surpass the capabilities of a classical one. Due to the experimental developments during the last years, it might become useful for commercial purposes [206, 207]. This potential breakthrough has boosted proposals of several algorithms in different areas, such as differential equations, linear algebra, and optimization problems [208], which have been implemented in small quantum computers as proof of principle. However, the applicability of these algorithms in the current noisy intermediate-scale quantum (NISQ) devices [117] is still under investigation. This is because of the difficulty to implement scalable error-correction protocols with the current and near-future devices, a bottle neck for fault-tolerant quantum computing.

In recent years, the use of adiabatic quantum optimization (AQO) algorithms to solve optimization problems has received interest due to its experimentally feasible implementation [11, 27, 28, 30, 209]. These algorithms solve optimization problems by codifying them in the ground state of a Hamiltonian and accessing it via adiabatic evolution from another Hamiltonian, whose ground state is trivial to prepare. Current technology allows the implementation of incoherent adiabatic quantum computers or quantum annealers with thousands of qubits. Nevertheless, due to the considerable time involved in an adiabatic evolution,

such devices have various limitations like noise and limited qubit connectivity. To overcome these difficulties, the use of digitized-adiabatic quantum computing (DAdQC) [36] methods has been developed and implemented. These techniques are similar to AQO, but they digitized the evolution to implement the corresponding algorithms in a gate-based quantum computer. The convenience of digitization is that any arbitrary interactions can be included in the target Hamiltonian, providing more flexibility in choosing the optimization problem. However, it requires a large number of gates, which reduces the fidelity of the algorithms and makes them still impractical to approach quantum advantage in NISQ devices without error correction.

Other types of algorithms to solve optimization problems are the hybrid quantum-classical algorithms, like quantum approximate optimization algorithm (QAOA) [210]. In QAOA, a sequence of two evolutions is applied iteratively to an initial state. The evolution times are considered as free parameters to be optimized to minimize the cost function that encodes the solution to the problem. These evolutions are governed by a mixing Hamiltonian. Typically, a Pauli-X operation is applied to all the qubits and a problem Hamiltonian that codifies the cost function. Finally, the elapsed time of each evolution is optimized by a classical algorithm. Although QAOA is simple, it presents some major problems like the number of algorithmic layers required to optimize the cost function. This issue, in general, is hard to solve for many-body Hamiltonians, limiting the possible scalability in current NISQ devices. Additionally, classical optimization does not guarantee the reach of the global minimum, as it can get stuck into local minima, or barren plateaus may appear [147–149].

To overcome these limitations, shortcuts to adiabaticity (STA) methods were proposed. These are known to improve the adiabatic processes by circumventing the need of slow driving [39]. STA includes methods like fast-forward [45, 46], invariant based inverse engineering [43, 44], and counterdiabatic (CD) driving [40, 41, 52, 93, 100]. Among these, CD driving, i.e., the addition of an extra term that suppresses the non-adiabatic transitions, has already shown improvements in adiabatic quantum computing [150, 211] and quantum annealing [60–62].

Recently, Hegade *et al.* showed the advantage of CD driving in DAdQC methods [150], which have shown interesting improvements in many-body ground state preparations and adiabatic quantum factorization problems [211]. It was also studied that the inclusion of these approximate counterdiabatic terms could enhance the performance of QAOA while solving combinatorial optimization problems and state preparation of many-body ground states [212–214]. This chapter considers the advantages of digitized-counterdiabatic quan-

tum computing (DCQC) and digitized-counterdiabatic quantum approximate optimization algorithms (DC-QAOA) in financial applications. In particular, we investigate the Markowitz portfolio optimization problem [215], a common problem used intensively by financial asset managers. This problem deals with how to optimize the weights of the assets in a portfolio to give out returns based on the requirements of the asset manager, as is the case of maximum return and minimum risk. We select a large number of data instances and solve the problem using the DAdQC combined with CD-driving protocols. By considering variational minimization techniques, we obtain the approximate CD terms, getting a drastic enhancement in the success probability for most of the selected instances. We also show that the inclusion of these CD terms in hybrid quantum-classical algorithms like QAOA, namely DC-QAOA, results in an improvement in success probabilities. This chapter demonstrates the relevance of CD driving, its limitations, and its applicability to finance industry problems in the NISQ era.

7.2 Markowitz portfolio optimization

Suppose an asset manager is willing to invest a budget b in a given portfolio with n number of assets. Markowitz portfolio optimization [215] answers the question: How to distribute the given budget b into n assets such that the asset manager would receive maximum returns at minimum risk. For example, the asset manager could invest evenly in all the assets, but that may not be the best choice. Given the expected returns of each asset x_i and the risk associated with the assets, applying Markowitz portfolio optimization, we can predict the distribution of the budget b to get the maximum returns out of the portfolio. Expected returns can be estimated from the preceding market return data, and the risk is assessed via a covariance matrix. As the name suggests, a covariance matrix shows the covariance of different stocks in the portfolio. Thus, these types of problems are classified as mean-variance portfolio optimization problems.

The portfolio optimization problem has two components, the cost function, and the constraints. The cost function includes quantities such as the average returns, the variance of the portfolio, and others that need to be maximized or minimized based on the need of the asset manager, while the constraints can include budget constraints or transition costs, or market inflation. Based on the constraints, portfolio optimization problems can be broadly divided into three types. The first type of optimization problem is unconstrained portfolio optimization, where the constraints are added as the penalty terms in the cost function with

the help of Lagrange multipliers. The second type is when the constraints can be represented as inequalities, and the third type is when the constraints are integer constraints, the so-called mixed-integer problem. Examples and computational complexities of all these problems are discussed in Ref. [216]. Different types of these portfolio optimization problems have been solved recently using quantum computing [217–224].

As far as the variables are concerned, portfolio optimization can be solved as a continuous-variable and discrete-variable problem. Discrete mean-variance optimization proves to be a beneficial method to optimize the given portfolio in cases where the assets are traded in lots, which are integer multiples of a base size of assets traded. Thus, the asset manager will only be interested in the number of lots which makes the problem discrete. In consequence, we will investigate here an unconstrained single-period discrete mean-variance portfolio optimization problem using the digitized-counterdiabatic quantum computing paradigm.

Our task is to distribute b budget into n assets with mean returns m_i and the co-variance matrix ρ_{ij} to maximize returns at a minimum variance. The problem can be formulated as

$$\max_x \sum_{i=1}^n \theta_1 m_i x_i - \theta_2 \rho_{ij} x_i x_j - \theta_3 (G_f b x_i - b)^2, \quad (7.1)$$

where x_i are the assets represented by integers. The first term of Eq. (7.1) indicates the expected returns, where m_i are the daily return data, and the second term shows the variance of the portfolio, where ρ_{ij} show the variance of j th asset with i . The market data (m_i and ρ_{ij}) is easily available and can be generated in various ways [225, 226]. The third term shows the constraint applied to the budget. Most of the times, asset managers have a certain budget to follow, so this term penalizes the solutions that do not satisfy the budget criteria. The term G_f in Eq. (7.1) shows the granularity function which is given by $G_f = 1/2^{(g-1)}$, where g is the number of slices of the budget. This implies that the fraction of the budget that can be chosen is $G_f b x_i$. To explain this, assume that we set $g = 2$, so the budget is cut into two slices giving $G_f = 1/2$. Therefore, we have $b/2$ weight of the budget that can be invested in required assets. In other words, granularity function decides how small a fraction of b you can invest in a particular stock. Thus, with increasing the value of slice g , we get the freedom to invest smaller fractions of the budget which will give us more precision while deciding the optimal results. θ_1 , θ_2 and θ_3 are the Lagrange multipliers and their role is to adjust weights of different terms to adjust constraints according to the manager's requirements. For instance, if the manager is less concerned about the risk and more interested about the returns, we can set θ_1 higher than θ_2 such that the expected return term is given more weight.

Once these terms are determined, we can convert Eq. (7.1) into an Ising Hamiltonian. To do so, we start with transforming Eq. (7.1) into a quadratic unconstrained binary optimization problem (QUBO) by encoding assets x_i integers into an g bit binary number. Apart from binary encoding, various ways of encoding like unary, sequential, and partition have been proposed [219]. Hence, x_i 's are given by

$$x_i = \sum_{k=1}^g 2^{k-1} z_{u(i,k)}, \quad (7.2)$$

where $u(i, k) = (i - 1)g + k$ and $z \in \{0, 1\}$. This problem can be transformed into a QUBO problem by substituting x_i 's from Eq. (7.2) into Eq. (7.1). After making some rearrangements and transformation $z_i = \frac{1}{2}(1 + \sigma_i^z)$, we get an Ising Hamiltonian given by

$$H_p = \sum_i h_i \sigma_i^z + \sum_{i,j} J_{ij} \sigma_i^z \sigma_j^z + \beta, \quad (7.3)$$

where J_{ij} shows the interaction coefficient between the spins i and j , while h_i shows the coefficient associated with the local field along the z -axis. Explicit forms of these coefficients read

$$J_{ij} = \frac{1}{4}(\theta_2 b^2 G_f^2 + \theta_3 \rho_{i,j}), \quad (7.4)$$

$$h_i = \frac{(-\theta_1 m_i - 2\theta_2 b^2 G_f)}{2} + \sum_j J_{i,j}, \quad (7.5)$$

with a constant β that can be ignored. In this manner, we have transformed Eq. (7.1) into an Ising Hamiltonian such that its ground state encodes the solution to the optimization problem. In the following sections we show application of digitized-counterdiabatic quantum computing methods to find this ground state.

7.3 Digitized-counterdiabatic quantum computing

To find the ground state of the Hamiltonian in Eq. (7.3), we follow the adiabatic theorem by starting with an initial Hamiltonian whose ground state can be easily prepared, and slowly turn on the problem Hamiltonian. The corresponding total Hamiltonian can be expressed as

$$H_{ad}(\lambda) = (1 - \lambda)H_i + \lambda H_p, \quad (7.6)$$

where λ is a time dependent scheduling function. We choose the initial Hamiltonian as $H_i = -\sum_i^N h^x \sigma_i^x$, whose ground state $|\psi(0)\rangle = 2^{-N/2}(|0\rangle + |1\rangle)^{\otimes N}$ can be easily prepared.

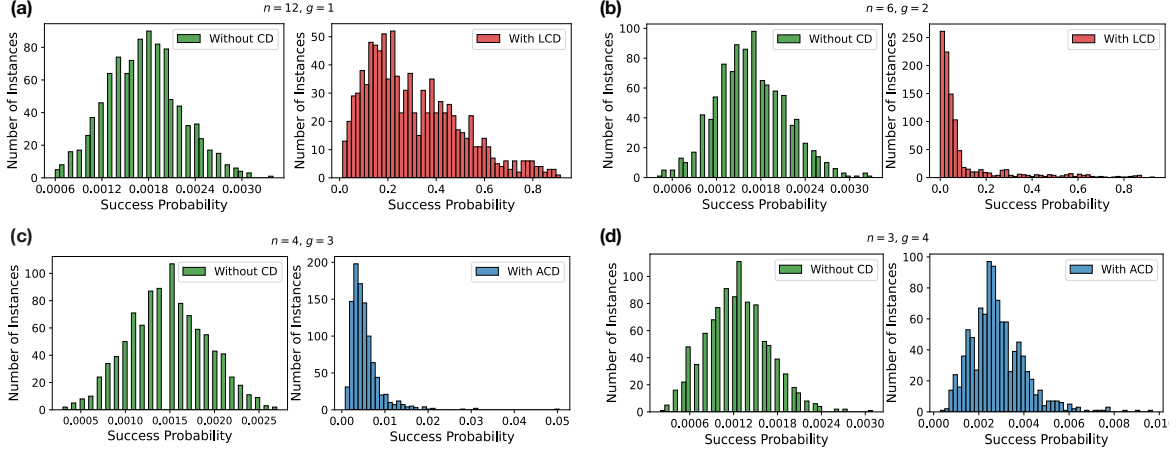


图 7.1 Histogram depicts the ground state success probability for 1000 randomly chosen instances of the portfolio optimization problem with and without CD driving. We considered 12 qubit systems with different numbers of assets (n) and partitions (g). When the number of partitions is smaller, the LCD in Eq. (7.8) gives a better enhancement. Whereas, when g is larger, ACD from Eq. (7.12) shows greater improvement. The simulation parameters are, total evolution time $T = 1$, and the step size $\Delta t = 0.05$.

If the evolution is slow enough, the adiabatic theorem guarantees that the final state will have a large overlap with the ground state of the problem Hamiltonian. In principle, to obtain the ground state with a higher success probability, one has to consider the total evolution time T much larger than the minimum energy gap Δ_{min} between the ground state and the first excited state. However, in practice, one can not rely on the adiabatic evolution due to limited coherence time, and device noise. One has to consider a short time evolution that will lead to non-adiabatic transitions between the eigenstates. In order to suppress these transitions, a technique called shortcuts to adiabaticity was developed [38, 191]. The idea is to introduce an additional term called counterdiabatic-driving term (CD term) so that the excitations due to the finite time evolution will be compensated, and the resulting evolution will be quasi-adiabatic. The modified Hamiltonian by adding the CD term takes the form

$$H(t) = H_{ad} + \dot{\lambda}A_\lambda, \quad (7.7)$$

where $\dot{\lambda}$ infers how fast our evolution is, and A_λ is called adiabatic gauge potential [13], which satisfies the condition $[i\partial_\lambda H_{ad} - [A_\lambda, H_{ad}], H_{ad}] = 0$. In principle, one can evolve the system very fast without any excitation by including the CD term. However, obtaining the exact gauge potential for a many-body system is a difficult task. Also, the operator form of the CD term for a many-body system with N interacting spins generally contains non-local N-body interaction terms, which makes it experimentally challenging to realize. To overcome this challenge a variational method was proposed to obtain an approximate CD

term [13]. And, many recent work shows the advantage of using variationally calculated local CD terms for different applications [100, 227, 228]. The main advantage of this method is that, the approximate local CD terms can be easily implemented in lab and its calculation does not require any knowledge of the instantaneous eigenstates. This feature makes it suitable for adiabatic quantum computation.

For the Hamiltonian (7.3), we choose the local CD term of the form $\tilde{A}_\lambda = \sum_i^N \alpha_i(t) \sigma_i^y$. Here, the CD coefficient $\alpha_i(t)$ is obtained by minimizing the action $S = \text{tr}[G_\lambda^2]$, where $G_\lambda = \partial_\lambda H_{ad} + i[\tilde{A}_\lambda, H_{ad}]$,

$$\alpha_i(t) = -\frac{h^x h_i^z}{2 \left(h^{x^2} [\lambda - 1]^2 + \lambda^2 \left[h_i^{z^2} + \sum_{i \neq j} J_{ij}^2 \right] \right)}. \quad (7.8)$$

The CD term should vanish at the beginning and end of the protocol, for that we consider the scheduling function as $\lambda(t) = \sin^2 \left[\frac{\pi}{2} \sin^2 \left(\frac{\pi t}{2T} \right) \right]$, also $\dot{\lambda}$, and $\ddot{\lambda}$ vanishes at $t = 0$ and $t = T$. The time evolution including the CD term is given by

$$|\psi(T)\rangle = \mathcal{T} e^{-i \int_0^T H(t) dt} |\psi(0)\rangle = U(0, T) |\psi(0)\rangle. \quad (7.9)$$

For the gate-model implementation of the evolution, we write the total Hamiltonian as sum of 2-local terms, i.e. $H(t) = \sum_j c_j(t) H_j(t)$. We discretize the total time into M parts with step size $\Delta t = T/M$. Using the Trotter-Suzuki formula, we approximate the time evolution operator as

$$U_{\text{dig}}(0, T) = \prod_{k=1}^M \prod_j \exp \{-i \Delta t c_j(k \Delta t) H_j\}. \quad (7.10)$$

In this study, we only considered first-order trotterization, which leads to an error of the order $\mathcal{O}(\Delta t^2)$. Using single-qubit and two-qubit gates, each matrix exponential term in Eq. (7.10) can be easily implemented. Since the Hamiltonian involves all-to-all connection between the qubits, extra swap gates might be needed on a device with only nearest neighbour interactions. We consider a wide range of portfolios where the data (m_i and ρ_{ij}) is randomly generated such that it mimics the real world trends. $\theta_1 = 0.3$, $\theta_2 = 0.5$ and $\theta_3 = 0.2$ are selected so that the budget constraint is given greater importance. We run 1000 different instances and system sizes upto $N = 14$ qubits with different number of stocks n and slicing g .

Since current NISQ devices can only implement circuits of limited depth, we consider a short-time evolution and compare the final success probability with and without including the CD term. In Fig. 7.1, the ground state success probability for 1000 randomly chosen

instances of the portfolio optimization problem is depicted for a system size $N = 12$. In Fig. 7.1a, the number of assets and the slices are chosen as $n = 12, g = 1$, respectively. And, in Fig. 7.1b, $n = 6, g = 2$. We fix the total evolution time $T = 1$, and step size $\Delta t = 0.05$ with total 20 Trotter steps. In both cases, the local CD (LCD) term $H_{LCD} = \dot{\lambda} \sum_i^N \alpha_i(t) \sigma_i^y$ is considered.

We observe that when the number of slices is less, the LCD terms drastically improves the success probability for most of the instances. However, as g becomes larger, the performance of LCD terms will be decreased. Previously, it was shown that the density of states close to the ground state would also become larger with the increasing number of slices, leading to an increase in the probability of transition to the higher excited states [218]. In order to suppress these transitions, we considered higher-order CD terms obtained by the nested commutator (NC) ansatz [14],

$$A_\lambda^{(l)} = i \sum_{k=1}^l \alpha_k(t) \underbrace{[H_{ad}, [H_{ad}, \dots, [H_{ad}, \partial_\lambda H_{ad}]]]}_{2k-1}. \quad (7.11)$$

Here, l corresponds to the expansion order, and when $l \rightarrow \infty$ we will get the exact gauge potential. By considering only the first-order expansion ($l = 1$), we obtain the approximate CD (ACD) term for the problem Hamiltonian in Eq. (7.3) as

$$H_{ACD} = 2\dot{\lambda} h^x \alpha_1(t) \left[\sum_i^N h_i^z \sigma_i^y + \sum_{i,j} J_{ij} (\sigma_i^y \sigma_j^z + \sigma_i^z \sigma_j^y) \right], \quad (7.12)$$

where $\alpha_1(t)$ is obtained as before by minimization of the action $S = \text{tr}[G_\lambda^2]$. The general expression for $\alpha_1(t)$ for an Ising spin-glass Hamiltonian is given in [229]. In Figs. 7.1c and 7.1d, we considered $g = 3$, and $g = 4$, respectively, and compare the probability of success for different instances by including ACD and without including the CD term. The CD solutions depend upon the choice of instances which can be either easy or hard depending on the value of the slicing parameter g . As follows from Eq. (7.4) and (7.5), the local field h_i is significantly large compared to the interaction term J_{ij} for lower values of g that translates into a weakly coupled Ising system. Consequently, for $h_i \gg J_{ij}$, the success probability can be improved drastically using the Local CD driving due to relatively larger energy gaps which are in accordance with Fig. 4.2a and 4.2b [150]. Such instances are referred to as easy ones. On the other hand, the hard instances occur when g is large, we obtain a strongly coupled Ising Hamiltonian where $h_i \approx J_{ij}$. In such cases, we need to take the aid of the approximate CD driving to show the enhancement in the success probability (see Fig. 4.2c and 4.2d). Nonetheless, in both cases, we can obtain an enhancement of at least up to an

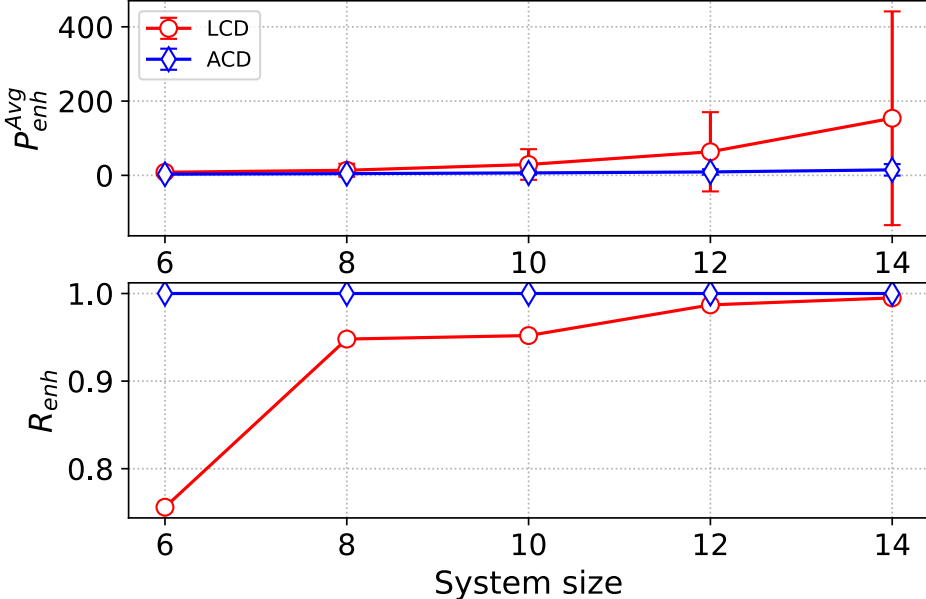


图 7.2 The upper plot depicts the average success probability enhancement (Eq. (7.14)), and the lower plot represents the enhancement ratio (Eq. (7.13)) for various system sizes with LCD and ACD. The error bars represent the standard deviation. Due to the huge variations in the success probability enhancement for different instances using LCD, the error bars have larger values.

order of magnitude.

To show the enhancement that results from applying the CD term, we define a metric called enhancement ratio,

$$R_{enh} = \frac{I}{I^0}, \quad (7.13)$$

where I^0 is the total number of instances considered, and I denotes the number of instances with enhanced success probability by including the CD term. The enhancement that results from applying the CD term is quantified by the success probability enhancement,

$$P_{enh} = \frac{P}{P^0}. \quad (7.14)$$

Here, P is the ground state success probability by including the CD term, and P^0 is the success probability obtained by naive evolution without the CD term. Fig. 7.2 depicts the average success probability enhancement and enhancement ratio for various system sizes by including the CD driving. We observed that for ACD the enhancement ratio is 1, indicating that it is always advantageous to include the approximate CD terms obtained from the first-order NC ansatz with fixed $g = 2$. The simulation result indicates that the enhancement with the CD term will increase with the system size. In Fig. 7.4, the ground state success probability as a function of total evolution time T is shown. The result shows that a huge

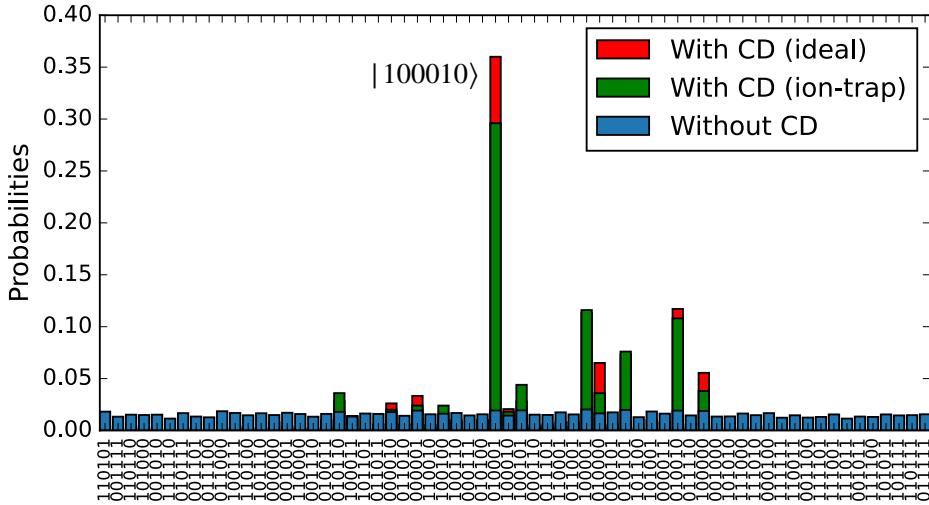


图 7.3 Output probability distribution of an instance with $n = 3$ and $g = 2$. We considered $T = 0.3$, and $\delta t = 0.1$. The green bar corresponds to the results obtained from Quantinuum's H1 emulator, which mimics the noise model of the hardware Model H1. The red and blue bars are for the ideal simulation results with and without including the CD terms, respectively. The ground-state bitstring is also shown.

enhancement can be obtained for both LCD and ACD. For Fig. 4.3, we selected 40 random instances, and each colored line depicts one of the instances considered. It can be observed that two particular instances achieve better success probability than the rest while using LCD. This is due to the fact that those particular easy instances have a significantly larger energy gap compared to other instances. This can be verified from Fig. 4.3a, where, even in the adiabatic case, those two instances give better success probability referring to the existence of a larger gap, which makes the suppression of non-adiabatic contributions easier with LCD.

To make our arguments even more concrete, we also implemented a $N = 6$ qubit system with $n = 3$, $g = 2$ on an emulator that closely mimics the noise model of the hardware *Quantinuum System Model H1*, which is an all-to-all connected trapped-ion quantum computing system with 20 qubits. Trapped-ion systems are a good choice for this problem because of their all-to-all connectivity, making it easier to implement the interactions without using any additional SWAP gates. In our implementation, we initialize all the qubits in $|+\rangle$ state, which corresponds to the ground state of the initial Hamiltonian and then apply the digitized time evolution with the help of the native gates provided by the device. As the two-qubit $ZZ(\theta)$ gate is native to this hardware, we can efficiently implement the matrix exponential terms in Eq. (7.10) without relying on the standard decomposition with CNOTs. And finally, we measure the final state on a computational basis. We have selected a total time evolution for the noisy simulation as $T = 0.3$, with step size $\delta t = 0.1$, which gives

three Trotter steps. The number of shots is set to $N_{shots} = 500$ and the ground-state of the instance we investigate is $GS = |100010\rangle$. Since the time scale we chose is small, the CD terms are dominant for this fast evolution. While implementing on the hardware, we could discard the term H_{ad} to reduce the gate counts without affecting the success probability. In Fig. 7.3, we have plotted the probability distribution obtained at the end of the evolution without CD term and with ACD. Even with just three Trotter steps, the evolution with ACD gives the ground state with very high success probability compared to the without CD case. We remark that this performance will be similar when the real device is used. Evidently, CD driving does perform well even in the presence of noise, and we can still get a drastic enhancement over the usual digitized adiabatic evolution making our algorithm suitable for NISQ devices.

7.4 Digitized-counterdiabatic quantum approximate optimization algorithm

Hybrid quantum-classical optimization algorithms like QAOA [210] have been of interest due to their applicability in the noisy intermediate-scale quantum (NISQ) devices. These algorithms fall under the class of variational quantum algorithms, where classical optimization routines are employed to find suitable parameters (γ, β) that optimize a cost function $C(\gamma, \beta)$. In our case, we have set $C(\gamma, \beta) = \langle \psi_f(\gamma, \beta) | H_p | \psi_f(\gamma, \beta) \rangle$ such that $C(\gamma, \beta)$ shows the expectation value of the problem Hamiltonian H_p and $|\psi_f(\gamma, \beta)\rangle$ is provided by

$$|\psi_f(\gamma, \beta)\rangle = U(\gamma, \beta) |\psi_i\rangle, \quad (7.15)$$

where $|\psi_i\rangle = |+\rangle^{\otimes N}$ is the initial state corresponds to the mixer Hamiltonian and

$$U(\gamma, \beta) = U_m(\beta_p) U_c(\gamma_p) U_m(\beta_{p-1}) U_c(\gamma_{p-1}) \dots U_m(\beta_1) U_c(\gamma_1). \quad (7.16)$$

Here, $U_b(\beta)$ and $U_c(\gamma)$ are two unitaries corresponding to the mixer and the problem Hamiltonian, respectively, applied iteratively for p layers. At $p \rightarrow \infty$, QAOA is expected to converge to the ground state of any problem Hamiltonian because it mimics the adiabatic evolution. However, experimentally realising large p circuits is difficult due to the noise, hence, significant research has been done recently to improve the performance of low p QAOA circuits. Over the years, many modifications have been reported in the standard QAOA [145, 146, 212–214, 230] to serve this purpose. Among them, the addition of

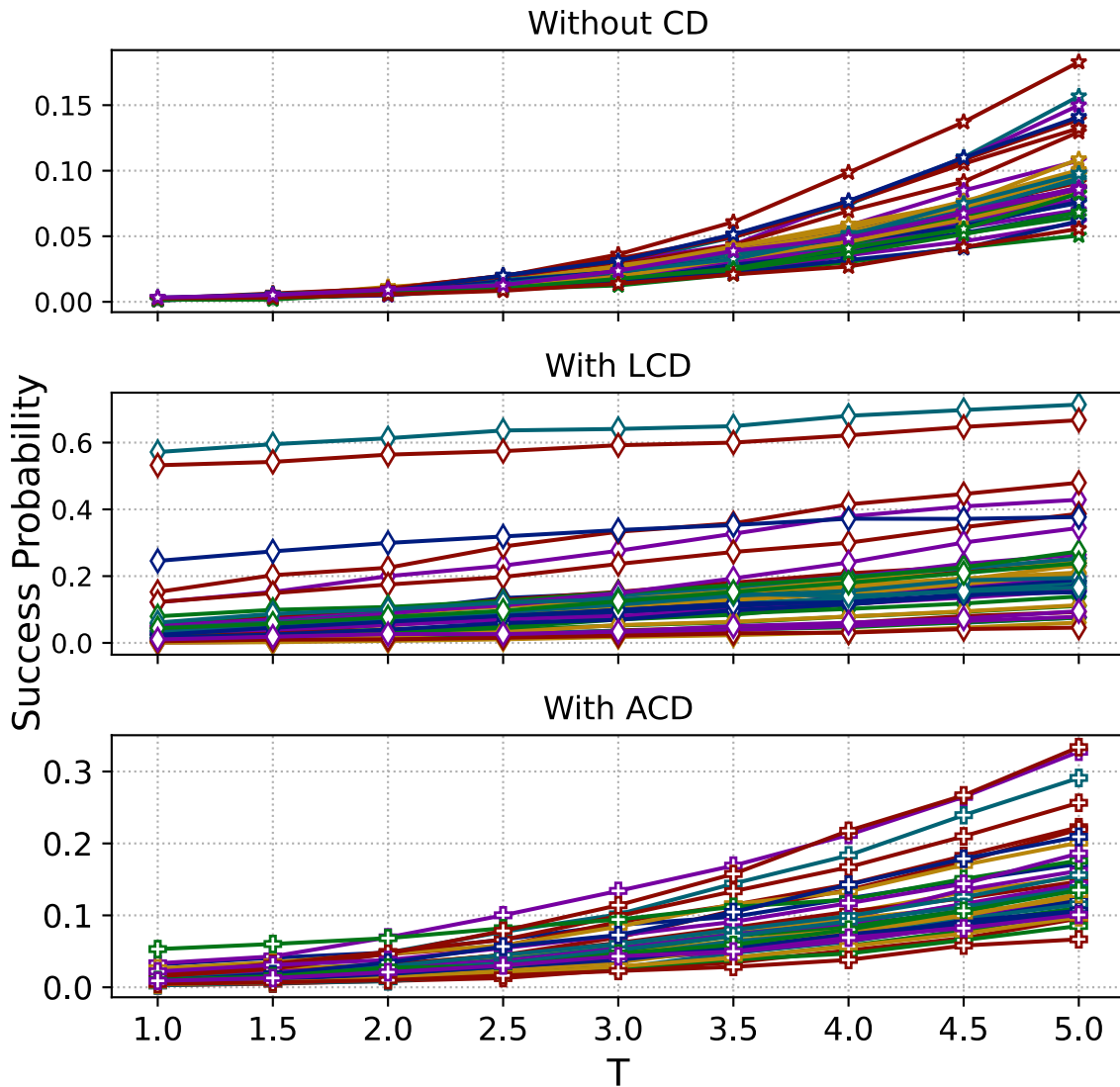


图 7.4 Success probability as a function of total evolution time T for randomly chosen 40 instances is depicted. Here we considered $n = 6$ assets and $g = 2$ partitions resulting in system size $N = 12$. A substantial improvement in success probability is obtained for most of the instances by including the local CD term H_{LCD} , and the approximate CD term H_{ACD} . Here, we considered the Trotter step size as $\Delta t = 0.1$. Different colored lines show each of the 40 instances.

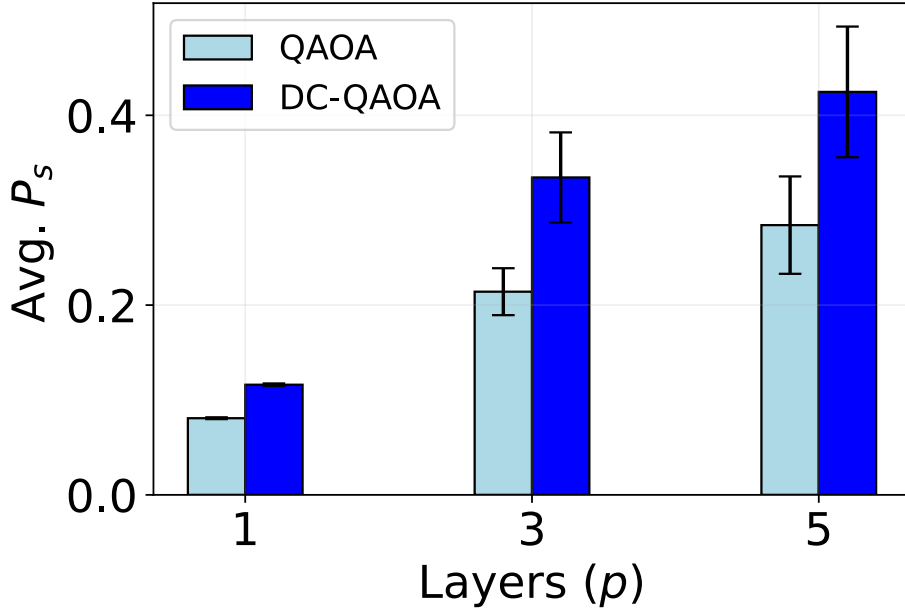


图 7.5 Average success probability (P_s) as a function of number of layers for a $N = 6$ system with $n = 3, g = 2$. Results show the mean success probability obtained after considering 10 instances and 20 random initialization in each instance. Error bars represent the variance of the distribution. Stochastic gradient descent based optimizer called adagrad optimizer with step size = 0.1 was used as the classical optimizer for all instances.

terms using counterdiabatic (CD) protocols has shown significant improvements, specially in finding the ground-state of many-body Hamiltonians [212–214]. One of the algorithms following the same principle is the digitized-counterdiabatic quantum approximate optimization algorithm (DC-QAOA) [213]. In DC-QAOA, CD protocol is utilized to introduce an additional CD unitary $U_D(\alpha)$. The form of CD unitary is chosen from the operator pool $A_\lambda^{(l)}$ obtained using the nested commutator (NC) method as mentioned in Sec. 7.3. Therefore, three unitaries $U_b(\beta)$, $U_c(\gamma)$ and $U_D(\alpha)$ are applied iteratively while performing DC-QAOA. In this section, we perform QAOA and DC-QAOA for 10 instances of portfolios with system size $N = 6$ qubits ($n = 3, g = 2$) with $\theta_1 = 0.3, \theta_2 = 0.5$ and $\theta_3 = 0.2$ to compare the obtained success probabilities (P_s) and demonstrate the advantage of CD induced variational quantum algorithms for portfolio optimization.

In QAOA, p -layers of $U_b(\beta) = e^{-i\beta \sum_i \sigma_i^x}$ and $U_p(\gamma) = e^{-i\gamma H_p}$, where H_p is given by Eq. (7.3), are applied to the initial state $|\psi_i\rangle$. In DC-QAOA, $U_D(\alpha) = e^{-i\alpha \sum_i h_i \sigma_i^y}$ is added, where σ^y is a local first-order term chosen from an operator pool $A_\lambda^{(2)} = \{\sigma^y, \sigma^z \sigma^y, \sigma^y \sigma^z, \sigma^x \sigma^y, \sigma^y \sigma^x\}$ which is obtained from Eq. (7.11). Parameters (γ, β, α) are updated using a stochastic gradient descent (SGD) based classical optimizer called Adagrad optimizer [160] with step size = 0.1.

Fig. 4.5 shows the mean success probabilities (P_s) as a function of number of layers (p) for $N = 6$ system with $n = 3, g = 2$. Results show the mean of the 10 different instances where each instance is the best output chosen from 20 runs of different random initial parameters for each layer. We observe that by using DC-QAOA, improvement in the P_s value is achieved for all the instances. The higher error bars show that even for the same system size and values of n and g , the performance of DC-QAOA and QAOA depends upon the energy landscape and the choice of the CD operator. This improvement by using DC-QAOA can be attributed to the fact that the introduction of a free parameter makes the Hilbert space more accessible to the optimizer, so it increases the expressibility of the circuit ansatz. The high variances can also be attributed to the fact that the performance of these algorithms depends upon the initial parameters and the classical optimizer chosen. In particular, classical optimizers and its step sizes play a significant role in improving the performance of the algorithm. Nevertheless, a considerable improvement can always be achieved using DC-QAOA over the conventional QAOA algorithm. Moreover, here we have used local CD operators only, but in the typical hard instances, higher-order CD terms might give more improvement. However, the inclusion of these higher-order CD terms might also increase the effective circuit depth to a larger extent which can induce errors, reducing the advantages of DC-QAOA.

7.5 Conclusion

We studied the financial portfolio optimization problem using digitized-counterdiabatic quantum algorithms. We computed the approximate CD terms that can be easily implemented on any current gate-based quantum computer. We compared the ground state success probability for the evolution with and without including the CD terms by fixing the total evolution time or the number of Trotter steps. We considered many instances of the portfolio optimization problem with randomly generated data. The results indicate that, for most cases, the inclusion of the local CD term and approximate CD term substantially improve the success probability. We also verified this behavior by considering the noisy emulator of a trapped-ion system with all-to-all connected qubits. As expected, we get an advantage over the state-of-the-art methods when noise is present in the system. Also, we consider the hybrid classical-quantum algorithms for tackling hard instances of the portfolio optimization problem. In particular, we considered QAOA and DC-QAOA methods and showed that CD-assisted QAOA gives better performance than the naive approach. However, for random

initialization, finding optimal parameters for QAOA and DC-QAOA is a challenging task due to the highly non-convex nature of the cost landscape. Moreover, a hybrid quantum-classical algorithm can face challenges such as local minima, noise-induced barren plateaus, and many more. In conclusion, adding the local and approximate CD terms provides a drastic enhancement for solving the portfolio optimization problem by finite-time adiabatic evolution and also for hybrid classical-quantum algorithms. The present study considers only 2-local CD terms. Extending this to higher-order terms is expected to give further enhancement. This chapter presents a novel approach to address the portfolio optimization problem using the digitized-counterdiabatic method. However, one should note that the counterdiabatic method is ubiquitous in nature and can be applied to a wide range of combinatorial optimization problems in the quantum computing paradigm. As an outlook, considering the development of a digital-analog quantum computing encoding, on top of the digitized-counterdiabatic quantum algorithm for solving the same problem, may approach us to quantum advantage for industrial use cases in the NISQ era.

第八章 Conclusions

In this thesis, we developed a new paradigm called digitized-counterdiabatic quantum computing as a means to perform adiabatic quantum computation assisted by approximate counterdiabatic protocols on a gate-based quantum computer and show its usefulness on noisy intermediate-scale quantum computers.

Inspired by the recently proposed variational methods to obtain approximate counterdiabatic terms, we develop a gate model approach to implement the quasi-adiabatic evolution assisted by CD terms for useful applications in the NISQ era. This variational method to construct counterdiabatic protocols does not require any knowledge of the Hamiltonian spectrum, which makes it suitable for performing adiabatic quantum computing without relying on slow adiabatic evolution. The approximate counterdiabatic terms partially suppress the non-adiabatic excitation during the fast Hamiltonian evolution. This helps to reduce the effect of decoherence and other sources of noise on current quantum computers. The digital approach to implementing the continuous counterdiabatic evolution provides the required flexibility to introduce any arbitrary counterdiabatic terms. Also, any higher-order multi-qubit counterdiabatic interactions can be efficiently realized using one and two-qubit quantum gates. Furthermore, we showed various applications of DCQC protocols in many-body ground state preparation, quantum chemistry, combinatorial optimization problems, prime factorization, and portfolio optimization. In all cases, the digitized counterdiabatic protocols outperform the finite-time adiabatic evolution and the quantum approximate optimization algorithms.

In summary, In chapter 1, we started by describing the main motivation behind this thesis. In chapter 2, we introduced the basics of adiabatic quantum computation by showing proof of the adiabatic theorem. The exact counterdiabatic protocols to completely suppress the non-adiabatic excitation were shown, and their limitations to many-body quantum systems were discussed. In order to apply the counterdiabatic protocols for adiabatic quantum computations, an approximate CD calculation based on a variational approach is discussed in detail. In chapter 3, for the practical implementation of the counterdiabatic protocols, we proposed digitized counterdiabatic driving techniques and showed their applications in many-body ground state preparations. Furthermore, we implemented the digitized counterdiabatic protocols on a superconducting quantum processor achieving higher ground state success probabilities with a shallow quantum circuit. Also, we provided numerical evidence

that significant enhancement of the digitized adiabatic quantum computing can be achieved using higher order counterdiabatic terms, this results in a decrease in the total computational cost and hence achieving the desired computation results within the coherence time of the device. In chapter 4, we showed that suitably designed non-stoquastic counterdiabatic terms help to escape from classical simulability and provide a polynomial enhancement in ground state success probability compared to the finite time stoquastic adiabatic quantum optimization. Consequently, we answered a long-debated problem in adiabatic quantum optimization, i.e., the speed-up role of non-stoquastic catalysts. Also, we experimentally demonstrate the performance of our algorithm on a cloud-based superconducting quantum processor and ion-trap quantum processor with up to 8 qubit system.

In chapter 5, we proposed a new variational ansatz inspired by the counterdiabatic protocols for hybrid classical-quantum algorithms. By starting with the standard QAOA ansatz, we add local CD terms, which helps in reaching the ground state of the problem Hamiltonian faster while decreasing the computational cost. In addition, this also reduces the size of the parameter space, which improves the performance of the classical optimizers. We benchmarked our algorithm by applying it to different problems and compared the obtained results with QAOA in finding the ground state of different types of Ising models, as well as in classical optimization problems like MaxCut, Sherrington-Kirkpatrick (SK) model, and the P-spin model. We found that DC-QAOA outperforms QAOA for each case studied, and we report significant improvement in the approximation ratios. These results are remarkable considering the fact that DC-QAOA requires lower circuit depth to reach unit approximation ratio, thus reducing computational cost, and making DC-QAOA more suitable for NISQ devices.

In chapter 6, we use the digitized counterdiabatic method to speed up the adiabatic quantum factorization algorithms. We consider two different approaches for solving the factorization problem by encoding them as an optimization problem. In both cases, we explicitly calculate the approximate CD terms for the respective problem Hamiltonians and show that introducing more control parameters can increase the success probability even with local CD terms. The Hamiltonian corresponding to the factorization problem contains up to four body interaction terms. Embedding such a Hamiltonian on analog quantum annealers is complex, and it costs extra auxiliary qubits. Also, for the Hamiltonian considered in our simulation, the calculated CD term is non-stoquastic in nature, making it challenging to simulate on existing quantum annealers. In this regard, DCQC proves to be much more efficient and provides the flexibility and universality to tackle any arbitrary

adiabatic algorithms. We study different instances of the factorization problem to show the efficiency of our algorithm. From the obtained result, we conclude that the inclusion of CD driving can decrease the circuit depth and total gates required for the computation, which enables us to factorize numbers bigger than those feasible using Shor's algorithm with the same number of qubits, which makes it more suitable for NISQ devices. We tested our algorithm on a superconducting quantum computer with up to six qubits, obtaining better fidelities in all the cases under study compared to the most popular factorization algorithms.

Finally, in chapter 7, we show the application of digitized CD protocol to solve the Markowitz portfolio optimization model, consisting of several assets to maximize the returns by minimizing the risks. We consider the pure DCQC approach to find the exact solution and the hybrid DCQC approach to find the approximate solution for the portfolio optimization problem. The former is compared with the finite-time adiabatic evolution, and the latter is compared with usual QAOA. In both cases, the results obtained from CD protocols show significant improvements in the success probabilities with a shallow quantum circuit.

The increasing interest in using quantum computing methods for useful research and industrial applications has recently led to numerous developments. Unfortunately, due to the current hardware limitations, it is crucial to perform computation faster and with a higher success probability of obtaining the correct solution. We believe that our methods serve this purpose, approaching us to the needed goal of NISQ advantage with the detailed developments presented in the thesis. However, there are many unaddressed questions and challenges that remain to be answered. For instance, identifying the most dominant terms while calculating the approximate CD terms using nested commutator ansatz. This will help to reduce the circuit depth by only considering the most relevant terms and discarding other terms which don't provide any significant improvement. Also, in this thesis, we considered the simplest digitization procedure using first-order product formulas. However, with the increasing order of the nested commutator ansatz, the number of non-commuting terms in the CD Hamiltonian will increase, which results in an increase in Trotter error. This might be circumvented by considering higher order product formulas, or the recently proposed commutator product formulas. As a final remark, DCQC provides an algorithmic enhancement for quantum computation, however, a more clever approach like digital-analog quantum computing is required for efficient hardware implementation of the counterdiabatic protocols to reach quantum advantage on NISQ devices.

插图索引

- 图 3.1 Circuit implementation for the digitized adiabatic evolution using CD driving, where T is the total evolution time, and Δt is the step size. The circuit is repeated $n = T/\Delta t$ times, where the Hamiltonian's satisfy the condition $\hat{H}_f(0) = \hat{H}_{CD}(0) = \hat{H}_{CD}(T) = \hat{H}_i(T) = 0$ 18
- 图 3.2 (a) The final ground state probability P_{gs} versus the simulation time for a single qubit using CD driving on `ibmq_essex` quantum computer (solid blue) compared to the ideal simulator (dashed blue). The simulation without CD driving in real device (solid brown) and ideal simulator (dotted brown). (b) Time evolution using DAdQC and STA methods for $T = 1$. Parameters are following: $\Delta t = 0.2$, $h_x = -1$, $h_z = 1$, and number of shots $N_{shots} = 1024$. 19
- 图 3.3 (a) The final ground state probability P_{gs} versus the simulation time for the two interacting spin system ($\Delta t = 0.5$). The red solid curve represents the time evolution using STA method, the solid blue curve represents the DAdQC on `ibmq_london` 5-qubit quantum processor. As the evolution time increases, the gate error starts to dominate, which is clearly inferred from the figure. (b) Implementation of the time evolution for two spin system without CD term (solid blue) and including CD term (solid red). Parameters are following: simulation time $T = 1$, $\Delta t = 0.2$, $h_x = -1$, $h_z^1 = h_z^2 = 1$, $J_0 = -0.1$, and $N_{shots} = 1024$. Both the curves are showing the expected profile. 22

- 图 3.4 (a) For the non-integrable Ising model, the probability of obtaining the final ground state using local CD term calculated from variational method for up to 5 qubit system is depicted. The experiment is performed on 5 qubit `ibmqx2` processor. The experimental parameters are $J_0 = -0.1$, $h_x = h_z = 1$, $N_{shots} = 8192$. (b) The probability of obtaining the final ground state as a function of coupling strength using local CD driving for up to 25 qubits are shown. The solid line is for the local CD term from the variational approach, and the dotted line is for the local CD term from Berry formula, see Eq. (3.7). The parameters chosen are $h_x = -1$, $h_z^j = 1$, $dt = 0.1$, and $T = 1$. The simulation was performed on a `qasm_simulator`..... 24
- 图 3.5 The fidelity of obtaining the final ground state $(|01\rangle + |10\rangle)/\sqrt{2}$ as a function of evolution time for local CD and NC ansatz ($l=1$) obtained from `ibmq_vigo`. The solid line represents the experimental result and the dashed line represents the result from ideal digital simulator. Parameters: $J_0 = 2$, $h_z = 0.6$, $T = 1$, $dt = 0.2$, and $N_{shots} = 8192$. 26
- 图 3.6 The density matrix representation of the final ground state obtained from state tomography. (a) Bell-state from `ibmq_ourense` and (b) GHZ-state from `ibmq_vigo`..... 28
- 图 3.7 Fidelity to prepare the GHZ state as a function of system size on an ideal digital simulator with CD term from nested commutator (NC) ansatz with different orders and the naive approach without CD term. Where the parameters are $T = 0.006$ and $\Delta t = 0.001$. 29
- 图 3.8 Visualization of the toric code Hamiltonian on a 2D lattice, where the shaded circles represents the qubits. $A_s = \sigma_i^x \sigma_j^x \sigma_k^x \sigma_l^x$, and $B_p = \sigma_i^z \sigma_j^z \sigma_k^z \sigma_l^z$ represents the star and the plaquette operators, respectively. 30
- 图 3.9 Fidelity as a function of evolution time for the ground state preparation of toric code model on a 2×2 square lattice. We compared the fidelity by including the CD term and without the CD term. For a short time, we can see a huge improvement in the fidelity with approximate CD driving obtained from first-order ($l=1$) NC ansatz. 31

- 图 3.10 Quantum circuit for the preparation of the ground state of toric code model. Two trotter steps are shown. The time chosen for the evolution is very small ($T = 0.02$), hence only the CD terms are significant, and the interactions corresponding to the Hamiltonian H_{TC} can be neglected. 32
- 图 3.11 Circuit implementation for the digitized-counterdiabatic evolution with two Trotter steps. (a) circuit decomposition using standard gate set (b) circuit decomposition using the native CR gate..... 34
- 图 4.1 Schematic of the quantum circuit implementation of digitized-counterdiabatic evolution using the first-order Trotter-Suzuki formula in Eq. (7.10). 46
- 图 4.2 The Average success probability of obtaining the ground state as a function of number of spins in the Ising spin-glass Hamiltonian is depicted. Here, we fix the total evolution time $T = 1$ and the number of Trotter steps to 20, *i.e.* $\delta t = 0.05$. The interaction strengths and the local fields are chosen randomly from a Gaussian distribution for 1000 random instances. The blue curve corresponds to the evolution without the CD term, the red curve is with the local single qubit CD term, and the green curve is for the 2-local CD term in Eq. (4.5). In the latter case, a polynomial enhancement in the success probability can be observed. 47
- 图 4.3 The average success probability enhancement (P_{enh}^{Avg}) and probability enhancement ratio (R_{enh}) as a function of system size for the Ising spin-glass problem is depicted. For the 2-local CD term from the first order NC ansatz, P_{enh}^{Avg} increases with the system size. Whereas for the local CD term (Y), a constant enhancement by a factor of 3 is observed. In the bottom panel, we see that the 2-local CD term always gives enhancement for all 1000 random instances, whereas the local CD has an average enhancement ratio of 0.756. . 48
- 图 4.4 The distribution of ground-state success probability for 1000 randomly chosen instances is illustrated. The red plot corresponds to the traditional stoquastic adiabatic Hamiltonian in Eq. (4.1), the green plot is for the local single-spin CD term, and the blue plot is for the non-stoquastic 2-local CD term in Eq. (4.5). 48

- 图 4.5 The energy gap between the ground state and the first excited state is plotted as a function of time for a system size $N = 10$. The blue curve corresponds to the stoquastic Hamiltonian in Eq. (4.1), while the green curve corresponds to the non-stoquastic Hamiltonian by including the 2-local CD term in Eq. 4.5.50 50
- 图 4.6 The plot shows success probability versus minimum gap for 250 random instances of the Ising spin glass problem with and without including the CD term. We can observe that adding the CD term will result in an increase in success probability and minimum gap. The parameters are $T = 1$, $\delta t = 0.05$ 51
- 图 4.7 Circuit implementation for the digitized-counterdiabatic evolution for 2 Trotter steps. The time chosen for the evolution is very small ($T = 0.1$); hence only the CD terms are significant, and the terms in H_{ad} are neglected. 51
- 图 4.8 Probability distribution obtained from digitized-counterdiabatic quantum evolution of Ising spin glass Hamiltonian is depicted. We considered random instances of all-to-all connected Ising spin-glass Hamiltonian with 5 to 8 spins. The system is evolved using Trotter–Suzuki approximation with and without including the CD terms given in Eq. (4.5). The experimental results are obtained from IBM’s transmon-based superconducting quantum processor `ibmq_montreal` and Quantinuum’s ion-trap quantum processor. The ground state success probability obtained after two Trotter steps are compared for the digitized-counterdiabatic quantum evolution with the non-adiabatic one. We observed that the experimental and ideal simulations using the DCQO approach have a large overlap with the exact ground state highlighted in the figure. The inset depicts the graph representation of the problem instance with coupling terms, and local field strengths are shown in color bars. 52
- 图 5.1 Schematic diagram with circuit used for DC-QAOA having additional CD term along with the Hamiltonian and mixing terms. 56

- 图 5.2 Comparison of approximation ratios (\mathcal{R}) as a function of number of layers (p) for three representative cases of Ising spin model. Green lines show results of QAOA whereas red lines show results of DC-QAOA. (a) shows \mathcal{R} variation of LFIM where $J_{ij} = 1$, $h_i = 1$, and $k_i = 0$. (b) depicts TFIM where $J_{ij} = 1$, $h_i = 0$, and $k_i = 1$, and (c) shows preparation of GHZ state where $J_{ij} = 1$, $h_i = 0$, and $k_i = 0$. System size for all the cases was kept to $L = 12$ qubits. ... 57
- 图 5.3 Comparison of approximation ratios obtained for different graph size using DC-QAOA and QAOA. (a) Unweighted 3-regular MaxCut for a randomly chosen 10 instances. (b) Approximation ratio vs number of layers (p) for SK model with 6-qubits (vertices) is depicted. Green line and red line show the values of QAOA and DC-QAOA respectively. On the right-bottom, a graph of 6 qubits with all-to-all connectivity is also shown. The results were obtained by considering 10 different randomly chosen instances of J_{ij} values. Error bars represents the standard error. 62
- 图 5.4 Comparison of approximation ratio (\mathcal{R}) with respect to number of iterations for $P = 4$ and $p = 1$. Panels (a) and (b) show the QAOA and DC-QAOA results for $h = 1$, respectively. The case with $h = 0$ is shown in panels (c) and (d) for QAOA and DC-QAOA results, respectively. The system size is $L = 6$. Each of the 10 random initial parameters chosen is represented by a color line. 63
- 图 5.5 Approximation ratio (\mathcal{R}) as a function of number of layers ($p = 1, 2, 3$) for $P = 3$ and $h = 1$. Green and red lines show the average results obtained from 10 random parameter initialization for QAOA and DC-QAOA, respectively. Standard deviations are of the order of 10^{-2} 65
- 图 6.1 Ground state probability as a function of total evolution time for factorizing 21 and 91. The blue line corresponds to the evolution with local CD driving and the orange line is for without CD driving. 71

- 图 6.2 The success probability of obtaining the ground state ($|0100\rangle$) as a function of total evolution time for the Hamiltonian in Eq. (6.8) corresponding to factoring the number $2479 = 37 \times 67$ using the CD term with multiple parameters from Eq. (6.11) (green and orange), the CD term obtained from NC ansatz in Eq. (6.10) (red), the local CD in Eq. (6.5) (blue) and the corresponding adiabatic case (purple) by simulating on `qasm` simulator. 73
- 图 6.3 Factorization of $217 = 7 \times 31$: (a) The success probability as a function of total evolution time with and without CD driving using `qasm` simulator. (b) Probability distribution from 7-qubit quantum processor `ibmq_casablanca`. Parameters chosen are: $T = 0.01$, $\Delta t = 0.001$, $N_{shots} = 8192$ 74
- 图 6.4 (a)The ground state fidelity as a function of evolution time for both with and without CD. Inset: scheduling parameter $\lambda(t)$ and the variational CD coefficient $\alpha_1(t)$ as a function of time. Experimental parameters: $T = 0.005$, $\Delta t = 0.001$, $h_x = -2$. (b) Probability distribution for factoring 235 using 4-qubits on `ibmq_casablanca` using only two trotter steps for $T = 0.02$, $\Delta t = 0.01$, $N_{shots} = 8192$ 76
- 图 7.1 Histogram depicts the ground state success probability for 1000 randomly chosen instances of the portfolio optimization problem with and without CD driving. We considered 12 qubit systems with different numbers of assets (n) and partitions (g). When the number of partitions is smaller, the LCD in Eq. (7.8) gives a better enhancement. Whereas, when g is larger, ACD from Eq. (7.12) shows greater improvement. The simulation parameters are, total evolution time $T = 1$, and the step size $\Delta t = 0.05$ 83
- 图 7.2 The upper plot depicts the average success probability enhancement (Eq. (7.14)), and the lower plot represents the enhancement ratio (Eq. (7.13)) for various system sizes with LCD and ACD. The error bars represent the standard deviation. Due to the huge variations in the success probability enhancement for different instances using LCD, the error bars have larger values. 86

图 7.3 Output probability distribution of an instance with $n = 3$ and $g = 2$. We considered $T = 0.3$, and $\delta t = 0.1$. The green bar corresponds to the results obtained from Quantinuum's H1 emulator, which mimics the noise model of the hardware Model H1. The red and blue bars are for the ideal simulation results with and without including the CD terms, respectively. The ground-state bitstring is also shown.	87
图 7.4 Success probability as a function of total evolution time T for randomly chosen 40 instances is depicted. Here we considered $n = 6$ assets and $g = 2$ partitions resulting in system size $N = 12$. A substantial improvement in success probability is obtained for most of the instances by including the local CD term H_{LCD} , and the approximate CD term H_{ACD} . Here, we considered the Trotter step size as $\Delta t = 0.1$. Different colored lines show each of the 40 instances.....	89
图 7.5 Average success probability (P_s) as a function of number of layers for a $N = 6$ system with $n = 3, g = 2$. Results show the mean success probability obtained after considering 10 instances and 20 random initialization in each instance. Error bars represent the variance of the distribution. Stochastic gradient descent based optimizer called adagrad optimizer with step size = 0.1 was used as the classical optimizer for all instances.	90
图 A.1 (a) Experimental parameters of the quantum processor <code>ibmq_vigo</code> , (b) device layout, (c) circuit implementation for the time evolution of the Hamiltonian to factorize $35 = 7 \times 5$ using CD driving (two trotter steps).	107
图 A.2 Probability distribution corresponding to the factorization of $2479 = 67 \times 37$ using three trotter steps obtained by considering three different CD terms. In all the cases the ground state $ 0100\rangle$ (read from right to left) has the highest probability. The simulation parameters are: $\Delta t = 0.1$, $T = 0.3$, and $N_{shots} = 10000$	107

表格索引

表 3.1	The state fidelity and the gate counts after circuit optimization is depicted.	... 38
表 3.2	We compare the number of quantum gates required for the successful implementation of adiabatic evolution on a digital quantum computer by including the CD term and excluding the CD term. 39
表 A.1	Multiplication table for $67 \times 37 = 2479$ in binary. 108

附录 A Additional Calculation and results for Digitized-Counterdiabatic Quantum Factorization.

A.1 Calculation of local CD term

To factor a number N into its prime factors x and y , we need $X = m(\lfloor \sqrt{N} \rfloor_o) - 1$, $Y = m(\lfloor \frac{N}{3} \rfloor) - 1$ qubits, where $\lfloor a \rfloor_o$ denotes the largest odd integer not larger than a , while $m(b)$ denotes the smallest number of bits required for representing b . In binary notation $x = (x_{l_1-1}x_{l_1-2}\dots x_1 1)$, $y = (y_{l_1+l_2-2}y_{l_1+l_2-3}\dots y_{l_1} 1)$. So we can write

$$x = \sum_{i=1}^{l_1-1} 2^i x_i + 1, \text{ and } y = \sum_{j=l_1}^{l_1+l_2-2} 2^j y_j + 1.$$

Since both x and y are odd prime numbers, $x_0 = y_0 = 1$. This problem can be mapped to an optimization problem where the minimum of a function $f(x, y) = (N - xy)^2$ gives the solution of the factorization problem. It is possible to encode the solution of a minimization problem in the ground state of a Hamiltonian,

$$H_f = \left[NI - \left(\sum_{l=1}^{n_x} 2^l \hat{x}_l + I \right) \left(\sum_{m=1}^{n_y} 2^m \hat{y}_m + I \right) \right]^2, \quad (\text{A.1})$$

where $\hat{x}_l = \frac{I - \sigma_l^z}{2}$ and $\hat{y}_m = \frac{I - \sigma_m^z}{2}$. This Hamiltonian can be written in a general form as

$$H_f = \sum_i \tilde{h}_i \sigma_i^z + \sum_{i < j} \tilde{J}_{ij} \sigma_i^z \sigma_j^z + \sum_{i < j < k} \tilde{K}_{ijk} \sigma_i^z \sigma_j^z \sigma_k^z + \sum_{i < j < k < l} \tilde{L}_{ijkl} \sigma_i^z \sigma_j^z \sigma_k^z \sigma_l^z, \quad (\text{A.2})$$

where \tilde{J}_{ij} , \tilde{K}_{ijk} and \tilde{L}_{ijkl} are the two, three, and four-body interaction terms, respectively. In order to find the ground state of this Hamiltonian, we follow the adiabatic theorem by preparing the ground state of an initial Hamiltonian $H_i = \sum_i \tilde{h}_i \sigma_i^x$ and evolve the system adiabatically to reach the final ground state of H_f . The total Hamiltonian for the adiabatic evolution is given by

$$H = (1 - \lambda)H_i + \lambda H_f. \quad (\text{A.3})$$

In order to speedup the slow adiabatic evolution and suppress the unwanted transitions, we add an extra term to the Hamiltonian called counter-diabatic (CD) driving term. The

calculation and implementation of the exact CD term is not useful for the practical purpose, so we consider an approximate local CD driving proposed by Sels *et al.* (see Ref. [23] in the main text),

$$\tilde{A}_\lambda = \sum_j \alpha_j(t) \sigma_j^y. \quad (\text{A.4})$$

For a specified control parameter λ , the CD term is given by $H_{CD} = \dot{\lambda} \tilde{A}_\lambda$, where \tilde{A}_λ is the approximate gauge potential responsible for the non-adiabatic transitions and $\alpha_j(t)$ is the corresponding CD coefficient. For the optimal solution, we have to minimize the operator distance between the exact gauge potential and the approximate gauge potential, which is equivalent to minimizing the action,

$$S_\lambda(\tilde{A}_\lambda) = \text{Tr} \left[G_\lambda^2(\tilde{A}_\lambda) \right], \quad (\text{A.5})$$

where the Hilbert-Schmidt norm G_λ is given by

$$G_\lambda(\tilde{A}_\lambda) = \partial_\lambda H + i \left[\tilde{A}_\lambda, H \right]. \quad (\text{A.6})$$

Moreover,

$$\partial_\lambda H = \frac{1}{\dot{\lambda}} \left(-\sum_i \dot{h}_i^x \sigma_i^x + \sum_i \dot{h}_i^z \sigma_i^z + \sum_{i < j} \dot{J}_{ij} \sigma_i^z \sigma_j^z + \sum_{i < j < k} \dot{K}_{ijk} \sigma_i^z \sigma_j^z \sigma_k^z + \sum_{i < j < k < l} \dot{L}_{ijkl} \sigma_i^z \sigma_j^z \sigma_k^z \sigma_l^z \right),$$

where, the scheduling function $\lambda(t)$ has been incorporated in the new set of parameters, $h_j^z(t) = \lambda(t) \tilde{h}_j^z$, $h_j^x(t) = \lambda(t) \tilde{h}_j^x$, $J_{ij}^z(t) = \lambda(t) \tilde{J}_{ij}^z$, and so on. Furthermore,

$$\begin{aligned} G_\lambda = & \sum_i \left(-\frac{\dot{h}_i^x}{\dot{\lambda}} - 2\alpha_i h_i^z \right) \sigma_i^x - 2 \sum_{i < j} \alpha_i J_{ij} (\sigma_i^x \sigma_j^z + \sigma_i^z \sigma_j^x) - 2 \sum_{i < j < k} \alpha_i K_{ijk} (\sigma_i^x \sigma_j^z \sigma_k^z \\ & + \sigma_i^z \sigma_j^x \sigma_k^z + \sigma_i^z \sigma_j^z \sigma_k^x) - 2 \sum_{i < j < k < l} \alpha_i L_{ijkl} (\sigma_i^x \sigma_j^z \sigma_k^z \sigma_l^z + \sigma_i^z \sigma_j^x \sigma_k^z \sigma_l^z + \sigma_i^z \sigma_j^z \sigma_k^x \sigma_l^z) + \\ & \sum_i \left(\frac{\dot{h}_i^z}{\dot{\lambda}} - 2\alpha_i h_i^x \right) \sigma_i^z + \sum_{i < j} \frac{\dot{J}_{ij}}{\dot{\lambda}} \sigma_i^z \sigma_j^z + \sum_{i < j < k} \frac{\dot{K}_{ijk}}{\dot{\lambda}} \sigma_i^z \sigma_j^z \sigma_k^z + \sum_{i < j < k < l} \frac{\dot{L}_{ijkl}}{\dot{\lambda}} \sigma_i^z \sigma_j^z \sigma_k^z \sigma_l^z. \end{aligned} \quad (\text{A.7})$$

The action is calculated as

$$\begin{aligned} S &= \text{Tr}(G_\lambda^2) \\ &= \sum_i \left(-\frac{\dot{h}_i^x}{\dot{\lambda}} - 2\alpha_i h_i^z \right)^2 + 8 \sum_{i < j} \alpha_i^2 J_{ij}^2 + 12 \sum_{i < j < k} \alpha_i^2 K_{ijk}^2 + 16 \sum_{i < j < k < l} \alpha_i^2 L_{ijkl}^2 \end{aligned}$$

$$+ \sum_i (\frac{\dot{h}_i^z}{\lambda} - 2\alpha_i h_i^x)^2 + \sum_{i < j} \frac{\dot{J}_{ij}^2}{\lambda^2} + \sum_{i < j < k} \frac{\dot{K}_{ijk}^2}{\lambda^2} + \sum_{i < j < k < l} \frac{\dot{L}_{ijkl}^2}{\lambda^2}. \quad (\text{A.8})$$

By minimizing the action $\frac{\partial S}{\partial \alpha_i} = 0$, we will get the CD coefficient

$$\alpha_i = \frac{h_i^x \dot{h}_i^z - h_i^z \dot{h}_i^x}{2\lambda \left(h_i^{x2} + h_i^{z2} + 2 \sum_j J_{ij}^2 + 3 \sum_{j < k} K_{ijk}^2 + 4 \sum_{j < k < l} L_{ijkl}^2 \right)}. \quad (\text{A.9})$$

Therefore the local CD driving can be calculated as

$$H_{CD}(t) = \dot{\lambda} \tilde{A}_\lambda = \sum_i \frac{h_i^x \dot{h}_i^z - h_i^z \dot{h}_i^x}{2 \left(h_i^{x2} + h_i^{z2} + 2 \sum_j J_{ij}^2 + 3 \sum_{j < k} K_{ijk}^2 + 4 \sum_{j < k < l} L_{ijkl}^2 \right)} \sigma_i^y. \quad (\text{A.10})$$

A.1.1 Example-1: quantum factorization of 217 using the direct optimization method

For the adiabatic quantum factorization using direct optimization method, we consider the example of factoring the number $N = 217 = 7 \times 31$, which requires $n_x = 3$, and $n_y = 5$ qubits to represent the factors. Hence, for the simulation we need total $(n_x - 1) + (n_y - 1) = 6$ qubits. The problem Hamiltonian can be calculated using Eq. (2) from the main paper,

$$\begin{aligned} H_f = & 16\sigma_1^z\sigma_2^z\sigma_3^z\sigma_4^z + 32\sigma_1^z\sigma_2^z\sigma_3^z\sigma_5^z + 64\sigma_1^z\sigma_2^z\sigma_3^z\sigma_6^z - 128\sigma_1^z\sigma_2^z\sigma_3^z + 64\sigma_1^z\sigma_2^z\sigma_4^z\sigma_5^z \\ & + 128\sigma_1^z\sigma_2^z\sigma_4^z\sigma_6^z - 256\sigma_1^z\sigma_2^z\sigma_4^z + 256\sigma_1^z\sigma_2^z\sigma_5^z\sigma_6^z - 512\sigma_1^z\sigma_2^z\sigma_5^z - 1024\sigma_1^z\sigma_2^z\sigma_6^z \\ & + 1364\sigma_1^z\sigma_2^z - 32\sigma_1^z\sigma_3^z\sigma_4^z - 64\sigma_1^z\sigma_3^z\sigma_5^z - 128\sigma_1^z\sigma_3^z\sigma_6^z - 178\sigma_1^z\sigma_3^z - 128\sigma_1^z\sigma_4^z\sigma_5^z \\ & - 256\sigma_1^z\sigma_4^z\sigma_6^z - 356\sigma_1^z\sigma_4^z - 512\sigma_1^z\sigma_5^z\sigma_6^z - 712\sigma_1^z\sigma_5^z - 1424\sigma_1^z\sigma_6^z + 4216\sigma_1^z - 64\sigma_2^z\sigma_3^z\sigma_4^z \\ & - 128\sigma_2^z\sigma_3^z\sigma_5^z - 256\sigma_2^z\sigma_3^z\sigma_6^z - 356\sigma_2^z\sigma_3^z - 256\sigma_2^z\sigma_4^z\sigma_5^z - 512\sigma_2^z\sigma_4^z\sigma_6^z - 712\sigma_2^z\sigma_4^z \\ & - 1024\sigma_2^z\sigma_5^z\sigma_6^z - 1424\sigma_2^z\sigma_5^z - 2848\sigma_2^z\sigma_6^z + 8432\sigma_2^z + 84\sigma_3^z\sigma_4^z + 168\sigma_3^z\sigma_5^z + 336\sigma_3^z\sigma_6^z \\ & + 1064\sigma_3^z + 336\sigma_4^z\sigma_5^z + 672\sigma_4^z\sigma_6^z + 2128\sigma_4^z + 1344\sigma_5^z\sigma_6^z + 4256\sigma_5^z + 8512\sigma_6^z + 26474I. \end{aligned}$$

The ground state of this Hamiltonian is $|111111\rangle$, which encodes the solution of the factorization problem $217 = 7 \times 31 = \underline{111} \times \underline{11111}$. To find the ground state, we use the 7-qubit quantum processor `ibmq_casablanca`, and the experimentally obtained result is shown in Fig. 3 (b), in the main text.

A.1.2 Example-2: quantum factorization of $35 = 7 \times 5$

To factorize the number 35 on a quantum processor, we consider the binary multiplication table method. After classical preprocessing, the number of qubits required for the

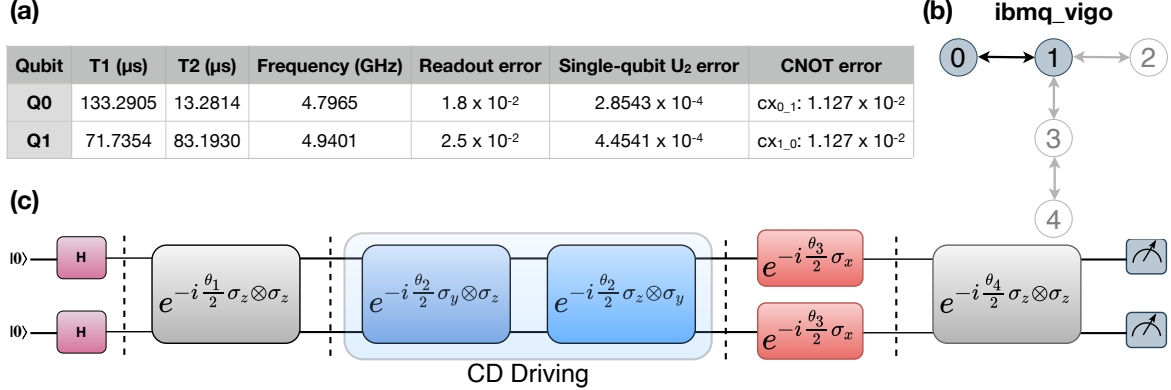


图 A.1 (a) Experimental parameters of the quantum processor `ibmq_vigo`, (b) device layout, (c) circuit implementation for the time evolution of the Hamiltonian to factorize $35 = 7 \times 5$ using CD driving (two trotter steps).

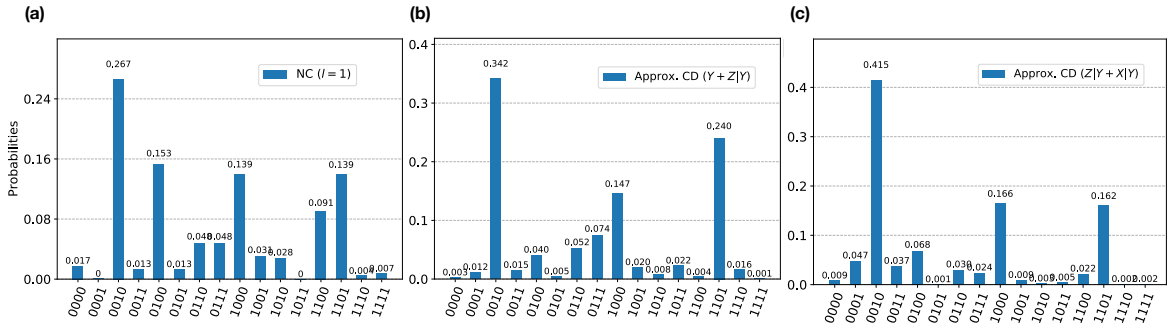


图 A.2 Probability distribution corresponding to the factorization of $2479 = 67 \times 37$ using three trotter steps obtained by considering three different CD terms. In all the cases the ground state $|0100\rangle$ (read from right to left) has the highest probability. The simulation parameters are: $\Delta t = 0.1$, $T = 0.3$, and $N_{shots} = 10000$.

factorization reduces to 2. Since the bit length of the factors 7 and 5 are same, the ground state is two fold degenerate due to exchange symmetry. The device layout, parameters and the quantum circuit for the digitized-adiabatic evolution using CD driving is shown in Fig. A.1.

A.1.3 Example-3: quantum factorization of 2479 using the binary multiplication table

The binary multiplication table for factoring 2479 is given in Table A.1. For simplicity, we assumed that the bit length of the factors are known, and we consider $n_x = 7$, and $n_y = 6$. We set the first and last bit of the factors to be 1. Adding each column leads to a set of factorization equations. To reduce the number of qubits we apply the classical preprocessing

表 A.1 Multiplication table for $67 \times 37 = 2479$ in binary.

	2^{11}	2^{10}	2^9	2^8	2^7	2^6	2^5	2^4	2^3	2^2	2^1	2^0
x						1	x_5	x_4	x_3	x_2	x_1	1
y						1	y_4	y_3	y_2	y_1	1	
						1	x_5	x_4	x_3	x_2	x_1	1
						y_1	y_1x_5	y_1x_4	y_1x_3	y_1x_2	y_1x_1	y_1
						y_2	y_2x_5	y_2x_4	y_2x_3	y_2x_2	y_2x_1	y_2
						y_3	y_3x_5	y_3x_4	y_3x_3	y_3x_2	y_3x_1	y_3
						y_4	y_4x_5	y_4x_4	y_4x_3	y_4x_2	y_4x_1	y_4
	1	x_5	x_4	x_3	x_2	x_1		1				
carries	$c_{10,11}$	$c_{9,10}$	$c_{8,9}$	$c_{7,8}$	$c_{6,7}$	$c_{5,6}$	$c_{4,5}$	$c_{3,4}$	$c_{2,3}$	$c_{1,2}$		
	$c_{9,11}$	$c_{8,10}$	$c_{7,9}$	$c_{6,8}$	$c_{5,7}$	$c_{4,6}$	$c_{3,5}$	$c_{2,4}$				
$x \times y = 2479$	1	0	0	1	1	0	1	0	1	1	1	1

scheme based on a binary logical constraints. we get the final set of equations as

$$\begin{aligned} x_3y_1 - y_1 &= 0 \\ x_3y_2 - y_1 &= 0 \\ x_3 + y_2 + c_{7,8} - 1 &= 0 \\ y_1 - y_2 - 2c_{7,8} + 1 &= 0 \\ x_3 - 2y_1y_2 - y_1 + y_2 - 1 &= 0. \end{aligned}$$

By squaring and summing all the equations, we get the cost function as

$$\begin{aligned} f(x, y, c) = & (x_3y_1 - y_1)^2 + (x_3y_2 - y_1)^2 + (x_3 + y_2 + c_{7,8} - 1)^2 + (y_1 - y_2 - 2c_{7,8} + 1)^2 \\ & + (x_3 - 2y_1y_2 - y_1 + y_2 - 1)^2. \end{aligned} \quad (\text{A.11})$$

The minimum of this cost function $f_{min}(x, y, c) = 0$. By mapping the binary variables to the qubit operator, we obtained the final Hamiltonian given in Eq. 8 in the main manuscript. The probability distribution obtained at the end of the evolution by considering different CD terms is shown in Fig. A.2. In all the cases the ground state $|0100\rangle$ is obtained with highest success probability with only three trotter steps.

参考文献

- [1] Benioff P. The computer as a physical system: A microscopic quantum mechanical Hamiltonian model of computers as represented by Turing machines [J]. *Journal of statistical physics*, 1980, 22 (5): 563–591.
- [2] Deutsch D. Quantum theory, the Church–Turing principle and the universal quantum computer [J]. *Proceedings of the Royal Society of London. A. Mathematical and Physical Sciences*, 1985, 400 (1818): 97–117.
- [3] Feynman R P. Simulating physics with computers [J/OL]. *Int. J. Theor. Phys*, 1999, 21 (6/7). <https://link.springer.com/article/10.1007/BF02650179>.
- [4] Shor P W. Algorithms for quantum computation: discrete logarithms and factoring [C/OL]. In *Proceedings 35th annual symposium on foundations of computer science*, 1994: 124–134. <https://ieeexplore.ieee.org/document/365700>.
- [5] Georgescu I M, Ashhab S, Nori F. Quantum simulation [J/OL]. *Reviews of Modern Physics*, 2014, 86 (1): 153. <https://journals.aps.org/rmp/abstract/10.1103/RevModPhys.86.153>.
- [6] Houck A A, Türeci H E, Koch J. On-chip quantum simulation with superconducting circuits [J/OL]. *Nature Physics*, 2012, 8 (4): 292. <https://www.nature.com/articles/nphys2251>.
- [7] Lanyon B P, Hempel C, Nigg D, et al. Universal digital quantum simulation with trapped ions [J/OL]. *Science*, 2011, 334 (6052): 57–61. <https://science.sciencemag.org/content/334/6052/57>.
- [8] Gerritsma R, Kirchmair G, Zähringer F, et al. Quantum simulation of the Dirac equation [J/OL]. *Nature*, 2010, 463 (7277): 68–71. <https://www.nature.com/articles/nature08688>.
- [9] Apolloni B, Carvalho C, De Falco D. Quantum stochastic optimization [J]. *Stochastic Processes and their Applications*, 1989, 33 (2): 233–244.
- [10] Apolloni B, Cesa-Bianchi N, De Falco D. A numerical implementation of “quantum annealing” [C]. In *Stochastic Processes, Physics and Geometry: Proceedings of the Ascona-Locarno Conference*, 1990: 97–111.
- [11] Farhi E, Goldstone J, Gutmann S, et al. A Quantum Adiabatic Evolution Algorithm Applied to Random Instances of an NP-Complete Problem [J/OL]. *Science*, 2001, 292 (5516): 472–475. <https://www.science.org/doi/abs/10.1126/science.1057726>.
- [12] Kato T. On the adiabatic theorem of quantum mechanics [J/OL]. *Journal of the Physical Society of Japan*, 1950, 5 (6): 435–439. <https://journals.jps.jp/doi/10.1143/JPSJ.5.435>.
- [13] Sels D, Polkovnikov A. Minimizing irreversible losses in quantum systems by local counterdiabatic driving [J/OL]. *Proceedings of the National Academy of Sciences*, 2017, 114 (20): E3909–E3916. <https://www.pnas.org/content/114/20/E3909>.
- [14] Claeys P W, Pandey M, Sels D, et al. Floquet-Engineering Counterdiabatic Protocols in Quantum Many-Body Systems [J/OL]. *Phys. Rev. Lett.*, 2019, 123: 090602. <https://link.aps.org/doi/10.1103/PhysRevLett.123.090602>.
- [15] Biamonte J, Wittek P, Pancotti N, et al. Quantum machine learning [J/OL]. *Nature*, 2017, 549 (7671): 195–202. <https://www.nature.com/articles/nature23474>.

- [16] Lloyd S, Mohseni M, Rebentrost P. Quantum algorithms for supervised and unsupervised machine learning [J/OL]. arXiv preprint arXiv:1307.0411, 2013. <https://arxiv.org/abs/1307.0411>.
- [17] Dunjko V, Taylor J M, Briegel H J. Quantum-enhanced machine learning [J/OL]. Physical review letters, 2016, 117 (13): 130501. <https://journals.aps.org/prl/abstract/10.1103/PhysRevLett.117.130501>.
- [18] Schuld M, Killoran N. Quantum machine learning in feature Hilbert spaces [J/OL]. Physical review letters, 2019, 122 (4): 040504. <https://journals.aps.org/prl/abstract/10.1103/PhysRevLett.122.040504>.
- [19] Moll N, Barkoutsos P, Bishop L S, et al. Quantum optimization using variational algorithms on near-term quantum devices [J/OL]. Quantum Science and Technology, 2018, 3 (3): 030503. <https://iopscience.iop.org/article/10.1088/2058-9565/aab822>.
- [20] Farhi E, Harrow A W. Quantum supremacy through the quantum approximate optimization algorithm [J/OL]. arXiv preprint arXiv:1602.07674, 2016. <https://arxiv.org/abs/1602.07674>.
- [21] Arute F, Arya K, Babbush R, et al. Quantum Approximate Optimization of Non-Planar Graph Problems on a Planar Superconducting Processor [J/OL]. arXiv preprint arXiv:2004.04197, 2020. <https://arxiv.org/abs/2004.04197>.
- [22] Gisin N, Ribordy G, Tittel W, et al. Quantum cryptography [J/OL]. Reviews of modern physics, 2002, 74 (1): 145. <https://journals.aps.org/rmp/abstract/10.1103/RevModPhys.74.145>.
- [23] Bennett C H, Brassard G. Quantum cryptography: Public key distribution and coin tossing [J/OL]. Theoretical Computer Science, 2014, 560: 7–11. <https://www.sciencedirect.com/science/article/pii/S0304397514004241?via%3Dhub>.
- [24] Arute F, Arya K, Babbush R, et al. Quantum supremacy using a programmable superconducting processor [J/OL]. Nature, 2019, 574 (7779): 505–510. <https://www.nature.com/articles/s41586-019-1666-5>.
- [25] Farhi E, Goldstone J, Gutmann S, et al. A quantum adiabatic evolution algorithm applied to random instances of an NP-complete problem [J/OL]. Science, 2001, 292 (5516): 472–475. <https://science.scienmag.org/content/292/5516/472>.
- [26] Ambainis A, Regev O. An elementary proof of the quantum adiabatic theorem [J/OL]. arXiv preprint quant-ph/0411152, 2004. <https://arxiv.org/abs/quant-ph/0411152>.
- [27] Young A, Knysh S, Smelyanskiy V. First-order phase transition in the quantum adiabatic algorithm [J/OL]. Physical review letters, 2010, 104 (2): 020502. <https://journals.aps.org/prl/abstract/10.1103/PhysRevLett.104.020502>.
- [28] Peng X, Liao Z, Xu N, et al. Quantum adiabatic algorithm for factorization and its experimental implementation [J/OL]. Physical review letters, 2008, 101 (22): 220405. <https://dx.doi.org/10.1103/PhysRevLett.101.220405>.
- [29] Reichardt B W. The Quantum Adiabatic Optimization Algorithm and Local Minima [C/OL]. 2004: 502–510. <https://doi.org/10.1145/1007352.1007428>.
- [30] Steffen M, van Dam W, Hogg T, et al. Experimental implementation of an adiabatic quantum optimization algorithm [J/OL]. Physical Review Letters, 2003, 90 (6): 067903. <https://journals.aps.org/prl/abstract/10.1103/PhysRevLett.90.067903>.

- [31] Bapst V, Foini L, Krzakala F, et al. The quantum adiabatic algorithm applied to random optimization problems: The quantum spin glass perspective [J/OL]. Physics Reports, 2013, 523 (3): 127–205. <https://www.sciencedirect.com/science/article/abs/pii/S037015731200347X>.
- [32] Das A, Chakrabarti B K. Colloquium: Quantum annealing and analog quantum computation [J/OL]. Reviews of Modern Physics, 2008, 80 (3): 1061. <https://journals.aps.org/rmp/abstract/10.1103/RevModPhys.80.1061>.
- [33] Johnson M W, Amin M H, Gildert S, et al. Quantum annealing with manufactured spins [J/OL]. Nature, 2011, 473 (7346): 194–198. <https://www.nature.com/articles/nature10012>.
- [34] Boixo S, Albash T, Spedalieri F M, et al. Experimental signature of programmable quantum annealing [J/OL]. Nature communications, 2013, 4 (1): 1–8. <https://www.nature.com/articles/ncomms3067>.
- [35] Aharonov D, Van Dam W, Kempe J, et al. Adiabatic quantum computation is equivalent to standard quantum computation [J/OL]. SIAM review, 2008, 50 (4): 755–787. <https://pubs.siam.org/doi/abs/10.1137/080734479?journalCode=siread>.
- [36] Barends R, Shabani A, Lamata L, et al. Digitized adiabatic quantum computing with a superconducting circuit [J/OL]. Nature, 2016, 534 (7606): 222–226. <https://doi.org/10.1038/nature17658>.
- [37] Torrontegui E, nez S I, Martínez-Garaot S, et al. Chapter 2 - Shortcuts to Adiabaticity [M] // Arimondo E, Berman P R, Lin C C. 2013: 2013: 117–169.
- [38] Guéry-Odelin D, Ruschhaupt A, Kiely A, et al. Shortcuts to adiabaticity: Concepts, methods, and applications [J/OL]. Rev. Mod. Phys., 2019, 91: 045001. <https://link.aps.org/doi/10.1103/RevModPhys.91.045001>.
- [39] Takahashi K. Hamiltonian engineering for adiabatic quantum computation: Lessons from shortcuts to adiabaticity [J/OL]. Journal of the Physical Society of Japan, 2019, 88 (6): 061002. <https://journals.jps.jp/doi/full/10.7566/JPSJ.88.061002>.
- [40] Demirplak M, Rice S A. Adiabatic Population Transfer with Control Fields [J/OL]. The Journal of Physical Chemistry A, 2003, 107 (46): 9937–9945. <http://dx.doi.org/10.1021/jp030708a>.
- [41] Demirplak M, Rice S A. Assisted Adiabatic Passage Revisited [J/OL]. The Journal of Physical Chemistry B, 2005, 109 (14): 6838–6844. <http://dx.doi.org/10.1021/jp040647w>.
- [42] Berry M V. Transitionless quantum driving [J/OL]. Journal of Physics A: Mathematical and Theoretical, 2009, 42 (36): 365303. <http://stacks.iop.org/1751-8121/42/i=36/a=365303>.
- [43] Chen X, Ruschhaupt A, Schmidt S, et al. Fast Optimal Frictionless Atom Cooling in Harmonic Traps: Shortcut to Adiabaticity [J/OL]. Phys. Rev. Lett., 2010, 104: 063002. <https://link.aps.org/doi/10.1103/PhysRevLett.104.063002>.
- [44] Chen X, Torrontegui E, Muga J G. Lewis-Riesenfeld invariants and transitionless quantum driving [J/OL]. Phys. Rev. A, 2011, 83: 062116. <https://link.aps.org/doi/10.1103/PhysRevA.83.062116>.
- [45] Masuda S, Nakamura K. Fast-forward problem in quantum mechanics [J/OL]. Phys. Rev. A, 2008, 78: 062108. <https://link.aps.org/doi/10.1103/PhysRevA.78.062108>.
- [46] Masuda S, Nakamura K. Fast-forward of adiabatic dynamics in quantum mechanics [J/OL]. Proceedings of the Royal Society of London A: Mathematical, Physical and Engineering Sciences, 2010, 466 (2116): 1135–1154. <http://rspa.royalsocietypublishing.org/content/466/2116/1135>.

- [47] Schaff J-F m c, Song X-L, Vignolo P, et al. Fast optimal transition between two equilibrium states [J/OL]. Phys. Rev. A, 2010, 82: 033430. <https://link.aps.org/doi/10.1103/PhysRevA.82.033430>.
- [48] An S, Lv D, Del Campo A, et al. Shortcuts to adiabaticity by counterdiabatic driving for trapped-ion displacement in phase space [J/OL]. Nature communications, 2016, 7: 12999. <https://www.nature.com/articles/ncomms12999>.
- [49] Du Y-X, Liang Z-T, Li Y-C, et al. Experimental realization of stimulated Raman shortcut-to-adiabatic passage with cold atoms [J/OL]. Nature communications, 2016, 7 (1): 1–7. <https://doi.org/10.1038/ncomms12479>.
- [50] Lucas A. Ising formulations of many NP problems [J/OL]. Frontiers in Physics, 2014, 2: 5. <https://www.frontiersin.org/articles/10.3389/fphy.2014.00005/full>.
- [51] del Campo A, Rams M M, Zurek W H. Assisted finite-rate adiabatic passage across a quantum critical point: exact solution for the quantum Ising model [J/OL]. Physical review letters, 2012, 109 (11): 115703. <https://journals.aps.org/prl/abstract/10.1103/PhysRevLett.109.115703>.
- [52] Özgüler A B i e i f m c, Joynt R, Vavilov M G. Steering random spin systems to speed up the quantum adiabatic algorithm [J/OL]. Phys. Rev. A, 2018, 98: 062311. <https://link.aps.org/doi/10.1103/PhysRevA.98.062311>.
- [53] Takahashi K. Transitionless quantum driving for spin systems [J/OL]. Physical Review E, 2013, 87 (6): 062117. <https://journals.aps.org/pre/abstract/10.1103/PhysRevE.87.062117>.
- [54] Hartmann A, Lechner W. Rapid counter-diabatic sweeps in lattice gauge adiabatic quantum computing [J/OL]. New Journal of Physics, 2019, 21 (4): 043025. <https://iopscience.iop.org/article/10.1088/1367-2630/ab14a0>.
- [55] Petziol F, Dive B, Mintert F, et al. Fast adiabatic evolution by oscillating initial Hamiltonians [J/OL]. Physical Review A, 2018, 98 (4): 043436. <https://journals.aps.org/pra/abstract/10.1103/PhysRevA.98.043436>.
- [56] Opatrný T, Mølmer K. Partial suppression of nonadiabatic transitions [J/OL]. New Journal of Physics, 2014, 16 (1): 015025. <https://iopscience.iop.org/article/10.1088/1367-2630/16/1/015025>.
- [57] Petziol F, Dive B, Carretta S, et al. Accelerating adiabatic protocols for entangling two qubits in circuit QED [J/OL]. Physical Review A, 2019, 99 (4): 042315. <https://journals.aps.org/pra/abstract/10.1103/PhysRevA.99.042315>.
- [58] Ji Y, Bian J, Chen X, et al. Experimental preparation of Greenberger-Horne-Zeilinger states in an Ising spin model by partially suppressing the nonadiabatic transitions [J/OL]. Physical Review A, 2019, 99 (3): 032323. <https://journals.aps.org/pra/abstract/10.1103/PhysRevA.99.032323>.
- [59] Zhou H, Ji Y, Nie X, et al. Experimental Realization of Shortcuts to Adiabaticity in a Nonintegrable Spin Chain by Local Counterdiabatic Driving [J/OL]. Physical Review Applied, 2020, 13 (4): 044059. <https://journals.aps.org/prapplied/abstract/10.1103/PhysRevApplied.13.044059>.
- [60] Vinci W, Lidar D A. Non-stoquastic Hamiltonians in quantum annealing via geometric phases [J/OL]. npj Quantum Information, 2017, 3 (1): 1–6. <https://www.nature.com/articles/s41534-017-0037-z>.
- [61] Takahashi K. Shortcuts to adiabaticity for quantum annealing [J/OL]. Physical Review A, 2017, 95 (1): 012309. <https://journals.aps.org/pra/abstract/10.1103/PhysRevA.95.012309>.

- [62] Passarelli G, Cataudella V, Fazio R, et al. Counterdiabatic driving in the quantum annealing of the p -spin model: A variational approach [J/OL]. Phys. Rev. Research, 2020, 2: 013283. <https://link.aps.org/doi/10.1103/PhysRevResearch.2.013283>.
- [63] Sieberer L M, Olsacher T, Elben A, et al. Digital quantum simulation, Trotter errors, and quantum chaos of the kicked top [J/OL]. npj Quantum Information, 2019, 5 (1): 1–11. <https://www.nature.com/articles/s41534-019-0192-5>.
- [64] Suzuki M. Generalized Trotter's formula and systematic approximants of exponential operators and inner derivations with applications to many-body problems [J/OL]. Communications in Mathematical Physics, 1976, 51 (2): 183–190. <https://link.springer.com/article/10.1007/BF01609348>.
- [65] IBM Quantum Experience.
- [66] Hatomura T. Shortcuts to adiabaticity in the infinite-range Ising model by mean-field counter-diabatic driving [J/OL]. Journal of the Physical Society of Japan, 2017, 86 (9): 094002. <https://journals.jps.jp/doi/10.7566/JPSJ.86.094002>.
- [67] Kolodrubetz M, Sels D, Mehta P, et al. Geometry and non-adiabatic response in quantum and classical systems [J/OL]. Physics Reports, 2017, 697: 1–87. <https://www.sciencedirect.com/science/article/abs/pii/S0370157317301989>.
- [68] Hatano N, Suzuki M. Finding exponential product formulas of higher orders [M] // Hatano N, Suzuki M. 2005: 2005: 37–68.
- [69] Poulin D, Qarry A, Somma R, et al. Quantum simulation of time-dependent Hamiltonians and the convenient illusion of Hilbert space [J/OL]. Physical review letters, 2011, 106 (17): 170501. <https://journals.aps.org/prl/abstract/10.1103/PhysRevLett.106.170501>.
- [70] Dawson C M, Nielsen M A. The solovay-kitaev algorithm [J/OL]. arXiv preprint quant-ph/0505030, 2005. <https://arxiv.org/abs/quant-ph/0505030>.
- [71] Qiskit: An Open-source Framework for Quantum Computing.
- [72] Maciejewski F B, Zimborás Z, Oszmaniec M. Mitigation of readout noise in near-term quantum devices by classical post-processing based on detector tomography [J/OL]. Quantum, 2020, 4: 257. <https://quantum-journal.org/papers/q-2020-04-24-257/>.
- [73] Fu Y, Anderson P W. Application of statistical mechanics to NP-complete problems in combinatorial optimisation [J/OL]. J. Phys. A: Math. Gen., 1986, 19 (9): 1605. <https://iopscience.iop.org/article/10.1088/0305-4470/19/9/033/meta>.
- [74] Albash T, Lidar D A. Adiabatic quantum computation [J/OL]. Rev. Mod. Phys., 2018, 90 (1): 015002. <https://journals.aps.org/rmp/abstract/10.1103/RevModPhys.90.015002>.
- [75] Barahona F. On the computational complexity of Ising spin glass models [J/OL]. J. Phys. A: Math. Gen., 1982, 15 (10): 3241. <https://iopscience.iop.org/article/10.1088/0305-4470/15/10/028>.
- [76] Gilyén A, Hastings M B, Vazirani U. (Sub)Exponential Advantage of Adiabatic Quantum Computation with No Sign Problem [J/OL]. Proceedings of the 53rd Annual ACM SIGACT Symposium on Theory of Computing, 2021. <http://dx.doi.org/10.1145/3406325.3451060>.
- [77] Hastings M B. The Power of Adiabatic Quantum Computation with No Sign Problem [J/OL]. Quantum, 2021, 5: 597. <https://quantum-journal.org/papers/q-2021-12-06-597/>.
- [78] Fujii K. Quantum speedup in stoquastic adiabatic quantum computation [J/OL]. arXiv:1803.09954, 2018. <https://arxiv.org/abs/1803.09954>.

- [79] Farhi E, Goldstone J, Gosset D, et al. Quantum Adiabatic Algorithms, Small Gaps, and Different Paths [J/OL]. arXiv:0909.4766, 2009. <https://arxiv.org/abs/0909.4766>.
- [80] Seki Y, Nishimori H. Quantum annealing with antiferromagnetic fluctuations [J/OL]. Phys. Rev. E, 2012, 85 (5): 051112. <https://journals.aps.org/pre/abstract/10.1103/PhysRevE.85.051112>.
- [81] Seki Y, Nishimori H. Quantum annealing with antiferromagnetic transverse interactions for the Hopfield model [J/OL]. J. Phys. A: Math. Theor., 2015, 48 (33): 335301. <https://iopscience.iop.org/article/10.1088/1751-8113/48/33/335301>.
- [82] Hormozi L, Brown E W, Carleo G, et al. Nonstoquastic Hamiltonians and quantum annealing of an Ising spin glass [J/OL]. Phys. Rev. B, 2017, 95 (18): 184416. <https://journals.aps.org/prb/abstract/10.1103/PhysRevB.95.184416>.
- [83] Vinci W, Lidar D A. Non-stoquastic Hamiltonians in quantum annealing via geometric phases [J/OL]. Npj Quantum Inf., 2017, 3 (1): 1–6. <https://www.nature.com/articles/s41534-017-0037-z>.
- [84] Nishimori H, Takada K. Exponential Enhancement of the Efficiency of Quantum Annealing by Non-Stoquastic Hamiltonians [J/OL]. Front. ICT, 2017, 4: 2. <https://www.frontiersin.org/articles/10.3389/fict.2017.00002/full>.
- [85] Outeiral C, Morris G M, Shi J, et al. Investigating the potential for a limited quantum speedup on protein lattice problems [J/OL]. New J. Phys., 2021, 23 (10): 103030. <https://arxiv.org/abs/2004.01118>.
- [86] Takada K, Sota S, Yunoki S, et al. Phase transitions in the frustrated Ising ladder with stoquastic and nonstoquastic catalysts [J/OL]. Phys. Rev. Res., 2021, 3 (4): 043013. <https://journals.aps.org/prresearch/abstract/10.1103/PhysRevResearch.3.043013>.
- [87] Crosson E, Albash T, Hen I, et al. De-Signing Hamiltonians for Quantum Adiabatic Optimization [J/OL]. Quantum, 2020, 4: 334. <https://quantum-journal.org/papers/q-2020-09-24-334/>.
- [88] Chen X, Ruschhaupt A, Schmidt S, et al. Fast Optimal Frictionless Atom Cooling in Harmonic Traps: Shortcut to Adiabaticity [J/OL]. Phys. Rev. Lett., 2010, 104: 063002. <https://link.aps.org/doi/10.1103/PhysRevLett.104.063002>.
- [89] Guéry-Odelin D, Ruschhaupt A, Kiely A, et al. Shortcuts to adiabaticity: Concepts, methods, and applications [J/OL]. Rev. Mod. Phys., 2019, 91 (4): 045001. <https://journals.aps.org/rmp/abstract/10.1103/RevModPhys.91.045001>.
- [90] Demirplak M, Rice S A. Adiabatic Population Transfer with Control Fields [J/OL]. J. Phys. Chem. A, 2003, 107 (46): 9937–9945. <https://pubs.acs.org/doi/abs/10.1021/jp030708a>.
- [91] Berry M V. Transitionless quantum driving [J/OL]. J. Phys. A: Math. Theor., 2009, 42 (36): 365303. <https://iopscience.iop.org/article/10.1088/1751-8113/42/36/365303/meta>.
- [92] Chen X, Lizuain I, Ruschhaupt A, et al. Shortcut to Adiabatic Passage in Two- and Three-Level Atoms [J/OL]. Phys. Rev. Lett., 2010, 105: 123003. <https://link.aps.org/doi/10.1103/PhysRevLett.105.123003>.
- [93] del Campo A. Shortcuts to adiabaticity by counterdiabatic driving [J/OL]. Physical review letters, 2013, 111 (10): 100502. <https://journals.aps.org/prl/abstract/10.1103/PhysRevLett.111.100502>.
- [94] Hegade N N, Paul K, Ding Y, et al. Shortcuts to Adiabaticity in Digitized Adiabatic Quantum Computing [J/OL]. Phys. Rev. Appl., 2021, 15 (2): 024038. <https://journals.aps.org/prapplied/abstract/10.1103/PhysRevApplied.15.024038>.

- [95] Hegade N N, Paul K, Albarrán-Arriagada F, et al. Digitized adiabatic quantum factorization [J/OL]. Phys. Rev. A, 2021, 104: L050403. <https://link.aps.org/doi/10.1103/PhysRevA.104.L050403>.
- [96] Hegade N N, Chandarana P, Paul K, et al. Portfolio Optimization with Digitized-Counterdiabatic Quantum Algorithms [J/OL]. arXiv:2112.08347, 2021. <https://arxiv.org/abs/2112.08347>.
- [97] Zhan Z, Run C, Zong Z, et al. Experimental Determination of Electronic States via Digitized Shortcut to Adiabaticity and Sequential Digitized Adiabaticity [J/OL]. Phys. Rev. Appl., 2021, 16 (3): 034050. <https://journals.aps.org/prapplied/abstract/10.1103/PhysRevApplied.16.034050>.
- [98] Takahashi K. Shortcuts to adiabaticity for quantum annealing [J/OL]. Phys. Rev. A, 2017, 95: 012309. <https://link.aps.org/doi/10.1103/PhysRevA.95.012309>.
- [99] Passarelli G, Cataudella V, Fazio R, et al. Counterdiabatic driving in the quantum annealing of the p-spin model: A variational approach [J/OL]. Phys. Rev. Res., 2020, 2: 013283. <https://link.aps.org/doi/10.1103/PhysRevResearch.2.013283>.
- [100] Prielinger L, Hartmann A, Yamashiro Y, et al. Two-parameter counter-diabatic driving in quantum annealing [J/OL]. Physical Review Research, 2021, 3 (1): 013227. <https://journals.aps.org/prresearch/abstract/10.1103/PhysRevResearch.3.013227>.
- [101] Hartmann A, Mbeng G B, Lechner W. Polynomial scaling enhancement in ground-state preparation of Ising spin models via counter-diabatic driving [J/OL]. arXiv:2109.04962, 2021. <https://arxiv.org/abs/2109.04962>.
- [102] Yao J, Lin L, Bukov M. Reinforcement Learning for Many-Body Ground-State Preparation Inspired by Counterdiabatic Driving [J/OL]. Phys. Rev. X, 2021, 11 (3): 031070. <http://dx.doi.org/10.1103/PhysRevX.11.031070>.
- [103] Wurtz J, Love P J. Counterdiabaticity and the quantum approximate optimization algorithm [J/OL]. arXiv:2106.15645, 2021. <https://arxiv.org/abs/2106.15645>.
- [104] Chandarana P, Hegade N N, Paul K, et al. Digitized-counterdiabatic quantum approximate optimization algorithm [J/OL]. arXiv:2107.02789, 2021. <https://arxiv.org/abs/2107.02789>.
- [105] Sels D, Polkovnikov A. Minimizing irreversible losses in quantum systems by local counterdiabatic driving [J/OL]. PNAS, 2017, 114 (20): E3909–E3916. <https://www.pnas.org/content/114/20/E3909>.
- [106] Hatomura T, Takahashi K. Controlling and exploring quantum systems by algebraic expression of adiabatic gauge potential [J/OL]. Phys. Rev. A, 2021, 103 (1): 012220. <https://journals.aps.org/prabstract/10.1103/PhysRevA.103.012220>.
- [107] Gentini L, Cuccoli A, Banchi L. Variational Adiabatic Gauge Transformation on real quantum hardware for effective low-energy Hamiltonians and accurate diagonalization [J/OL]. arXiv:2111.08771, 2021. <https://arxiv.org/abs/2111.08771>.
- [108] Yao J, Köttering P, Gundlach H, et al. Noise-Robust End-to-End Quantum Control using Deep Autoregressive Policy Networks [J/OL]. arXiv:2012.06701, 2020. <https://arxiv.org/abs/2012.06701>.
- [109] Hegde P R, Passarelli G, Scocco A, et al. Genetic optimization of quantum annealing [J/OL]. arXiv:2108.03185, 2021. <https://arxiv.org/abs/2108.03185>.
- [110] Kadowaki T, Nishimori H. Greedy parameter optimization for diabatic quantum annealing [J/OL]. arXiv:2111.13287, 2021. <https://arxiv.org/abs/2111.13287>.

- [111] Ozfidan I, Deng C, Smirnov A, et al. Demonstration of a Nonstoquastic Hamiltonian in Coupled Superconducting Flux Qubits [J/OL]. Phys. Rev. Appl., 2020, 13 (3): 034037. <https://journals.aps.org/prapplied/abstract/10.1103/PhysRevApplied.13.034037>.
- [112] Fowler A G, Mariantoni M, Martinis J M, et al. Surface codes: Towards practical large-scale quantum computation [J/OL]. Phys. Rev. A, 2012, 86 (3): 032324. <https://journals.aps.org/pra/abstract/10.1103/PhysRevA.86.032324>.
- [113] Endo S, Benjamin S C, Li Y. Practical Quantum Error Mitigation for Near-Future Applications [J/OL]. Phys. Rev. X, 2018, 8 (3): 031027. <https://journals.aps.org/prx/abstract/10.1103/PhysRevX.8.031027>.
- [114] Chen Y-A, Childs A M, Hafezi M, et al. Efficient Product Formulas for Commutators and Applications to Quantum Simulation [J/OL]. arXiv:2111.12177, 2021. <https://arxiv.org/abs/2111.12177>.
- [115] Yi C. Success of digital adiabatic simulation with large Trotter step [J/OL]. arXiv:2107.06404, 2021. <https://journals.aps.org/pra/abstract/10.1103/PhysRevA.104.052603>.
- [116] Könz M S, Lechner W, Katzgraber H G, et al. Embedding Overhead Scaling of Optimization Problems in Quantum Annealing [J/OL]. PRX Quantum, 2021, 2: 040322. <https://link.aps.org/doi/10.1103/PRXQuantum.2.040322>.
- [117] Preskill J. Quantum Computing in the NISQ era and beyond [J/OL]. Quantum, 2018, 2: 79. <https://doi.org/10.22331/q-2018-08-06-79>.
- [118] Bharti K, Cervera-Lierta A, Kyaw T H, et al. Noisy intermediate-scale quantum (NISQ) algorithms [J], 2021.
- [119] Colless J I, Ramasesh V V, Dahlen D, et al. Computation of Molecular Spectra on a Quantum Processor with an Error-Resilient Algorithm [J/OL]. Phys. Rev. X, 2018, 8: 011021. <https://link.aps.org/doi/10.1103/PhysRevX.8.011021>.
- [120] Grimsley H R, Economou S E, Barnes E, et al. An adaptive variational algorithm for exact molecular simulations on a quantum computer [J/OL]. Nature Communications, 2019, 10 (1): 3007. <https://doi.org/10.1038/s41467-019-10988-2>.
- [121] Cao Y, Romero J, Olson J P, et al. Quantum Chemistry in the Age of Quantum Computing [J/OL]. Chemical Reviews, 2019, 119 (19): 10856–10915. <https://doi.org/10.1021/acs.chemrev.8b00803>.
- [122] Kandala A, Mezzacapo A, Temme K, et al. Hardware-efficient variational quantum eigensolver for small molecules and quantum magnets [J/OL]. Nature, 2017, 549 (7671): 242–246. <https://doi.org/10.1038/nature23879>.
- [123] Nam Y, Chen J-S, Pisenti N C, et al. Ground-state energy estimation of the water molecule on a trapped-ion quantum computer [J/OL]. npj Quantum Information, 2020, 6 (1): 33. <https://doi.org/10.1038/s41534-020-0259-3>.
- [124] Hempel C, Maier C, Romero J, et al. Quantum Chemistry Calculations on a Trapped-Ion Quantum Simulator [J/OL]. Phys. Rev. X, 2018, 8: 031022. <https://link.aps.org/doi/10.1103/PhysRevX.8.031022>.
- [125] Cade C, Mineh L, Montanaro A, et al. Strategies for solving the Fermi-Hubbard model on near-term quantum computers [J/OL]. Physical Review B, 2020, 102 (23). <http://dx.doi.org/10.1103/PhysRevB.102.235122>.

- [126] Endo S, Kurata I, Nakagawa Y O. Calculation of the Green's function on near-term quantum computers [J/OL]. Physical Review Research, 2020, 2 (3). <http://dx.doi.org/10.1103/PhysRevResearch.2.033281>.
- [127] Bravo-Prieto C, Lumbrales-Zarapico J, Tagliacozzo L, et al. Scaling of variational quantum circuit depth for condensed matter systems [J/OL]. Quantum, 2020, 4: 272. <https://doi.org/10.22331/q-2020-05-28-272>.
- [128] Bravo-Prieto C, LaRose R, Cerezo M, et al. Variational Quantum Linear Solver [J], 2020.
- [129] Liu X, Angone A, Shaydulin R, et al. Layer VQE: A Variational Approach for Combinatorial Optimization on Noisy Quantum Computers [J], 2021.
- [130] Nannicini G. Performance of hybrid quantum-classical variational heuristics for combinatorial optimization [J/OL]. Physical Review E, 2019, 99 (1). <http://dx.doi.org/10.1103/PhysRevE.99.013304>.
- [131] Anschuetz E R, Olson J P, Aspuru-Guzik A, et al. Variational Quantum Factoring [J], 2018.
- [132] Karamlou A H, Simon W A, Katabarwa A, et al. Analyzing the Performance of Variational Quantum Factoring on a Superconducting Quantum Processor [J], 2021.
- [133] Peruzzo A, McClean J, Shadbolt P, et al. A variational eigenvalue solver on a photonic quantum processor [J/OL]. Nature Communications, 2014, 5 (1): 4213. <https://doi.org/10.1038/ncomms5213>.
- [134] O'Malley P J J, Babbush R, Kivlichan I D, et al. Scalable Quantum Simulation of Molecular Energies [J/OL]. Phys. Rev. X, 2016, 6: 031007. <https://link.aps.org/doi/10.1103/PhysRevX.6.031007>.
- [135] McClean J R, Romero J, Babbush R, et al. The theory of variational hybrid quantum-classical algorithms [J/OL]. New Journal of Physics, 2016, 18 (2): 023023. <https://doi.org/10.1088/1367-2630/18/2/023023>.
- [136] McClean J R, Kimchi-Schwartz M E, Carter J, et al. Hybrid quantum-classical hierarchy for mitigation of decoherence and determination of excited states [J/OL]. Phys. Rev. A, 2017, 95: 042308. <https://link.aps.org/doi/10.1103/PhysRevA.95.042308>.
- [137] Barkoutsos P K, Gonthier J F, Sokolov I, et al. Quantum algorithms for electronic structure calculations: Particle-hole Hamiltonian and optimized wave-function expansions [J/OL]. Phys. Rev. A, 2018, 98: 022322. <https://link.aps.org/doi/10.1103/PhysRevA.98.022322>.
- [138] Romero J, Babbush R, McClean J R, et al. Strategies for quantum computing molecular energies using the unitary coupled cluster ansatz [J/OL]. Quantum Science and Technology, 2018, 4 (1): 014008. <https://doi.org/10.1088/2058-9565/aad3e4>.
- [139] Lee J, Huggins W J, Head-Gordon M, et al. Generalized Unitary Coupled Cluster Wave functions for Quantum Computation [J/OL]. Journal of Chemical Theory and Computation, 2019, 15 (1): 311–324. <https://doi.org/10.1021/acs.jctc.8b01004>.
- [140] Shen Y, Zhang X, Zhang S, et al. Quantum implementation of the unitary coupled cluster for simulating molecular electronic structure [J/OL]. Phys. Rev. A, 2017, 95: 020501. <https://link.aps.org/doi/10.1103/PhysRevA.95.020501>.
- [141] Pagano G, Bapat A, Becker P, et al. Quantum approximate optimization of the long-range Ising model with a trapped-ion quantum simulator [J/OL]. Proceedings of the National Academy of Sciences, 2020, 117 (41): 25396–25401. <https://www.pnas.org/content/117/41/25396>.

- [142] Farhi E, Goldstone J, Gutmann S. A Quantum Approximate Optimization Algorithm [J], 2014.
- [143] Willsch M, Willsch D, Jin F, et al. Benchmarking the quantum approximate optimization algorithm [J/OL]. *Quantum Information Processing*, 2020, 19 (7). <http://dx.doi.org/10.1007/s11128-020-02692-8>.
- [144] Wauters M M, Mbeng G B, Santoro G E. Polynomial scaling of QAOA for ground-state preparation of the fully-connected p-spin ferromagnet [J], 2020.
- [145] Zhu L, Tang H L, Barron G S, et al. An adaptive quantum approximate optimization algorithm for solving combinatorial problems on a quantum computer [J/OL], 2020. <https://arxiv.org/abs/2005.10258>.
- [146] Headley D, Müller T, Martin A, et al. Approximating the quantum approximate optimisation algorithm [J/OL]. arXiv preprint arXiv:2002.12215, 2020. <https://arxiv.org/abs/2002.12215>.
- [147] McClean J R, Boixo S, Smelyanskiy V N, et al. Barren plateaus in quantum neural network training landscapes [J/OL]. *Nature Communications*, 2018, 9 (1): 4812. <https://doi.org/10.1038/s41467-018-07090-4>.
- [148] Cerezo M, Sone A, Volkoff T, et al. Cost function dependent barren plateaus in shallow parametrized quantum circuits [J/OL]. *Nature Communications*, 2021, 12 (1). <http://dx.doi.org/10.1038/s41467-021-21728-w>.
- [149] Grant E, Wossnig L, Ostaszewski M, et al. An initialization strategy for addressing barren plateaus in parametrized quantum circuits [J/OL]. *Quantum*, 2019, 3: 214. <https://doi.org/10.22331/q-2019-12-09-214>.
- [150] Hegade N N, Paul K, Ding Y, et al. Shortcuts to Adiabaticity in Digitized Adiabatic Quantum Computing [J/OL]. *Phys. Rev. Applied*, 2021, 15: 024038. <https://link.aps.org/doi/10.1103/PhysRevApplied.15.024038>.
- [151] Hartmann A, Lechner W. Rapid counter-diabatic sweeps in lattice gauge adiabatic quantum computing [J/OL]. *New Journal of Physics*, 2019, 21 (4): 043025. <https://doi.org/10.1088/1367-2630/ab14a0>.
- [152] Opatrný T, Mølmer K. Partial suppression of nonadiabatic transitions [J/OL]. *New Journal of Physics*, 2014, 16 (1): 015025. <https://doi.org/10.1088/1367-2630/16/1/015025>.
- [153] Hegade N N, Paul K, Albarrán-Arriagada F, et al. Digitized-Adiabatic Quantum Factorization [J], 2021.
- [154] Yao J, Lin L, Bukov M. Reinforcement Learning for Many-Body Ground State Preparation based on Counter-Diabatic Driving [J], 2020.
- [155] Saberi H, Opatrný T, Mølmer K, et al. Adiabatic tracking of quantum many-body dynamics [J/OL]. *Physical Review A*, 2014, 90 (6): 060301. <https://journals.aps.org/pra/abstract/10.1103/PhysRevA.90.060301>.
- [156] Hatomura T, Takahashi K. Controlling and exploring quantum systems by algebraic expression of adiabatic gauge potential [J/OL]. *Phys. Rev. A*, 2021, 103: 012220. <https://link.aps.org/doi/10.1103/PhysRevA.103.012220>.
- [157] Qian N. On the momentum term in gradient descent learning algorithms [J/OL]. *Neural Networks*, 1999, 12 (1): 145–151. <https://www.sciencedirect.com/science/article/pii/S0893608098001166>.

- [158] Duchi J, Hazan E, Singer Y. Adaptive Subgradient Methods for Online Learning and Stochastic Optimization [J/OL]. *Journal of Machine Learning Research*, 2011, 12 (61): 2121–2159. <http://jmlr.org/papers/v12/duchi11a.html>.
- [159] Dean J, Corrado G, Monga R, et al. Large Scale Distributed Deep Networks [J/OL]. *Advances in Neural Information Processing Systems*, 2012, 25. <https://proceedings.neurips.cc/paper/2012/file/6aca97005c68f1206823815f66102863-Paper.pdf>.
- [160] Ruder S. An overview of gradient descent optimization algorithms [J/OL], 2017. <https://arxiv.org/abs/1609.04747>.
- [161] Brush S G. History of the Lenz-Ising Model [J/OL]. *Rev. Mod. Phys.*, 1967, 39: 883–893. <https://link.aps.org/doi/10.1103/RevModPhys.39.883>.
- [162] Ising E. Beitrag zur Theorie des Ferromagnetismus [J/OL]. *Zeitschrift für Physik*, 1925, 31 (1): 253–258. <https://doi.org/10.1007/BF02980577>.
- [163] Lifshitz E M, Pitaevskii L P. Statistical physics: theory of the condensed state [M/OL]. Elsevier, 2013. <https://books.google.co.in/books?id=lgIBDAAAQBAJ>.
- [164] Leibfried D, Barrett M D, Schaetz T, et al. Toward Heisenberg-Limited Spectroscopy with Multiparticle Entangled States [J/OL]. *Science*, 2004, 304 (5676): 1476–1478. <https://science.sciencemag.org/content/304/5676/1476>.
- [165] Giovannetti V, Lloyd S, Maccone L. Quantum-Enhanced Measurements: Beating the Standard Quantum Limit [J/OL]. *Science*, 2004, 306 (5700): 1330–1336. <https://science.sciencemag.org/content/306/5700/1330>.
- [166] Degen C L, Reinhard F, Cappellaro P. Quantum sensing [J/OL]. *Rev. Mod. Phys.*, 2017, 89: 035002. <https://link.aps.org/doi/10.1103/RevModPhys.89.035002>.
- [167] Choi S, Yao N Y, Lukin M D. Quantum metrology based on strongly correlated matter [J], 2017.
- [168] Nachtergaelie B, Sims R. Lieb-Robinson Bounds in Quantum Many-Body Physics [J], 2010.
- [169] Ho W W, Hsieh T H. Efficient variational simulation of non-trivial quantum states [J/OL]. *SciPost Phys.*, 2019, 6: 29. <https://scipost.org/10.21468/SciPostPhys.6.3.029>.
- [170] Binder K, Young A P. Spin glasses: Experimental facts, theoretical concepts, and open questions [J/OL]. *Rev. Mod. Phys.*, 1986, 58: 801–976. <https://link.aps.org/doi/10.1103/RevModPhys.58.801>.
- [171] Sherrington D, Kirkpatrick S. Solvable Model of a Spin-Glass [J/OL]. *Phys. Rev. Lett.*, 1975, 35: 1792–1796. <https://link.aps.org/doi/10.1103/PhysRevLett.35.1792>.
- [172] Harrigan M P, Sung K J, Neeley M, et al. Quantum approximate optimization of non-planar graph problems on a planar superconducting processor [J/OL]. *Nature Physics*, 2021, 17 (3): 332–336. <https://doi.org/10.1038/s41567-020-01105-y>.
- [173] Farhi E, Goldstone J, Gutmann S, et al. The Quantum Approximate Optimization Algorithm and the Sherrington-Kirkpatrick Model at Infinite Size [J], 2020.
- [174] Jörg T, Krzakala F, Kurchan J, et al. Energy gaps in quantum first-order mean-field-like transitions: The problems that quantum annealing cannot solve [J/OL]. *EPL (Europhysics Letters)*, 2010, 89 (4): 40004. <https://doi.org/10.1209/0295-5075/89/40004>.

- [175] Wauters M M, Fazio R, Nishimori H, et al. Direct comparison of quantum and simulated annealing on a fully connected Ising ferromagnet [J/OL]. *Phys. Rev. A*, 2017, 96: 022326. <https://link.aps.org/doi/10.1103/PhysRevA.96.022326>.
- [176] Filippone M, Dusuel S, Vidal J. Quantum phase transitions in fully connected spin models: An entanglement perspective [J/OL]. *Physical Review A*, 2011, 83 (2). <http://dx.doi.org/10.1103/PhysRevA.83.022327>.
- [177] Caneva T, Fazio R, Santoro G E. Adiabatic quantum dynamics of a random Ising chain across its quantum critical point [J/OL]. *Phys. Rev. B*, 2007, 76: 144427. <https://link.aps.org/doi/10.1103/PhysRevB.76.144427>.
- [178] Seki Y, Nishimori H. Quantum annealing with antiferromagnetic fluctuations [J/OL]. *Phys. Rev. E*, 2012, 85: 051112. <https://link.aps.org/doi/10.1103/PhysRevE.85.051112>.
- [179] Seoane B, Nishimori H. Many-body transverse interactions in the quantum annealing of the p-spin ferromagnet [J/OL]. *Journal of Physics A: Mathematical and Theoretical*, 2012, 45 (43): 435301. <https://doi.org/10.1088/1751-8113/45/43/435301>.
- [180] Shor P W. Polynomial-time algorithms for prime factorization and discrete logarithms on a quantum computer [J/OL]. *SIAM review*, 1999, 41 (2): 303–332. <https://pubs.siam.org/doi/pdf/10.1137/S0036144598347011>.
- [181] Lu C-Y, Browne D E, Yang T, et al. Demonstration of a Compiled Version of Shor’s Quantum Factoring Algorithm Using Photonic Qubits [J/OL]. *Phys. Rev. Lett.*, 2007, 99: 250504. <https://link.aps.org/doi/10.1103/PhysRevLett.99.250504>.
- [182] Lanyon B P, Weinhold T J, Langford N K, et al. Experimental Demonstration of a Compiled Version of Shor’s Algorithm with Quantum Entanglement [J/OL]. *Phys. Rev. Lett.*, 2007, 99: 250505. <https://link.aps.org/doi/10.1103/PhysRevLett.99.250505>.
- [183] Martin-Lopez E, Laing A, Lawson T, et al. Experimental realization of Shor’s quantum factoring algorithm using qubit recycling [J/OL]. *Nature photonics*, 2012, 6 (11): 773–776. <https://www.nature.com/articles/nphoton.2012.259>.
- [184] Amico M, Saleem Z H, Kumph M. Experimental study of Shor’s factoring algorithm using the IBM Q Experience [J/OL]. *Phys. Rev. A*, 2019, 100: 012305. <https://link.aps.org/doi/10.1103/PhysRevA.100.012305>.
- [185] Burges C J. Factoring as optimization [J/OL]. Microsoft Research MSR-TR-200, 2002. <https://www.microsoft.com/en-us/research/publication/factoring-as-optimization/>.
- [186] Xu N, Zhu J, Lu D, et al. Quantum Factorization of 143 on a Dipolar-Coupling Nuclear Magnetic Resonance System [J/OL]. *Phys. Rev. Lett.*, 2012, 108: 130501. <https://link.aps.org/doi/10.1103/PhysRevLett.108.130501>.
- [187] Xu K, Xie T, Li Z, et al. Experimental Adiabatic Quantum Factorization under Ambient Conditions Based on a Solid-State Single Spin System [J/OL]. *Phys. Rev. Lett.*, 2017, 118: 130504. <https://link.aps.org/doi/10.1103/PhysRevLett.118.130504>.
- [188] Jiang S, Britt K A, McCaskey A J, et al. Quantum Annealing for Prime Factorization [J/OL]. *Scientific reports*, 2018, 8 (1): 1–9. <https://www.nature.com/articles/s41598-018-36058-z>.
- [189] Dridi R, Alghassi H. Prime factorization using quantum annealing and computational algebraic geometry [J/OL]. *Scientific reports*, 2017, 7 (1): 1–10. <https://www.nature.com/articles/srep43048>.

- [190] Gibney E. D-Wave upgrade: How scientists are using the world's most controversial quantum computer [J/OL]. *Nature*, 2017, 541 (7638). <https://www.nature.com/articles/541447b>.
- [191] Torrontegui E, Ibáñez S, Martínez-Garaot S, et al. Shortcuts to adiabaticity [J/OL]. *Advances in atomic, molecular, and optical physics*, 2013, 62: 117–169. <https://www.sciencedirect.com/science/article/pii/B9780124080904000025>.
- [192] Deffner S, Jarzynski C, del Campo A. Classical and Quantum Shortcuts to Adiabaticity for Scale-Invariant Driving [J/OL]. *Phys. Rev. X*, 2014, 4: 021013. <https://link.aps.org/doi/10.1103/PhysRevX.4.021013>.
- [193] Campbell S, De Chiara G, Paternostro M, et al. Shortcut to Adiabaticity in the Lipkin-Meshkov-Glick Model [J/OL]. *Phys. Rev. Lett.*, 2015, 114: 177206. <https://link.aps.org/doi/10.1103/PhysRevLett.114.177206>.
- [194] Hartmann A, Mukherjee V, Niedenzu W, et al. Many-body quantum heat engines with shortcuts to adiabaticity [J/OL]. *Phys. Rev. Research*, 2020, 2: 023145. <https://link.aps.org/doi/10.1103/PhysRevResearch.2.023145>.
- [195] Berry D W, Childs A M, Su Y, et al. Time-dependent Hamiltonian simulation with L^1 -norm scaling [J/OL]. *Quantum*, 2020, 4: 254. <https://doi.org/10.22331/q-2020-04-20-254>.
- [196] Schaller G, Schützhold R. The Role of Symmetries in Adiabatic Quantum Algorithms [J/OL]. *Quantum Info. Comput.*, 2010, 10 (1): 109–140. <https://dl.acm.org/doi/10.5555/2011438.2011447>.
- [197] Dattani N S, Bryans N. Quantum factorization of 56153 with only 4 qubits [J/OL]. arXiv preprint arXiv:1411.6758, 2014. <https://arxiv.org/abs/1411.6758>.
- [198] Anschuetz E R, Olson J P, Aspuru-Guzik A, et al. Variational quantum factoring [J/OL]. arXiv preprint arXiv:1808.08927, 2018. <https://arxiv.org/abs/1808.08927>.
- [199] Karamlou A H, Simon W A, Katabarwa A, et al. Analyzing the performance of variational quantum factoring on a superconducting quantum processor [J/OL]. *npj Quantum Information*, 2021, 7 (1): 1–6. <https://www.nature.com/articles/s41534-021-00478-z>.
- [200] Albash T. Role of nonstoquastic catalysts in quantum adiabatic optimization [J/OL]. *Physical Review A*, 2019, 99 (4): 042334. <https://journals.aps.org/prabstract/10.1103/PhysRevA.99.042334>.
- [201] Raeisi S, Wiebe N, Sanders B C. Quantum-circuit design for efficient simulations of many-body quantum dynamics [J/OL]. *New Journal of Physics*, 2012, 14 (10): 103017. <https://iopscience.iop.org/article/10.1088/1367-2630/14/10/103017>.
- [202] Skosana U, Tame M. Demonstration of Shor's factoring algorithm for $N = 21$ on IBM quantum processors [J/OL]. *Scientific Reports*, 2021, 11 (1): 1–12. <https://www.nature.com/articles/s41598-021-95973-w>.
- [203] Ender K, ter Hoeven R, Niehoff B E, et al. Parity Quantum Optimization: Compiler [J/OL]. arXiv preprint arXiv:2105.06233, 2021. <https://arxiv.org/abs/2105.06233>.
- [204] Drieb-Schön M, Javanmard Y, Ender K, et al. Parity Quantum Optimization: Encoding Constraints [J/OL]. arXiv preprint arXiv:2105.06235, 2021. <https://arxiv.org/abs/2105.06235>.
- [205] Fellner M, Ender K, ter Hoeven R, et al. Parity Quantum Optimization: Benchmarks [J/OL]. arXiv preprint arXiv:2105.06240, 2021. <https://arxiv.org/abs/2105.06240>.
- [206] Mohseni M, Read P, Neven H, et al. Commercialize quantum technologies in five years [J/OL]. *Nature News*, 2017, 543 (7644): 171. <https://www.nature.com/articles/543171a>.

- [207] Bova F, Goldfarb A, Melko R G. Commercial applications of quantum computing [J/OL]. EPJ quantum technology, 2021, 8 (1): 2. <https://doi.org/10.1140/epjqt/s40507-021-00091-1>.
- [208] Montanaro A. Quantum algorithms: an overview [J/OL]. npj Quantum Information, 2016, 2 (1): 1–8. <https://www.nature.com/articles/npjqi201523>.
- [209] Bapst V, Foini L, Krzakala F, et al. The quantum adiabatic algorithm applied to random optimization problems: The quantum spin glass perspective [J/OL]. Physics Reports, 2013, 523 (3): 127–205. <https://www.sciencedirect.com/science/article/pii/S037015731200347X>.
- [210] Farhi E, Goldstone J, Gutmann S. A quantum approximate optimization algorithm [J/OL]. arXiv preprint arXiv:1411.4028, 2014. <https://arxiv.org/abs/1411.4028>.
- [211] Hegade N N, Paul K, Albarrán-Arriagada F, et al. Digitized adiabatic quantum factorization [J/OL]. Phys. Rev. A, 2021, 104: L050403. <https://link.aps.org/doi/10.1103/PhysRevA.104.L050403>.
- [212] Yao J, Lin L, Bukov M. Reinforcement Learning for Many-Body Ground-State Preparation Inspired by Counterdiabatic Driving [J/OL]. Physical Review X, 2021, 11 (3). <http://dx.doi.org/10.1103/PhysRevX.11.031070>.
- [213] Chandarana P, Hegade N, Paul K, et al. Digitized-counterdiabatic quantum approximate optimization algorithm [J/OL]. arXiv preprint arXiv:2107.02789, 2021. <https://arxiv.org/abs/2107.02789>.
- [214] Wurtz J, Love P J. Counterdiabaticity and the quantum approximate optimization algorithm [J/OL]. arXiv preprint arXiv:2106.15645, 2021. <https://arxiv.org/abs/2106.15645>.
- [215] Markowitz H. Portfolio Selection [J/OL]. The Journal of Finance, 1952, 7 (1): 77–91. <http://www.jstor.org/stable/2975974>.
- [216] Bouland A, van Dam W, Joorati H, et al. Prospects and challenges of quantum finance [J/OL]. arXiv preprint arXiv:2011.06492, 2020. <https://arxiv.org/abs/2011.06492>.
- [217] Hodson M, Ruck B, Ong H, et al. Portfolio rebalancing experiments using the Quantum Alternating Operator Ansatz [J/OL]. arXiv preprint arXiv:1911.05296, 2019. <https://arxiv.org/abs/1911.05296>.
- [218] Grant E, Humble T S, Stump B. Benchmarking Quantum Annealing Controls with Portfolio Optimization [J/OL]. Physical Review Applied, 2021, 15 (1). <http://dx.doi.org/10.1103/PhysRevApplied.15.014012>.
- [219] Rosenberg G, Haghnegahdar P, Goddard P, et al. Solving the Optimal Trading Trajectory Problem Using a Quantum Annealer [J/OL]. IEEE Journal of Selected Topics in Signal Processing, 2016, 10 (6): 1053–1060. <http://dx.doi.org/10.1109/JSTSP.2016.2574703>.
- [220] Venturelli D, Kondratyev A. Reverse quantum annealing approach to portfolio optimization problems [J/OL]. Quantum Machine Intelligence, 2019, 1 (1-2): 17–30. <http://dx.doi.org/10.1007/s42484-019-00001-w>.
- [221] Marzec M. Portfolio optimization: Applications in quantum computing [J/OL]. Handbook of high-frequency trading and modeling in finance, 2016: 73–106. <https://dx.doi.org/10.2139/ssrn.2278729>.
- [222] Rebentrost P, Lloyd S. Quantum computational finance: quantum algorithm for portfolio optimization [J/OL]. arXiv preprint arXiv:1811.03975, 2018. <https://arxiv.org/abs/1811.03975>.
- [223] Orús R, Mugel S, Lizaso E. Quantum computing for finance: Overview and prospects [J/OL]. Reviews in Physics, 2019, 4: 100028. <https://www.sciencedirect.com/science/article/pii/S2405428318300571>.

- [224] Mugel S, Kuchkovsky C, Sanchez E, et al. Dynamic portfolio optimization with real datasets using quantum processors and quantum-inspired tensor networks [J/OL]. arXiv preprint arXiv:2007.00017, 2020. <https://arxiv.org/abs/2007.00017>.
- [225] Huang X. Mean-Variance Models for Portfolio Selection Subject to Experts' Estimations [J/OL]. Expert Syst. Appl., 2012, 39 (5): 5887–5893. <https://doi.org/10.1016/j.eswa.2011.11.119>.
- [226] Martin I. What is the Expected Return on the Market? [J/OL]. The Quarterly Journal of Economics, 2016, 132 (1): 367–433. <https://doi.org/10.1093/qje/qjw034>.
- [227] Hartmann A, Mukherjee V, Mbeng G B, et al. Multi-spin counter-diabatic driving in many-body quantum Otto refrigerators [J/OL]. Quantum, 2020, 4: 377. <https://quantum-journal.org/papers/q-2020-12-24-377/>.
- [228] Iram S, Dolson E, Chiel J, et al. Controlling the speed and trajectory of evolution with counter-diabatic driving [J/OL]. Nature Physics, 2021, 17 (1): 135–142. <https://www.nature.com/articles/s41567-020-0989-3>.
- [229] Hegade N N, Chen X, Solano E. Digitized-Counterdiabatic Quantum Optimization [J/OL]. arXiv preprint arXiv:2201.00790, 2022. <https://arxiv.org/abs/2201.00790>.
- [230] Hadfield S, Wang Z, O' Gorman B, et al. From the Quantum Approximate Optimization Algorithm to a Quantum Alternating Operator Ansatz [J/OL]. Algorithms, 2019, 12 (2): 34. <http://dx.doi.org/10.3390/a12020034>.

作者在攻读博士学位期间发表的论文与研究成果

发表的学术论文

1. Hegade, Narendra N., Koushik Paul, Yongcheng Ding, Mikel Sanz, Francisco Albarrán-Arriagada, Enrique Solano and Xi Chen. "Shortcuts to adiabaticity in digitized adiabatic quantum computing". *Physical Review Applied* 15.2 (2021): 024038. (SCI 收录)
2. Chandarana, Pranav, Hegade, Narendra N., Koushik Paul, Francisco Albarrán-Arriagada, Enrique Solano, Adolfo Del Campo, and Xi Chen. "Digitized-counterdiabatic quantum approximate optimization algorithm". *Physical Review Research* 4.1 (2022): 013141. (SCI 收录)
3. Hegade, Narendra N., Koushik Paul, Francisco Albarrán-Arriagada, Xi Chen and Enrique Solano. "Digitized adiabatic quantum factorization". *Physical Review A* 104.5 (2021): L050403. (SCI 收录)
4. Hegade, Narendra. N., Chandarana, Pranav, Koushik Paul, Xi Chen, Francisco Albarrán-Arriagada and Enrique Solano. "Portfolio optimization with digitized-counterdiabatic quantum algorithms". *Physical Review Research* 4.4 (2022): 043204. (SCI 收录)
5. Hegade, Narendra N., Xi Chen, and Enrique Solano. "Digitized counterdiabatic quantum optimization". *Physical Review Research* 4.4 (2022): L042030. (SCI 收录)

Other published works not included in this thesis

1. Kumar, S., Cárdenas-López, F. A., Hegade, Narendra N., Chen, X., Albarrán-Arriagada, F., Solano, E., and Barrios, G. A. "Entangled quantum memristors". *Physical Review A*, 104.6, 062605 (2021).
2. Kumar, S., Cárdenas-López, F. A., Hegade, Narendra N., Albarrán-Arriagada, F., Solano, E., and Barrios, G. A. "Tripartite entanglement in quantum memristors". *Physical Review Applied* 18.3: 034004 (2022).
3. Chandarana, Pranav, Pablo S. Vieites, Narendra N. Hegade, Enrique Solano, Yue Ban,

- and Xi Chen. "Meta-Learning Digitized-Counterdiabatic Quantum Optimization". arXiv preprint arXiv:2206.09966 (2022).
4. Chandarana, Pranav, Hegade, Narendra N., Montalban, I., Solano, E., Chen, X. "Digitized-Counterdiabatic Quantum Algorithm for Protein Folding". arXiv preprint arXiv:2212.13511 (2022).

作者在攻读博士学位期间所作的项目

My Ph.D. research was supported by the China Scholarship Council (CSC) since 2019-2023, CSC number: 2019DFH022311.

致 谢

Foremost, I would like to express my sincere gratitude and regard to my Ph.D. supervisor Prof. Dr. Enrique Solano for the continuous support of my Ph.D. study and research, for his patience, motivation, enthusiasm, and immense knowledge. His guidance helped me in all the time of research and writing of this thesis. He introduced me to many interesting people and opportunities. I could not have imagined having a better advisor and mentor for my Ph.D. thesis.

I would like to express my sincere gratitude to Prof. Xi Chen, University of the Basque Country, Spain, for all his support, encouragement, and guidance. I'll always be glad to him for introducing me to the concept of shortcuts to adiabaticity.

A special thanks to Dr. Koushik Paul, who not only contributed to the development of my research but also guided me in every step of the project. Also, Dr. Francisco Albarrán-Arriagada for his guidance during the initial days of my Ph.D. work.

I would also like to give my special thanks to the following people who have contributed to my Ph.D. study and research in many different ways: Shubham Kumar, Pranav Chandarana, Dr. Francisco A Cárdenas-López, and Dr. Gabriel Alvarado Barrios.

I want to acknowledge the support and encouragement I received from the staff and students of the QuArtist Center at Shanghai University. In particular, I thank Dr. Minjia Hao and Mrs. Zhao Dong for all the help.

Finally, I would like to thank my family and friends for their moral and financial support as well as their valuable advice. I would especially like to thank my brother for his continuous guidance throughout my career and my Mom for her love, patience, and constant encouragement.